THE STUDY OF CHEMILUMINESCENT REACTIONS IN THE GAS PHASE

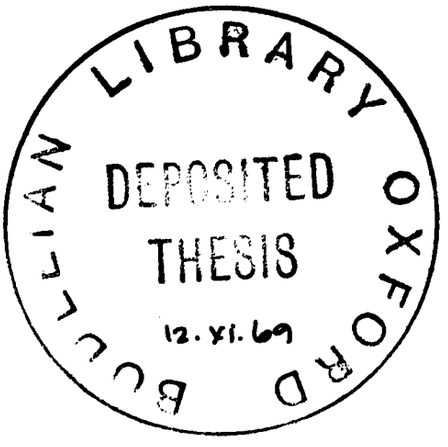
by

Thomas Paul John Izod

of

Christ Church

Oxford



ABSTRACT

The two lowest lying singlet electronic states of molecular oxygen $O_2(^1\Delta g)$ and $O_2(^1\Sigma g^+)$ are present in the atmosphere and undergo optical transitions to the ground state molecule giving rise to the atmospheric bands:

$$O_2(^1\Sigma g^+) \leftrightarrow O_2(^3\Sigma g^-) \quad (0,0) \quad 762 \text{ nm}$$

and the infra-red atmospheric bands:

$$O_2(^1\Delta g) \leftrightarrow O_2(^3\Sigma g^-) \quad (0,0) \quad 1268 \text{ nm}.$$

Possible mechanisms for the production of the excited speciesswere studied in the laboratory. The reactions were carried out in time resolved flow systems and the species observed by their optical emission with the aid of photomultipliers and photo conductors in conjunction with phase sensitive detection circuitry.

The ultra violet photolysis of ozone with λ = 253.7 nm was studied as a source of $O_2(^1\Sigma g^+)$ and $O_2(^1\Delta g)$. $O_2(^1\Delta g)$ was observed in the photolysis of ozone-oxygen mixtures with λ = 253.7 nm and its production was attributed to the energy transfer process:

$$O(^1D) + O_2(^3\Sigma g^-) \rightarrow O(^3P) + O_2(^1\Delta g).$$

$O_2(^1\Sigma g^+)$ was observed in a system involving the photolysis of oxygen with λ = 147 nm by an analogous reaction:

$$O(^1D) + O_2(^3\Sigma g^-) \rightarrow O(^3P) + O_2(^1\Sigma g^+)$$

The atom recombination reaction:

$$O(^3P) + O(^3P) + M \rightarrow O_2(\text{singlet}) + M$$

and the chemiluminescent reaction:

$$NO + O_3 \rightarrow NO_2 + O_2 + h\nu$$

were studied but found not to produce significant quantities of excited molecular oxygen.

The excited species have relatively long lifetimes and generally undergo physical or chemical deactivation reactions in preference to radiative transitions. The reactions of $O_2(^1\Sigma g^+)$ and $O_2(^1\Delta g)$ with ozone:

$$O_3 + O_2(^1\Sigma g^+) \rightarrow 2O_2 + O(^3P)$$
$$O_3 + O_2(^1\Delta g) \rightarrow 2O_2 + O(^3P)$$

and the quenching reactions:

$$O_2(^1\Sigma g^+) + M \rightarrow O_2 + M$$

where M = O_2, N_2 and Ar were studied and rate constants evaluated. A value for the efficiency of deactivation of $O_2(^1\Sigma g^+)$ at a pyrex surface was also obtained and the rate of the energy pooling process $O_2(^1\Delta g) + O_2(^1\Delta g) \rightarrow O_2(^1\Sigma g^+) + O_2(^3\Sigma g^-)$ was estimated.

The rates of the following $O(^1D)$ atom reactions:

$$O(^1D) + N_2 \rightarrow O(^3P) + N_2$$
$$O(^1D) + Ar \rightarrow O(^3P) + Ar$$
$$O(^1D) + O_3 \rightarrow O_2 + O_2$$
$$O(^1D) + O_2 \rightarrow O_2(^1\Sigma g^+) + O(^3P)$$
$$O(^1D) + O_2 \rightarrow O_2(^1\Delta g) + O(^3P)$$

were estimated.

Calculations were carried out to test the importance of the various mechanistic schemes studied as sources of excited singlet oxygen in the atmosphere. In addition the major loss processes of excited oxygen molecules and atoms were calculated and the results compared with atmospheric data.

ORIGINALITY OF THIS WORK

The experimental work described in this dissertation is original and was performed by the author. Acknowledgements to others is given where necessary. The dissertation was written solely by him. References are always given in discussions of other workers' data.

Thomas P. J. Izod

PREFACE

I wish to thank Dr. R.P. Wayne for his supervision over the past three years. He was a constant source of inspiration and encouragement.

I would like to thank Dr. C.D. Walshaw of the Clarendon Laboratory, Oxford, for carrying out the computations described in Chapter 6 and for numerous stimulating discussions on atmospheric topics.

My thanks are extended to Mr. I.D. Clark for the use of his high vacuum pumping system and Mr. I.T.N. Jones for the use of his cross beam absorption apparatus.

Finally, I would like to thank all the staff at the Physical Chemistry Laboratory for their technical advice, in particular Mr. K. Calkin for constructing many pieces of glassware, and Mr. J. Jessop for building the electronics of the detection system. Thanks are also due to the Science Research Council for a maintenance grant, during the tenure of which the work was performed.

To J.E.K.

CONTENTS

		Page
1	Introduction	1
2	Experimental Techniques	
	2.1 Preparation and purification of gases	
	(a) Ozone	17
	(b) Nitric Oxide	20
	(c) Oxygen and Nitrogen	21
	(d) Xenon	21
	2.2 Measurement of ozone purity	21
	2.3 Gold plating of bulb	22
	2.4 Preparation of photolysis lamps	24
	2.5 Flow and gas storage apparatus	26
	2.6 Optical components	
	(a) Filters	30
	(b) Monochromator	30
	(c) Detectors	31
	2.7 Electronics	
	(a) phase sensitive detector	44
	(b) D.C. amplifier	46
3	Ultra Violet Photolysis of Ozone	
	3.1 Summary	48
	3.2 Flow apparatus and materials	49
	3.3 Optical components	49
	3.4 Nitrogeneous impurities	51
	3.5 Ozone photolysis	51
	3.6 Use of monochromator	56
	3.7 Kinetic measurements	59
	3.8 Kinetic analysis	69
	3.9 Deactivation of $O_2(^1\Delta g)$ by reaction with ozone	77
	3.10 Photolysis of ozone with $\lambda \geq 266$ nm	81
4	Ultra Violet Photolysis of Oxygen	
	4.1 Summary	83
	4.2 Choice of system	84
	4.3 Flow apparatus and materials	86
	4.4 Optical components	86
	4.5 Preliminary studies	87
	4.6 Kinetic Studies	88
	4.7 Effect of discharge power on α	89
	4.8 Reaction of $O_2(^1\Sigma g^+)$ with ozone	91
	4.9 Quenching of $^2O_2(^1\Sigma g^+)$ by argon and nitrogen	94
	4.10 Reaction of $O_2(^1\Sigma g^+)$ with oxygen	96
	4.11 Reaction of $O(^1D)$ atoms	99
	4.12 Attempts to detect $O_2(^1\Delta g)$	109
	4.13 Further work	111

		Page
5	Miscellaneous reactions	
	5.1 Atom recombination reaction	112
	5.2 NO + O_3 reaction	115
	5.3 Photosensitization reactions	119
6.	Atmospheric discussion	122
	References	134

CHAPTER 1

INTRODUCTION

The Earth receives virtually all its energy from space in the form of solar electromagnetic radiation. The spectral distribution of the sun is complex, containing dark Fraunhoffer lines [1]. However, the solar spectral distribution is very similar to that of a black body source of 6000^{o}K and this is shown in figure 1. It is evident that most of the solar radiation lies in the ultra violet region. Part of this radiation is prevented from reaching the surface of the Earth by the complex gaseous layer surrounding the planet. The structure of the atmospheric layer is shown in simplified form in figure 2, illustrating some of the atmospheric parameters, such as temperature, pressure and composition with altitude.

Two atmospheric gases of particular importance are ozone and oxygen. Figures 3 and 4 show the extinction coefficient-wavelength relationship of these gases. It is evident that ozone absorbs strongly radiation between λ = 200 nm and λ = 300 nm, and oxygen radiation below λ = 175 nm. Therefore, a great deal of harmful ultra violet radiation is prevented from reaching the surface of the Earth by these two gases and destroying life in its present form. Not only are these two atmospheric

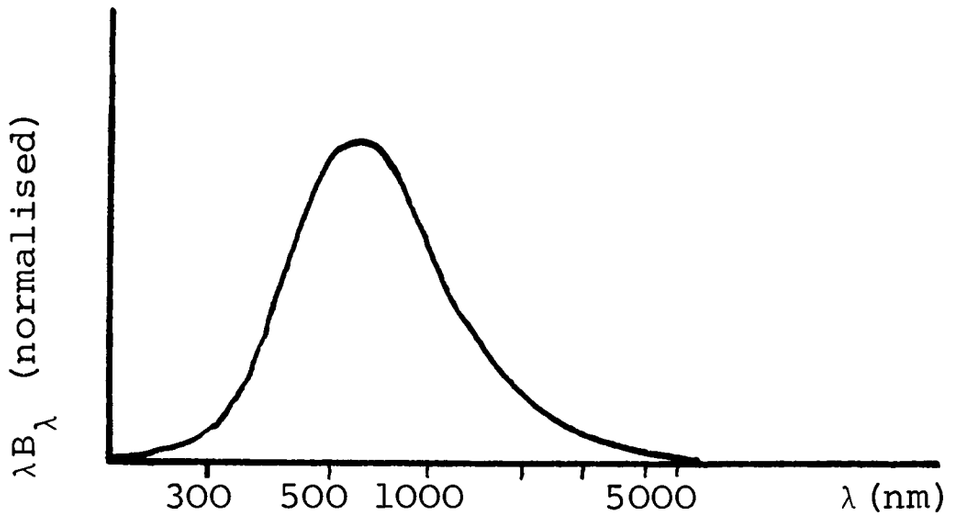


Figure 1. Spectral distribution of a black body source at 6000°K [1]

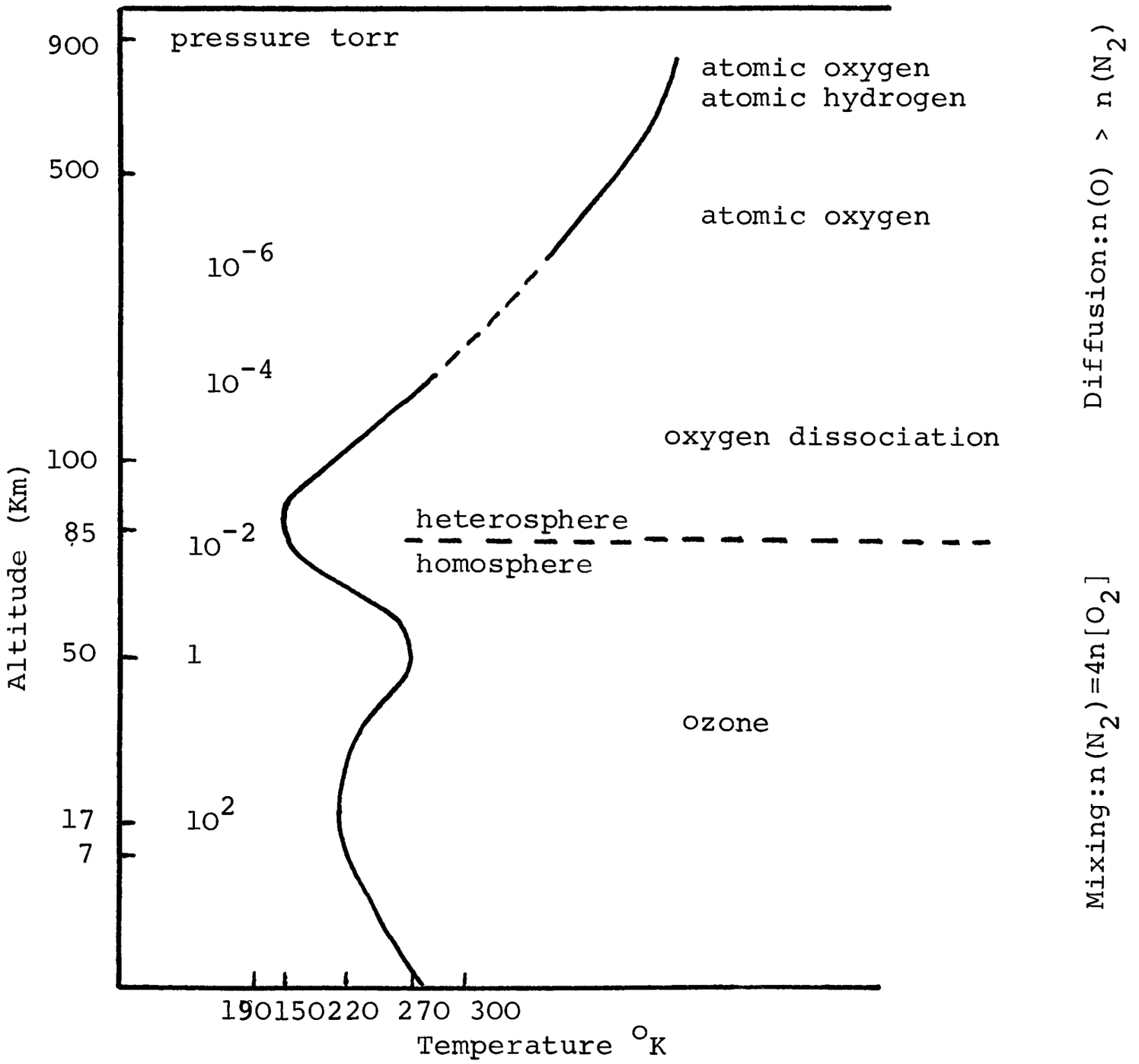


Figure 2. Diagramatic representation of the atmosphere [2]

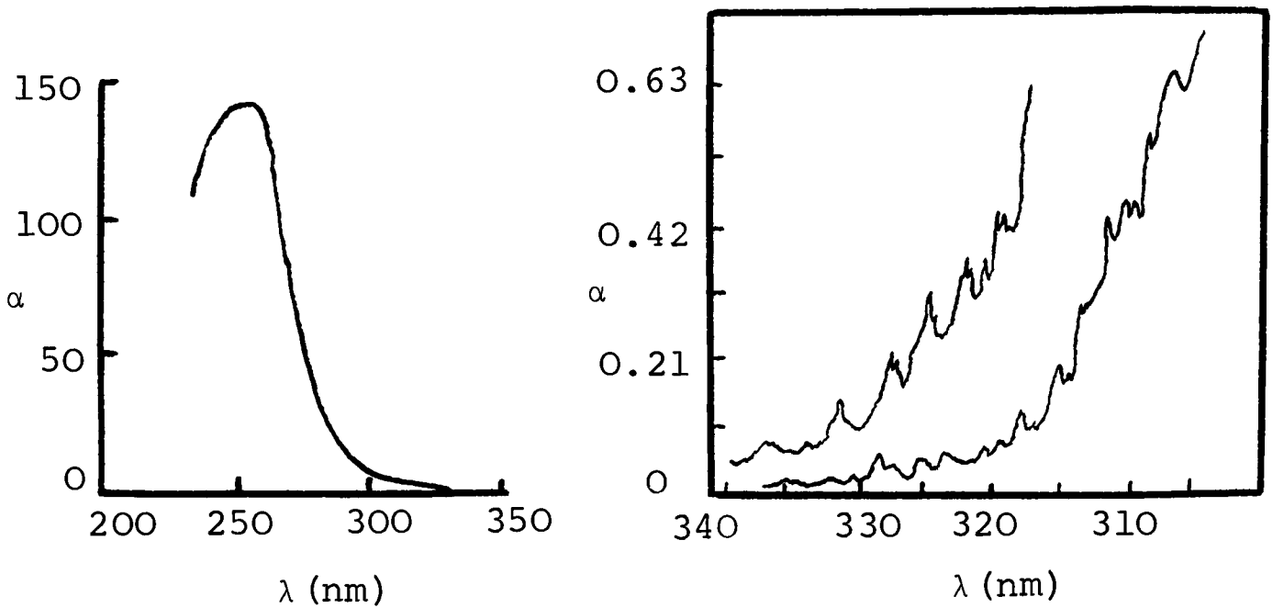


Figure 3. Extinction coefficients of ozone [3]

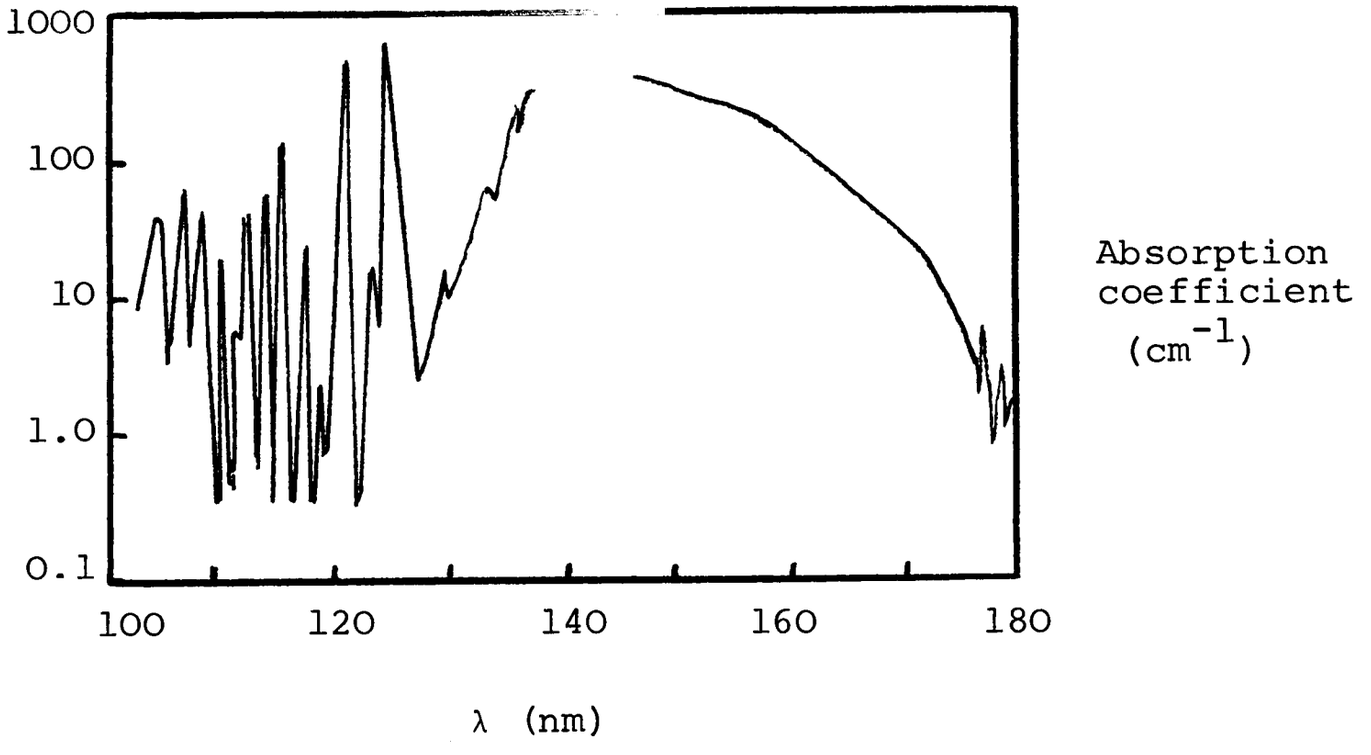


Figure 4. Absorption coefficients of oxygen [4]

constituents essential for maintaining life on this planet, but often the interaction with the sun's radiation leads to the formation of energetically excited atoms or molecules. Indeed, the two lowest lying excited singlet states of molecular oxygen are present in the atmosphere [5,6]. The study of these two species form the basis of this thesis.

The lowest electron configuration of oxygen is:

$$KK(\sigma g2s)^2(\sigma u2s)^2(\sigma g2p)^2(\pi u2p)^4(\pi g2p)^2.$$

This gives rise to the states $^3\sum g^-$, $^1\Delta g$ and $^1\sum g^+$ with $^3\sum g^-$ being the ground state. An energy level diagram, figure 5, indicates some of the energies of the states and their dissociation products.

Magnetic dipole interactions are possible for the $^1\Delta g \leftrightarrow {}^3\sum g^-$ & $^1\sum g^+ \leftrightarrow {}^3\sum g^-$ transitions in oxygen although since they are forbidden they are naturally weak. Herzberg and Herzberg [8] observed the (0,0) and (1,0) bands of the $^1\Delta g \leftrightarrow {}^3\sum g^-$ transition at 1268.3 nm and 1067.4 nm, respectively in absorption experiments. The (0,0) and (0,1) bands of this transition at 1268.3 nm and 1580.0 nm were observed in the airglow emission by Vallance Jones and Harrison [9]. These bands are frequently termed the "infra-red atmospheric" bands. The $^1\sum g^+ \leftrightarrow {}^3\sum g^-$ transition in oxygen gives rise to the "atmospheric" bands. This has (0,0) and (0,1) bands at 761.9 nm and 868.2 nm respectively [10].

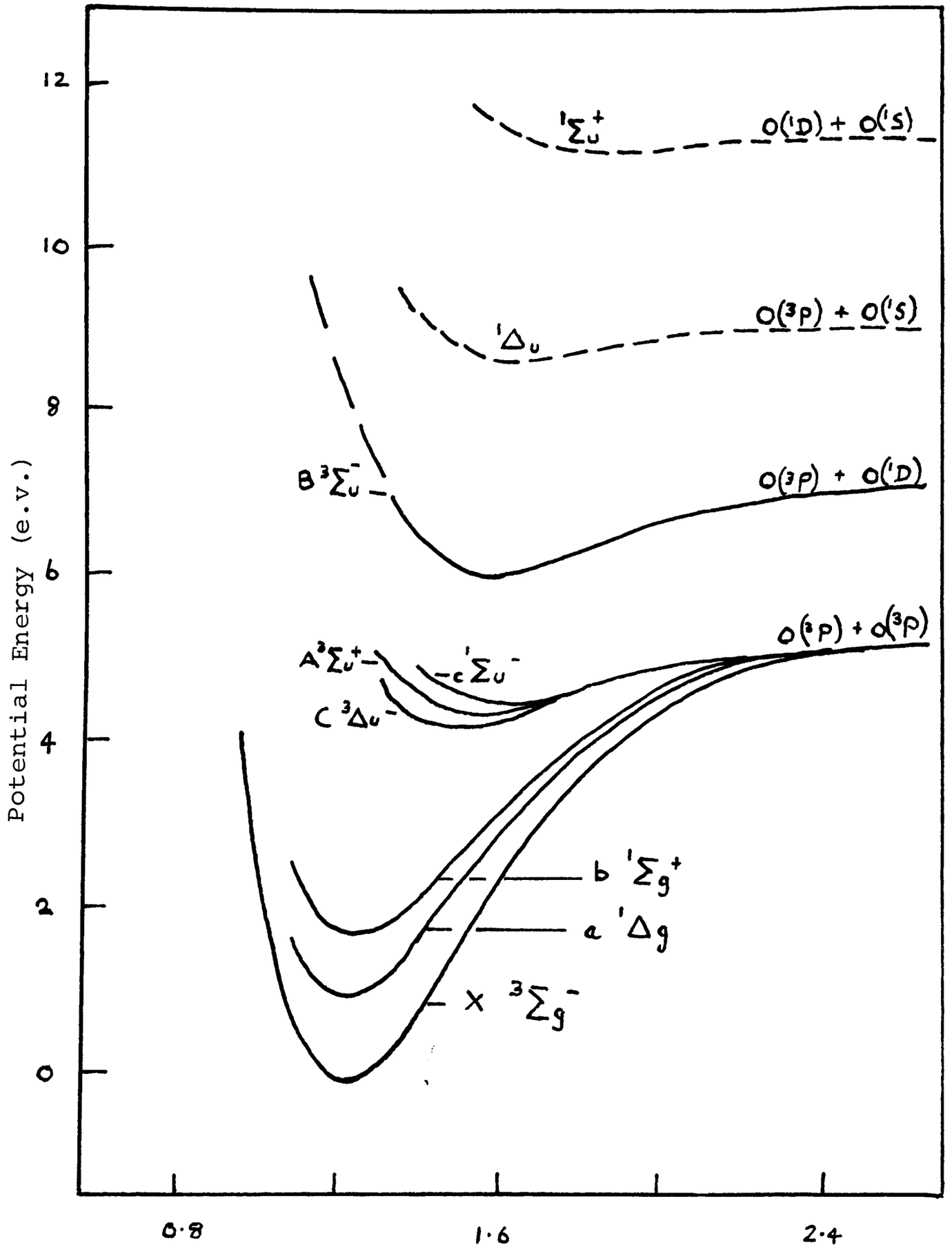


Figure 5. Potential Curves for oxygen molecules [7]

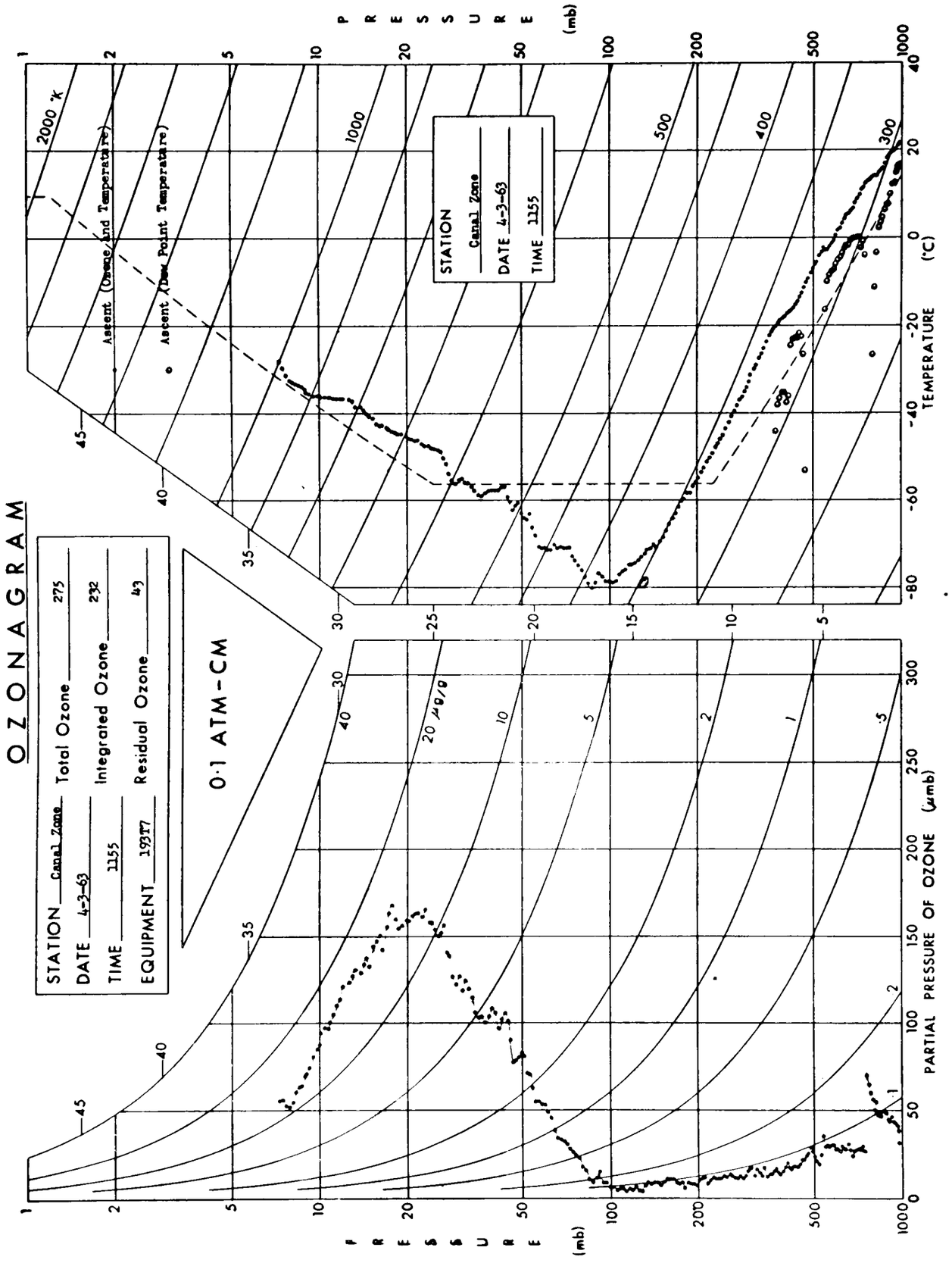


Figure 6. Atmospheric ozone distribution curves [19]

The absolute transition probabilities for the "atmospheric" and "infra-red atmospheric" bands are needed if emission intensities are to be used in the estimation of the concentrations of $O_2(^1\Delta g)$ and $O_2(^1\Sigma g^+)$. The Einstein A factor for the $^1\Sigma g^+ \leftrightarrow {}^3\Sigma g^-$ transition was determined as A = 0.145 sec^{-1} [11,12] for the (0,0) band. Recently, Wallace and Hunsten [13] have suggested an A value of 0.085 sec^{-1}. Clearly further experiments are required in this respect to resolve the discrepancy. The A factor for the $^1\Delta g \leftrightarrow {}^3\Sigma g^-$ transition was calculated by Badger et al [14] to be 2.58 x 10^{-4} sec^{-1} for the (0,0) band. Table 1 lists the wavelengths of band origins, relative intensities and transition probabilities of the "atmospheric" and "infra-red atmospheric" band systems.

The oxygen bands are present in the airglow. The airglow is the radiation emitted by the Earth's upper atmosphere, other than that due to aurora. The airglow is extremely feeble, the illumination it gives to the ground, according to Bates [16], being of the same order as that from a candle at a height of 100 meters. The presence of these excited oxygen species in the atmosphere raises the question of their mode of formation. Photolysis of atmospheric constituents by solar radiation may lead to the formation of excited species in the primary or secondary processes. If the excited species loses its energy by the

Table 1. Wavelengths of band origins and relative intensities of the $O_2(^1\Delta g \leftrightarrow {}^3\Sigma g^-)$ and $O_2(^1\Sigma g^+ \leftrightarrow {}^3\Sigma g^-)$ systems [15]

$^1\Delta_g \leftrightarrow {}^3\Sigma g^-$; $A = 2.58 \times 10^{-4}$ sec^{-1} [14]

V' / V"		0	1
0	λ (nm)	1268.6	1062.0
	I	100	2.2
1		1592.8	1280.2
		0.66	95

$^1\Sigma g^+ \leftrightarrow {}^3\Sigma g^-$; $A = 0.145$ sec^{-1} [11,12]

V' / V"	0	1
0	761.9	685.7
	100	9.9
1	868.2	770.5
	4.9	82

emission of radiation, then a phenomenon similar to fluorescence is observed. The process is not identical to fluorescence, since fluorescence is generally taken to mean the emission of radiation by the absorbing species. The phenomenon under consideration involves the transfer of energy by chemical means and the term "chemiluminescence" is used to describe this sort of process. If the process is initiated photochemically then the term "photo-chemiluminescence" is used.

Part of the work, Chapters 3, 4 and 5, is directed toward the study in the laboratory of a number of likely atmospheric chemiluminescent processes. Here it is intended to give a brief outline of some of the proposed mechanisms to indicate the types of systems, relevant to later experiments, that might yield excited singlet oxygen molecules.

The production of $O_2(^1\Sigma g^+)$ and $O_2(^1\Delta g)$ in the atmosphere is the subject of much speculation and numerous mechanisms have been postulated and reviewed [17,18]. The likely precursors of excited oxygen are probably ozone, oxygen and oxygen atoms.

Ozone is formed between 120 and 80 K.meters by the photodissociation of oxygen at wavelengths shorter than λ = 200 nm.

$$O_2 + h\nu \xrightarrow[<200\ nm]{} O + O \qquad 1.1$$

$$O_2 + O + M \rightarrow O_3 + M \qquad 1.2$$

$$O + O_3 \rightarrow 2O_2 \qquad 1.3$$

$$O_3 + h\nu \rightarrow O_2 + O \qquad 1.4$$

Air motions transport the ozone to lower levels. By consideration of the equilibrium between the formation and removal reactions 1.1 to 1.4 the maximum ozone concentration is predicted as being about 30 Km. This is in fairly good agreement with observation [19] which indicate the maximum ozone level at about 26 Km. More detailed calculations tend to predict too small a total ozone concentration and incorrect distribution [20]. A concentration-altitude profile carried out by rocket observation over the Canal Zone is shown in figure 6.

Consideration of the ozone extinction coefficient curves, figure 3, and the solar distribution, figure 1, indicate that most of the absorption of radiation by ozone occurs around the tail of the Hartley-Huggins band. Houghton [21] has shown that if ozone photolysis precedes the oxygen band emissions then the various steps leading to these species need only be 0.3% efficient. The photolysis of ozone has therefore to be considered as a likely source of $O_2(^1\Delta g)$ and $O_2(^1\Sigma g^+)$. The laboratory experiments of Norrish and Wayne [22] on the ultraviolet photolysis of pure dry ozone indicated that the quantum yield was a

linear function of pressure, extrapolating to a value of four at zero pressure. The following mechanism was proposed:

$O_3 + h\nu$	$\xrightarrow[\text{ultra violet}]{}$	$O_2 + O(^1D)$	1.4
$O(^1D) + O_2$	$\rightarrow$	$O_2^+ + O$	1.5
$O_2^+ + O_3$	$\rightarrow$	$2O_2 + O(^1D)$	1.6
$O_2^+ + O_3$	$\rightarrow$	$2O_2 + O(^3P)$	1.7

O_2^+ is an energy rich molecule, and clearly it must produce an $O(^1D)$ atom in 1.6 to propagate the chain, whilst in 1.7 the production of an $O(^3P)$ atom is effectively a terminating process. Neither $O_2(^1\Delta g)$ nor $O_2(^1\Sigma g^+)$ satisfy the requirements for O_2^+ since their reactions in 1.6 are endothermic to the extent of 47 Kcals. $mole^{-1}$ and 32 Kcals. $mole^{-1}$ respectively. The state of O_2^+ has been suggested as $O_2(^3\Sigma u^+)$ or vibrationally excited $O_2(^3\Sigma g^-)$ [22].

The presence of the $O(^1D)$ atom in the primary photolytic step was confirmed by De More and Raper [23] and Norrish and McGrath [24,25]. De More and Raper, by photolysing ozone in low temperature solvents, have shown that the quantum yield for $O(^1D)$ formation was approximately unity at $\lambda < 300$ nm. while it drops to .4(± .15) at $\lambda =$ 313 nm. However, the sum of the primary quantum yields for $O(^1D)$ and $O(^3P)$ atoms remains unity throughout the wavelengths studied [26,27].

The oxygen molecule formed in the primary photolytic

step, 1.4, could be $O_2(^1\Delta g)$ or $O_2(^1\Sigma g^+)$. Huffman [28] has observed intense absorption bands lying between 83 nm and 90 nm in the photolysis products of ozone. He concluded that metastable oxygen was a photolysis product. Consideration of spin conservation suggests that the oxygen molecule produced is likely to be a singlet as the oxygen atom produced and the ozone molecule decomposed are singlets. The reaction is written, with the long wavelength limits in brackets, as follows:

$$O_3(^1A) + h\nu \begin{cases} \longrightarrow O_2(^1\Delta g) + O(^1D) \ [310 \text{ nm}] & 1.4a \\ \longrightarrow O_2(^1\Sigma g^+) + O(^1D) \ [266 \text{ nm}] & 1.4b \end{cases}$$

The spin conservation rules, however, are not necessarily rigorous when the absorption is weak, which is the case in the atmosphere.

Recent laboratory studies of Jones and Wayne [29] suggest that a singlet oxygen molecule may be produced at wavelengths greater than 310 nm. They studied the photolysis of ozone at λ = 253.7 nm, 313 nm and 334 nm, measuring the amount of ozone decomposed by an absorption technique. The results indicate that even at λ = 334, when no $O(^1D)$ atoms are produced in the primary step the quantum yield gives a value of four when extrapolated to zero pressure. Explanation of this observation requires that a singlet oxygen molecule together with an $O(^3P)$ atom is produced in the primary step. If the oxygen were not a singlet then

the quantum yield would be two as shown by Castellano and Schumacher [30,31], from the measurement of ozone photolysis at λ = 600 nm. Thus at λ > 310 nm the following spin-forbidden reaction may be of importance:

$$O_3 + h\nu \rightarrow O_2(^1\Sigma g^+) + O(^3P) \quad [463 \text{ nm}] \qquad 1.4c$$

$$O_3 + h\nu \rightarrow O_2(^1\Delta g) + O(^3P) \quad [590 \text{ nm}] \qquad 1.4d$$

$$O_3 + h\nu \rightarrow O_2(^3\Sigma g^-) + O(^3P) \quad [1180 \text{ nm}] \qquad 1.4e$$

Laboratory experiments were carried out on the photolysis of pure, dry ozone at λ = 253.7 nm, using a flow technique in an attempt to observe either $O_2(^1\Sigma g^+)$ or $O_2(^1\Delta g)$ [32]. The observations are described in Chapter 3. $O_2(\Sigma g^+)$ was not observed, though its absence may be understood by the very fast loss process with ozone [33]:

$$O_3 + O_2(^1\Sigma g^+) \rightarrow 2O_2 + O(^3P) \qquad 1.8$$

$O_2(^1\Delta g)$ was observed but <u>only</u> in the presence of excess molecular oxygen [32]. The significance of this observation is discussed later in terms of an electronic energy transfer process.

Evans [34], Noxon [18], Wallace and Hunter [13] have inferred from rocket measurements of the "infra-red atmospheric" and "atmospheric" band concentration-altitude profiles that reaction 1.4a and 1.4b are the main sources of $O_2(^1\Sigma g^+)$ and $O_2(^1\Delta g)$ in the atmosphere. Evans [34] has also suggested that $O_2(^1\Delta g)$ is produced at λ > 266 nm

and $O_2(^1\Sigma g^+)$ at $\lambda < 266$ nm to account for his observations. Laboratory experiments were carried out to test this and are presented in Chapter 3. The results were negative, but this was perhaps due to the weak photolysis source employed and the small extinction coefficient of ozone at $\lambda > 266$ nm.

Another scheme proposed by Vallance Jones and Galtinger [35], De More and Raper [36] for excited singlet oxygen production involves an energy transfer reaction:

$$O(^1D) + O_2(^3\Sigma g^-) \begin{cases} \longrightarrow O_2(^1\Sigma g^+) + O(^3P) & 1.9 \\ \searrow O_2(^1\Delta g) + O(^3P) & 1.10 \end{cases}$$

This reaction on energetic spin conservation considerations could yield either $O_2(^1\Delta g)$ or $O_2(^1\Sigma g^+)$ being 25 Kcals $mole^{-1}$ and 11 Kcals $mole^{-1}$ exothermic respectively.

$O_2(^1\Sigma g^+)$ was observed by Young and Black [37] in a system involving the photolysis of oxygen with radiation of $\lambda = 147$ nm. Young and Black [38] have subsequently irradiated oxygen at various wavelengths between $\lambda = 120$ nm and $\lambda = 184$ nm. They observed $O_2(^1\Sigma g^+)$ as the only emitting product between 600 nm and 800 nm with photolytic radiation of $\lambda < 175$ nm. The reaction scheme was suggested as follows:

$$O_2 + h\nu \xrightarrow{\lambda < 175 \text{ nm}} O(^1D) + O(^3P) \qquad 1.11$$

$$O(^1D) + O_2(^3\Sigma g^-) \rightarrow O_2(^1\Sigma g^+) + O(^3P) \qquad 1.9$$

More recent work by Noxon [39] and Young and Black [40] indicated that the $O(^1D) \leftrightarrow O(^3P)$ transition at 634.0 nm is also an emitting product in the above reaction scheme. For the production of $O_2(^1\Sigma g^+)$ by the energy transfer process a resonance condition is taken into account. If the product $O_2(^1\Sigma g^+)$ were in v' = 2 vibrational level then a resonance condition exists and rapid vibrational relaxation with ground state oxygen would then lead to a high concentration of the v' = 0 state.

De More and Raper [36] suggest that the electronic energy transfer reaction proceeds via an excited triplet ozone molecule:

$$O(^1D) + O_2(^3\Sigma g^-) \longrightarrow O_3(\text{triplet}) \rightarrow O_2(^1\Delta g) + O(^3P) \qquad 1.10a$$

$$O(^1D) + O_2(^3\Sigma g^-) \longrightarrow O_3(\text{triplet}) \rightarrow O_2(^1\Sigma g^+) + O(^3P) \qquad 1.9b$$

This scheme is directly analogous to the quenching reaction of $O(^1D)$ atoms by nitrogen:

$$O(^1D) + N_2(^1\Sigma g^+) \rightarrow O(^3P) + N_2(^1\Sigma g^+) \qquad 1.12$$

Reaction 1.12 is neither energy matched nor spin permitted and is thought to involve a predissociation from vibrationally excited $N_2O(^1\Sigma g^+)$ from spectroscopic evidence. The presence of $O_2(^1\Delta g)$ when ozone-oxygen mixtures were irradiated with λ = 253.7 nm [32], where relatively high concentrations of $O(^1D)$ atoms were produced in the primary step can thus be understood in terms of the energy transfer

reaction 1.10. $O_2(^1\Sigma g^+)$ should also be produced in this system by reaction 1.9 but was not observed. This was again due to the fast removal rate of $O_2(^1\Sigma g^+)$ by ozone in our experimental system.

The recombination of ground state oxygen atoms might account for the formation of singlet excited oxygen [41]. It is evident from figure 5 that $O_2(^1\Delta g)$ and $O_2(^1\Sigma g^+)$ lie on the same potential energy curves as two ground state $O(^3P)$ atoms. The suggested scheme for singlet oxygen production is:

$$O(^3P) + O(^3P) + M \rightarrow O_2(\text{singlet}) + M \qquad 1.13$$

Young and Sharpless [41] have produced oxygen atoms by the reaction:

$$N + NO \rightarrow N_2 + O(^3P) \qquad 1.14$$

in a discharge flow tube and found some evidence for $O_2(^1\Sigma g^+)$ formation. The rate constant for $O_2(^1\Sigma g^+)$ formation via reaction 1.13 was evaluated as 5×10^5 moles^{-2}l^2 sec^{-1}. However, Clyne, Thrush and Wayne [42] were unable to detect any $O_2(^1\Sigma g^+)$. A search was made using essentially the same system for $O_2(^1\Delta g)$ production. This is described in Chapter 5. No $O_2(^1\Delta g)$ was observed and consideration of the lowest detectable absolute concentration of $O_2(^1\Delta g)$ enabled the evaluation of an upper limit for the rate constant of reaction 1.13 as

$k_{13} < 10^6$ mole^{-2} l^2 sec^{-1}.

A further reaction for possible singlet oxygen formation, but involving another minor atmospheric constituent, nitric oxide, is the chemiluminescent reaction [43,44]:

$$NO + O_3 \rightarrow NO_2^* + O_2 \qquad 1.15$$

$$NO + O_3 \rightarrow NO_2 \text{(ground state)} + O_2 \qquad 1.16$$

$$NO_2^* \rightarrow NO_2 + h\nu \qquad 1.17$$

$$M + NO_2 \rightarrow NO_2 + M \qquad 1.18$$

The chemiluminescence is thought to come solely from excited NO_2. As the reaction is 49Kcals mole^{-1} exothermic, some energy might appear as excitation of oxygen in one of its singlet states. The reaction was investigated for production of $O_2(^1\Delta g)$ and $O_2(^1\Sigma g^+)$ and described in Chapter 5. Observation indicated that neither of the excited species was present.

The relatively long radiative lifetimes of $O_2(^1\Delta g)$ and $O_2(^1\Sigma g^+)$, see Table 1, suggests that in the atmosphere these species probably undergo deactivation or reaction with other atmospheric constituents, in preference to radiative transitions. Clearly a knowledge of the efficiencies of such reactions affecting the excited species is essential to enable an overall assessment of the atmospheric processes of $O_2(^1\Delta g)$ and $O_2(^1\Sigma g^+)$. Chapters 3 and 4 are directed toward the kinetic study of $O_2(^1\Delta g)$

and $O_2(^1\Sigma g^+)$.

There are numerous laboratory techniques for studying $O_2(^1\Delta g)$ and $O_2(^1\Sigma g^+)$. These are reviewed by Wayne [15]. In all experiments described in this work the excited species were observed by their optical transitions with the aid of photomultipliers and photo conductors. The photo-chemiluminescent reactions were carried out in controlled flow systems. This avoided the disadvantage encountered with static systems of rapid consumption of reactants and light scattering [45]. The experimental techniques involved in all experiments are described fully in Chapter 2.

Chapter 4 describes experiments carried out to measure the rate constants for the following reactions:

$O_3 + O_2(^1\Sigma g^+)$	$\rightarrow 2O_2 + O(^3P)$	1.8
$N_2 + O_2(^1\Sigma g^+)$	$\rightarrow N_2 + O_2$	1.19
$O_2(^3\Sigma g^-) + O_2(^1\Sigma g^+)$	$\rightarrow 2O_2$	1.20
$O_2(^1\Sigma g^+)$	$\xrightarrow{\text{wall}} O_2$	1.21

The source of $O_2(^1\Sigma g^+)$ for these experiments was obtained, via the energy transfer reaction 1.9, by photolysing molecular oxygen with radiation of $\lambda = 147$ nm. This method was chosen in preference to the more conventional microwave or radio frequency discharge through oxygen for the following reason. Electrical discharge through molecular oxygen produces about 5% $O_2(^1\Delta g)$ [46,47] and

about 2×10^{-2}% $O_2(^1\Sigma g^+)$ [48] of the total gas flow. The presence of a large excess of $O_2(^1\Delta g)$ renders the "energy pooling" process [49] as an important source of $O_2(^1\Sigma g^+)$:

$$O_2(^1\Delta g) + O_2(^1\Delta g) \rightarrow O_2(^1\Sigma g^+) + O_2(^3\Sigma g^-) \qquad 1.22$$

The rate constant for reaction 1.22 is not well established and errors occur when correcting for $O_2(^1\Sigma g^+)$ concentrations in a microwave discharge flow system. Most rate constant determinations for $O_2(^1\Sigma g^+)$ reactions and deactivations were previously carried out in systems involving molecular oxygen discharge [46,50]. It is clearly essential to repeat these kinetic studies using a system where $O_2(^1\Delta g)$ is <u>not</u> in large excess of $O_2(^1\Sigma g^+)$ such that the energy pooling reaction does not play an important role. Rate constants for reactions 1.8, 1.19, 1.20 and 1.21 were obtained and the results are discussed in the light of other workers in Chapter 4. An analogous reaction to 1.8 for $O_2(^1\Delta g)$ is:

$$O_2(^1\Delta g) + O_3 \rightarrow 2O_2 + O(^3P) \qquad 1.24$$

The rate constant for this reaction was studied in a system producing $O_2(^1\Delta g)$ by the photolysis of ozone-oxygen mixtures at λ = 253.7 nm. This is presented in Chapter 3.

As pointed out earlier the energy transfer process could account for excited singlet oxygen production in the

atmosphere. The efficiencies of these transfer reactions and also the quenching efficiencies of $O(^1D)$ atoms with other atmospheric constituents are therefore required. These atom reactions have been fully reviewed by McGrath and McGarvey [51] and more recently by Zipf [52]. The efficiencies of the following reactions were evaluated:

$$O_2(^3\Sigma g^-) + O(^1D) \rightarrow O_2(^1\Sigma g^+) + O(^3P) \qquad 1.9$$

$$O_2(^3\Sigma g^-) + O(^1D) \rightarrow O_2(^1\Delta g) + O(^3P) \qquad 1.10$$

$$N_2 + O(^1D) \rightarrow N_2 + O(^3P) \qquad 1.25$$

$$Ar + O(^1D) \rightarrow Ar + O(^3P) \qquad 1.26$$

$$O_3 + O(^1D) \rightarrow O_2 + O_2 \qquad 1.5$$

Chapter 3 presents the estimated efficiencies of the reactions 1.10 and 1.5 and Chapter 4 those of reactions 1.9, 1.25 and 1.26. These are compared with the values obtained by other workers.

The (O,O) bands at 762 nm and 1270 nm of the two atmospheric band systems were observed from elevated altitudes and balloons. Ground observations are exceedingly difficult due to reabsorption of the bands by the atmosphere. More recently the use of high altitude aircraft and rockets [34] has enabled the variation of integrated intensity of a band, corrected for reabsorption, to be used in calculating the concentration distribution of the excited molecules in the atmosphere. The methods available for this are reviewed by Packer [53].

These atmospheric observations, though not always in agreement, offer a means of testing the importance of any particular reaction mechanism in producing $O_2(^1\Delta g)$ and $O_2(^1\Sigma g^+)$. Chapter 6 describes calculations carried out on a number of mechanistic schemes studied in earlier chapters, to compare theoretical intensities and concentrations of the atmospheric bands with observed data. The rate constants used are, wherever possible, those derived from this work, and where not, the most reasonable values from other workers [54,15]. All rate constants refer to laboratory temperature. This is clearly a source of error in the calculations since it is evident from figure 2 that temperature in the atmosphere varies with altitude. However, using a simplified approach it was possible to assess not only the importance of certain production mechanisms of $O_2(^1\Delta g)$ and $O_2(^1\Sigma g^+)$, but also the major loss processes that control the overall intensity and concentration distribution of the atmospheric oxygen bands. The results are compared and discussed with reference to atmospheric observations and suggestions are made for improving the calculation scheme.

CHAPTER 2

EXPERIMENTAL TECHNIQUES

2.1 Preparation and purification of gases.

(a) Ozone.

Ozone is 34 Kcals. $mole^{-1}$ endothermic with respect to $\frac{3}{2}$ oxygen and thus it is necessary to supply energy to the system when preparing the gas from oxygen. This can be achieved in a number of ways, for example by irradiation of molecular oxygen at wavelengths below its absorption limit near 200 nm [55], radiolysis of oxygen by γ rays using a Co source [56] or, more conveniently, by using a silent electrical discharge in oxygen.

A Siemens' ozoniser of the type shown in figure 7 was employed for the preparation of the gas. The efficiency of the ozoniser depends critically on the geometry of the system, pressure and flow-rate of the oxygen. It was found that oxygen, at a little above atmospheric pressure, when passed at about 5 $m.l.sec^{-1}$ through four ozonisers yielded up to 8% ozone in oxygen. The potential applied was 12,500 volts A.C. Above this limit, sparking occurred, with resulting decomposition of the ozone.

There are a number of ways of purifying ozonised oxygen. The boiling point of ozone is $-112.3^{o}C$ and thus it is possible to condense the ozone-oxygen mixture using a liquid nitrogen trap, pumping off the oxygen whilst cold,

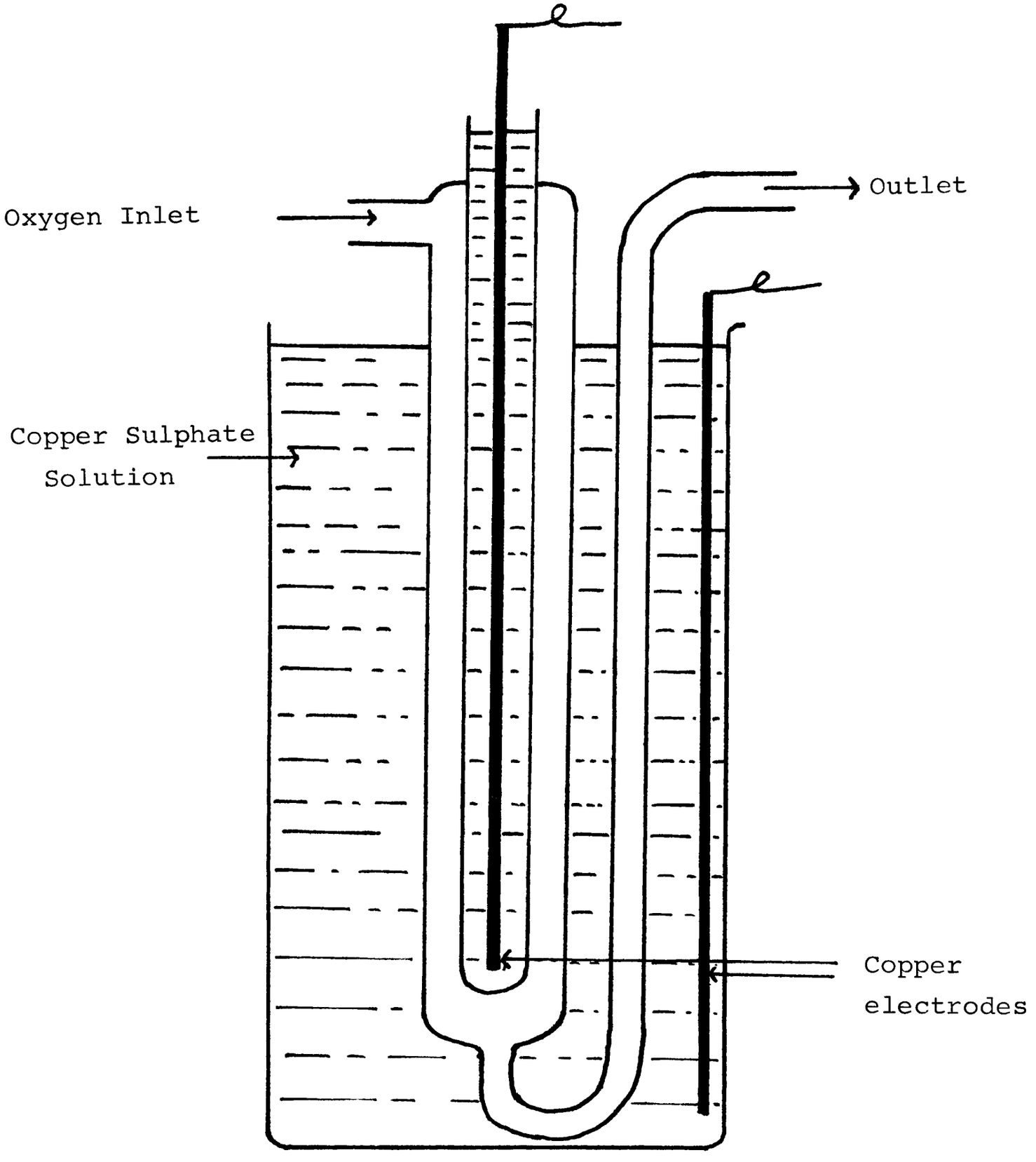


Figure 7. Siemens Ozoniser

and then allowing the liquid ozone to evaporate slowly into a gas storage system [22,57]. A serious drawback to this method is that liquid ozone is exceedingly dangerous and can detonate after thermal or mechanical shock or if exposed to traces of impurities. The method requires elaborate safety precautions [22,58].

A safer method was employed for all ozone purification which involved the separation of ozone from oxygen by adsorption of the ozone at low temperature on silica gel [59]. The capacity of the silica gel to take up ozone increases with decreasing temperature. When ozonised oxygen was passed through a trap packed with silica gel at -80°C (trichloroethylene-cardice slush) the ozone was adsorbed by the silica gel, giving a deep purple colouration when saturated. Occluded oxygen was then pumped off and the ozone desorbed into an evacuated storage bulb by allowing the trap to warm up. The complete system is shown in diagramatic form in figure 8. The B.O.C. cylinder oxygen was dried by passing through two P_2O_5 drying tubes, a trap packed with glass wool at -80°C, before and after the ozoniser, before entering the silica gel trap. The pump used to remove occluded ozonised oxygen was protected by a trap filled with activated charcoal. This glowed fiercely during pumping off, but prevented any ozone reaching the pump and thus harming it.

In the initial construction of this system difficulty

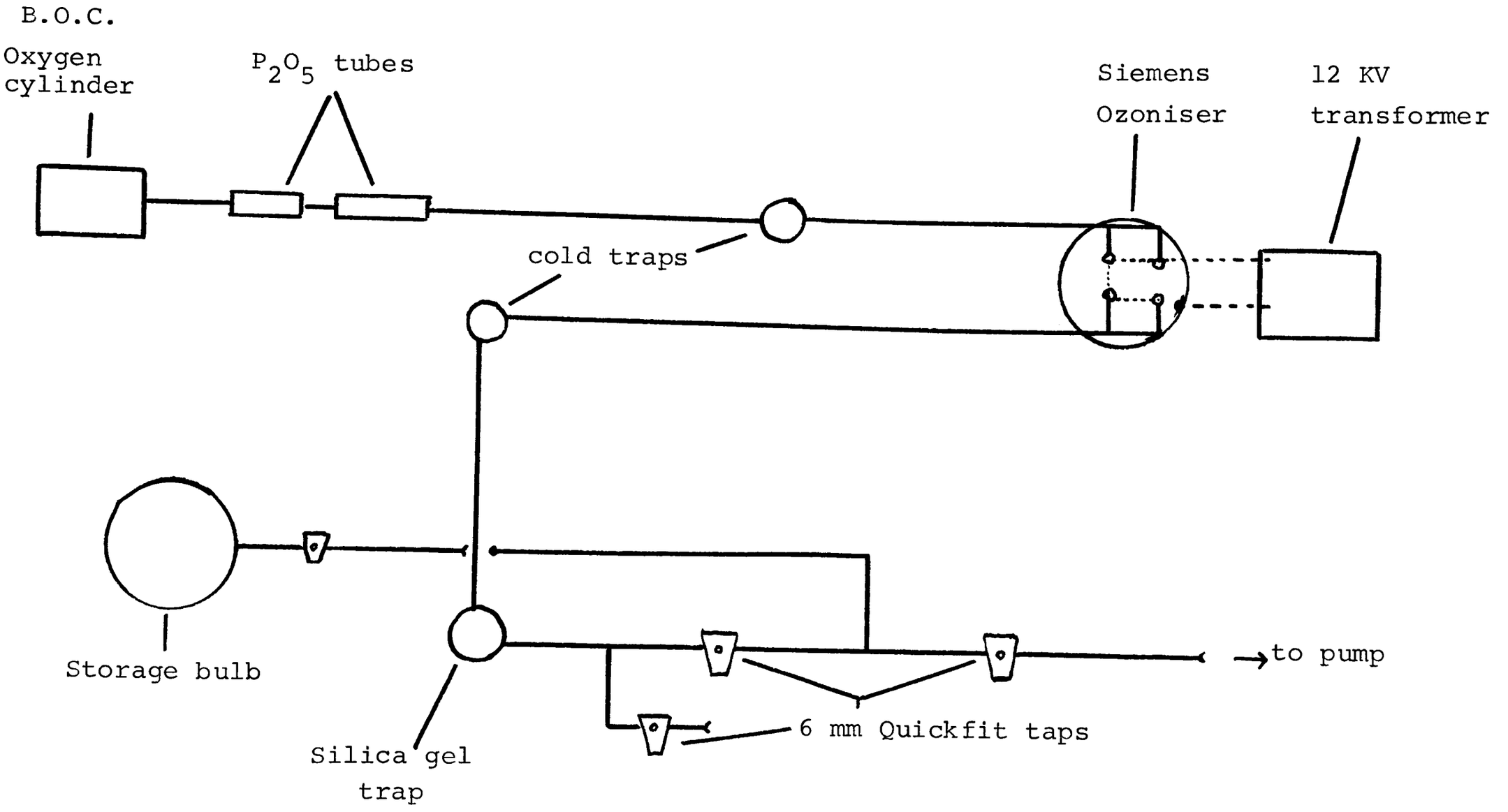


Figure 8. Layout of Ozone preparation apparatus

was encountered over the type of silica gel used [60]. The main problem was that the early gel decomposed the ozone during the desorption stages. This was due to trace inorganic impurities in the gel, supplied by Messrs. B.D.H. The silica gel finally adopted was Hopkins and Williams 6/22 mesh CO type. The only preparation necessary before use was drying by heating under vacuum and pumping off through a liquid nitrogen cold trap, or heating whilst passing an inert gas through the gel. After drying it was necessary to pass ozonised oxygen through the gel for three hours, before collecting, in order to "age" the gel.

The experiments carried out using ozone demanded the gas should be as pure as possible, the only acceptable impurity being oxygen. Wayne [83] found that the small nitrogen impurity (cf 0.1%) present in B.O.C. oxygen gave rise to the production of oxides of nitrogen in the silent discharge of the ozoniser, yielding nitrogen pentoxide as the most stable oxide. The presence of nitrogen oxides in ozone photolysis experiments is undesirable (see section 3.4). Attempts were made to produce nitrogen free oxygen from the electrolysis of dilute sodium hydroxide solution using platinum electrodes. An "H" design electrolysis cell was adopted and the oxygen produced at the anode was passed through silica gel to remove water, then paladised asbestos at 350^{o}C to remove any hydrogen, and finally

through a P_2O_5 tube before entering the ozoniser. However, this did not produce a fast enough flow of oxygen for the ozoniser to be effective. Attempts to increase the flow rate by increasing the D.C. current to the electrodes were hindered by the large heat dissipation of the cell. Even immersing the cell in a thermostated water bath did not solve the overheating problem. This method was not adopted for oxygen preparation, and in all ozone preparations B.O.C. oxygen was used.

In a typical run, five hours of ozonising yielded about 15 cms Hg in 5 liters of about 80% ozone in oxygen. In 24 hours the ozone decomposed about 10% when stored in the dark. This mode of preparation was found to be very safe during three years of constant operation by a number of operators. However, at the end of ozonising for a final set of experiments a spectacular explosion took place, leaving little of the ozoniser in recognisable form. Fortunately, no one was nearby and a large perspex shield in front of the apparatus prevented flying glass causing serious injury.

(b) Nitric Oxide.

Nitric oxide was prepared by the action of sulphuric acid on sodium nitrite solution in the presence of mercury. The impure gas, containing nitrogen dioxide, nitrogen

trioxide and water vapour, was introduced into a vacuum system containing two traps, each of which could be isolated. As much of the material as possible was condensed into the first trap at liquid nitrogen temperature, any gas remaining being pumped away. The material in the first trap was allowed to evaporate into the vacuum line and the nitric oxide (B.pt 112^{o}K) which evaporated first was condensed down into the second trap and isolated. The higher boiling point impurities which appeared as blue coloured solids were pumped away. The whole distillation was repeated three times until a white solid was obtained on condensing. From about an atmosphere of impure gas about 30 cms Hg in 2 liters of pure nitric oxide was obtained.

(c) Oxygen and nitrogen.

B.O.C. oxygen and oxygen-free nitrogen were obtained from cylinders. These were dried by passing through P_2O_5 tubes on the high pressure side of the flow apparatus and by cardice or liquid nitrogen traps on the low pressure side.

(d) Xenon and hydrogen.

These gases were supplied by B.O.C. as grade "X" spectroscopically pure. No purification was carried out.

2.2 Measurement of ozone purity.

The purity of the ozone prepared was obtained by

measuring the optical density (O.D.) at λ = 254 nm of a small known pressure of the sample in a 1 cm quartz cell using a Unicam S.P. 500 spectrophotometer. The total gas pressure was measured using a manometer containing di-butyl phthalate (specific gravity 1.04). The optical density is given by:

$$O.D. = \alpha.c.d$$

where d = cell path length

α = extinction coefficient of ozone at λ = 254 nm.

c = ozone concentration.

The value of α adopted was that of Vigroux [61], although it should be pointed out that Inn and Tanaka [62], Griggs [63] and Hearn [64] all have slightly differing values at λ = 254 nm. The value of α determined by Vigroux was 126 cm^{-1} to the base 10 at λ = 254 nm. The values of the other workers cited are higher, the highest being that of Inn and Tanaka, of α = 133 cm^{-1} (base 10). This method is thus open to an error, due to the inconsistency in the value of α, of about 5%. The percentage purity of ozone can thus be calculated, and was found to give reproducible results to within 3%. In addition, this method was quick and convenient to use.

2.3 Gold plating of bulb.

A number of experiments described in this work involved the detection of very weak optical emissions. It

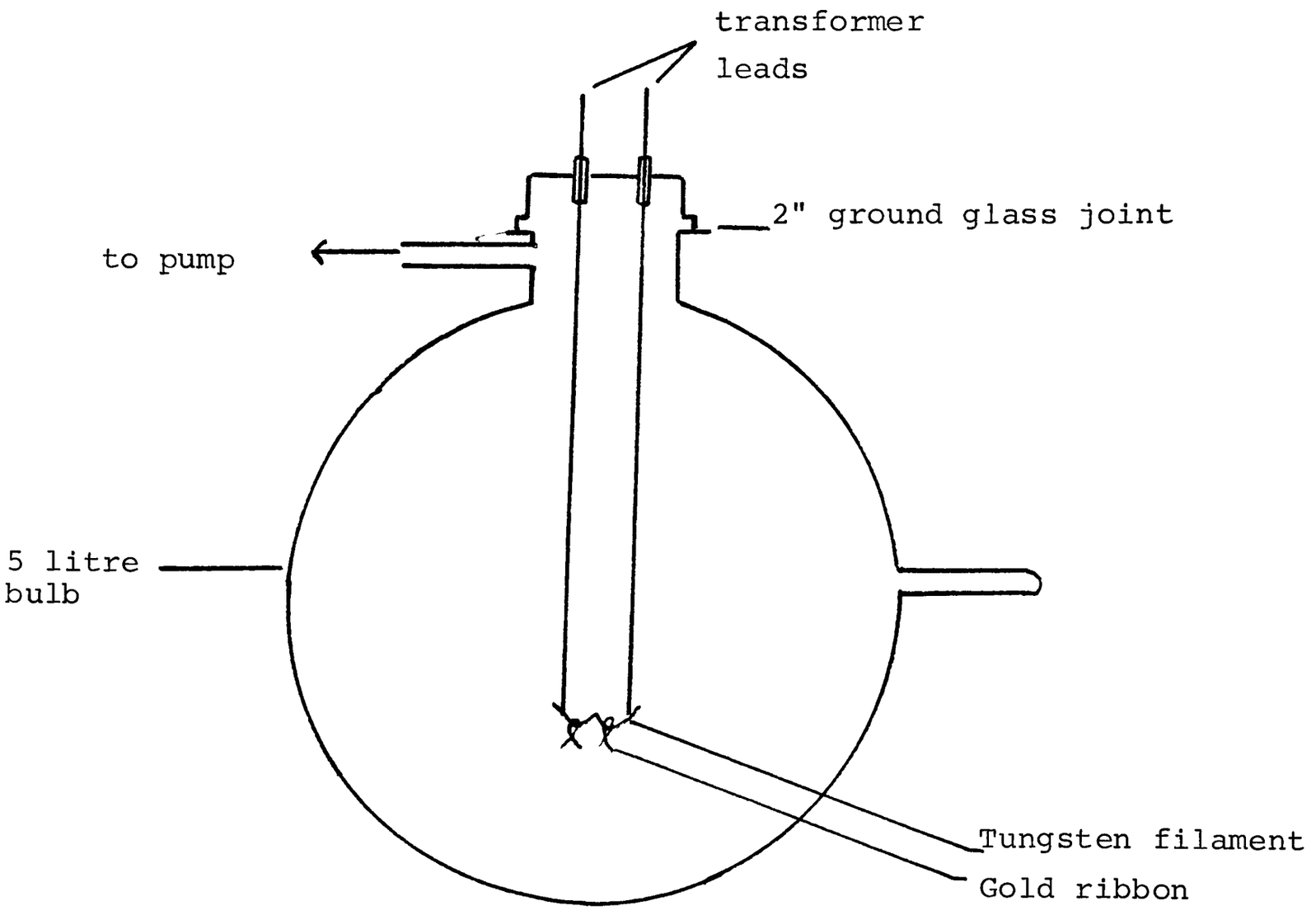


Figure 9. Apparatus for evaporation of gold

was necessary to have a large, highly reflective observation vessel to increase the likelihood of detecting these emissions. For this purpose, a gold plated surface was employed since gold has a high reflectivity in near infra-red region of the spectrum.

The observation vessel was a five liter bulb with a 2" ground glass opening. Before attempting to gold plate the bulb it was necessary to clean the internal surface thoroughly three times with hydrofluoric acid, wash with distilled water many times and dry in an oven.

Gold ribbon was wound around a tungsten filament. The filament was heated by means of an electric current to cause the gold to melt (melting point of gold 1063^{o}C) and evaporate. Difficulty was encountered in trying to wet the tungsten filament with the gold ribbon when the filament was heated, contrary to Caldwell [65]. However, platinum wire was found to be an effective intermediate. This wetted the tungsten filament when heated in an oxygen flame. The experimental set-up for the evaporation of the gold is shown in figure 9. The bulb was pumped down to about 10^{-3} to 10^{-4} torr for about three hours. The filament was then heated by means of a transformer until the gold formed globules on the filament and a metallic layer formed on the inside of the bulb. This procedure was repeated three times and the surface left

to harden for several days. The result was a thick, highly reflective, durable metallic surface.

2.4 Preparation of photolysis lamps.

For studying the photolysis of oxygen (Chapter 4) and ozone (Chapter 3) it was necessary to use lamps that had considerable output in the ultra violet region. A review of photolytic lamps has been given by Wayne [66].

(a) Xenon resonance lamp.

For the oxygen photolysis experiments light of $\lambda < 175$ nm was required. A low pressure xenon lamp was employed, this giving a main resonance line at 147 nm [67] which is near the oxygen absorption maximum, see figure 4. The design of the lamp is shown in figure 10 and is essentially the same as that of Okabe [68]. The lamp was constructed from pyrex except for the transmission window. Pure, cleaved lithium fluoride supplied by Messrs. Hilger and Watts was used. This transmitted above $\lambda = 104$ nm [69]. The lithium fluoride was piceined to the lamp. The lamp was pumped at 10^{-4} to 10^{-5} torr for five hours and then filled to about 0.2 torr with grade "X" Xenon. Getterising was not considered necessary as the lengthy pumping yielded a lamp which gave a fairly pure spectrum, figure 11. The spectrum was obtained using a vacuum ultra violet grating spectrometer with Ilford HP 140 plates. Exposure time was three minutes. The prints were kindly

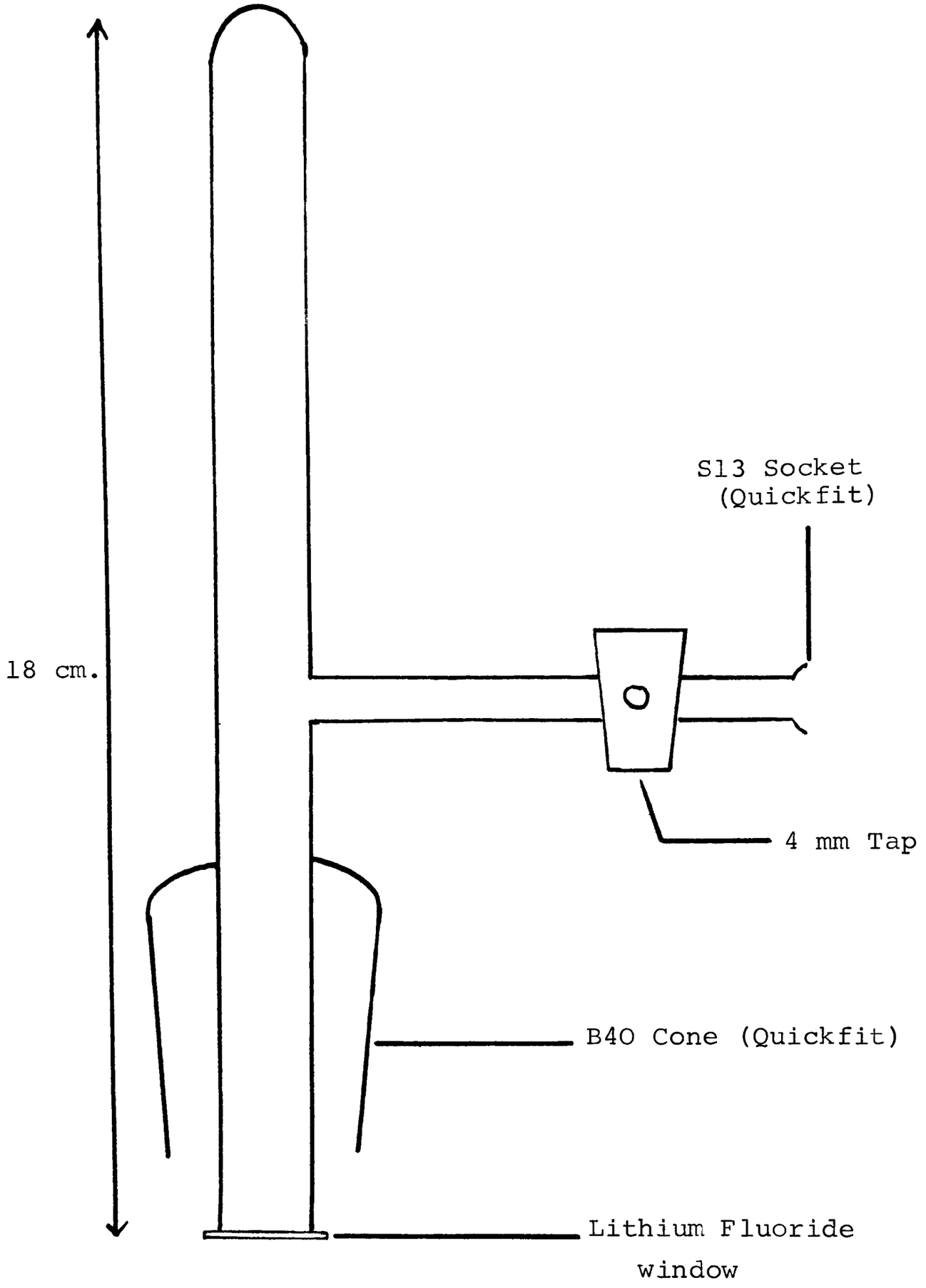


Figure 10. Design of Xenon Resonance Lamp

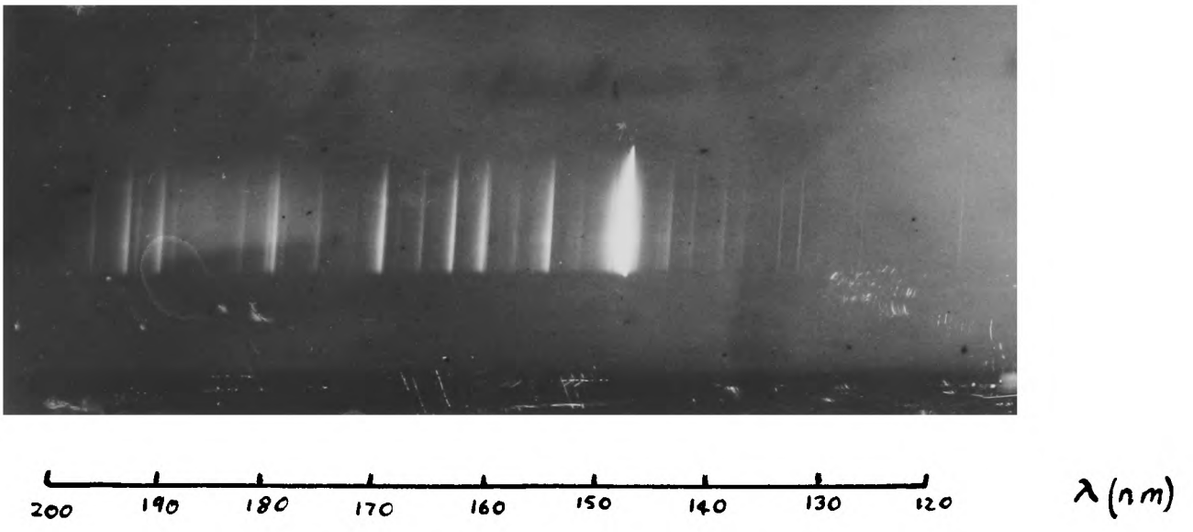


Figure 11. Spectrum of Xenon lamp

prepared by Mr. A. Simpkins. The lamp was operated by a "Microtron 200" microwave supply with variable power between 0 and 200 watts. The transmission of the lithium fluoride deteriorates fairly rapidly near its cut-off level [69], but at 147 nm it was found that the window retained its transmission throughout all experiments. The magnitude of the power produced by the lamp is discussed later in Chapter 4.

(b) Mercury resonance lamp.

For the ultra violet photolysis of ozone experiments low pressure mercury resonance lamps were employed. These give a high output at 253.7 nm, although there are contributions from other lines [70]. In the initial experiments, Chapter 3, "U" shaped Hanovia mercury lamps were used. However, for subsequent experiments a quartz spiral lamp which facilitated moving it up and down the irradiation flow-tube, was constructed.

To fill the lamp, a drop of clean mercury was introduced into the spiral and then evacuated for 15 minutes. 1 cm Hg of Neon was introduced and the lamp cleansed by passing an electric discharge through for 10 minutes. The lamp was then evacuated and refilled with 1 cm Hg pressure of grade "X" neon. The lamp was operated from a 6000 volt stray field transformer (neon sign) controlled by a Variac.

2.5 Flow and storage apparatus.

The flow system comprised essentially of a reaction area and an observation area through which the gases under consideration were pumped by a large mechanical pump (Edwards type E.S. 250). The pump had a large ballast, to stabilise pressure and flow patterns, past the main flow line tap. The pump was connected to the flow line by a reinforced nylon P.V.C. tube, supplied by Messrs. Griflex. The flow line was constructed from pyrex except for the reaction area which was quartz to allow transmission of the ultra violet radiation. The apparatus could be dismantled and altered fairly easily by means of Quickfit connectors. The design of the flow system for each experiment is discussed in the relevant chapter.

The pressure in the flow line was measured down-stream of the observation area by means of a silicone oil manometer. Ozone was found to cause a skin on the surface of the oil after long exposure, thus making readings difficult. Di-butyl phthalate was later used as a manometer fluid. This fluid was unattacked by ozone.

Reactant gases were introduced into the main flow system from storage bulbs via needle valves (type LB1A) and inlet jets. The needle valves have ¼" brass unions which were sealed to closely fitting glass tubing with a

small quantity of Araldite. The jets faced upstream to ensure rapid mixing.

Nitric oxide was stored in a 2.5 litre bulb. Because nitric oxide attacks mercury a spiral gauge was used to measure the pressure in the bulb. The gauge was calibrated against a mercury manometer and 1 cm Hg pressure corresponded to 1.7 cms of scale deflection on the spiral gauge.

Ozone was stored in a heavily protected 5 litre bulb. A spiral gauge was also employed to measure the ozone pressure and it was found that 1 cm Hg pressure corresponded to 2.8 cms scale deflection on the spiral gauge.

Oxygen, oxy-free nitrogen and argon were stored in cylinders and could be introduced directly into the flow line. The high pressure side of the needle valve was measured with mercury manometers.

All taps were greased with Edwards Apiezon M vacuum grease, except those in contact with ozone. Ozone attacked Apiezon M rapidly. Edwards silicon grease was initially used for the ozone line taps but even this, on lengthy exposure to ozone, formed a polymer and resulted in the taps leaking. A fluoro-carbon grease, KLF 90, was finally employed and was found not to be attacked by ozone.

The volume of each section of the storage apparatus was obtained by observing the pressure change when a standard known volume, containing a known pressure of dry

gas, was introduced into the evacuated section under consideration.

The flow rate of the gas through the flow system was measured by means of capillary flow meters. These use the principle of measuring the pressure drop along a capillary tube. The type used were similar to those described by Gowenlock and Melville [71]. The main advantage in design of this type being the ease of removal and replacement of the capillary. The capillaries were sealed on B10 joints (Quickfit) with picein wax. The flow meter fluid was di-butyl phthalate.

The rate $^{dv}/_{dt}$ of laminar flow of a gas having a viscosity z through a narrow tube of radius r and length l under a driving pressure Δp is given by Poiseuille's equation:

$$\frac{dv}{dt} = \frac{\pi \Delta p r^4}{8zl} \qquad 2.A$$

If the pressure drop Δp (cm oil) is much less than the total pressure P (cm Hg), the molar flow rate F is given by:

$$\frac{dM}{dt} = F = \frac{P\pi \Delta p r^4}{8RTlz} \qquad 2.B$$

$$= K.P.\Delta P. \qquad 2.C$$

where K is a constant appropriate to the units of F, P and ΔP. In our experiments K was expressed in mole sec^{-1} $(cm\ Hg)^{-1}(cm\ oil)^{-1}$.

No attempt was made to calibrate the flow meter by the use of Poiseuille's law, since constancy in the internal diameter of the capillary tubing is not guaranteed by the manufacturers and also most of the capillaries had been pulled down in an oxygen flame. Instead, gas of a known initial pressure was pumped through the flow meter from a vessel of known volume and the rate of pressure drop for a given flow meter reading was measured. A graph of pressure against time was used to obtain the rate of pressure drop $\frac{dP}{dt}$ (cm Hg sec^{-1}). The constant K at $T^{o}K$ is given by the equation:

$$K = \frac{(\text{volume of reservoir}) \times 273}{P \times \Delta P \times T \times 22400} \times \frac{dP}{76\ dt} \text{ mole } sec^{-1} (\text{cm Hg})^{-1} (\text{cm oil}) \qquad 2.D$$

The capillaries accurately obey Poiseuille's law [72] in that the pressure drop varies as the reciprocal of the viscosity. Each capillary was calibrated with the gas for which it was going to be used as a flow meter. This avoided correcting for the viscosity, which in the case of ozone is not well established.

The flow velocity V $cm.sec^{-1}$ in the flow tube was calculated, assuming plug flow, from the equation:

$$V = \frac{1}{a} \frac{F}{c} \qquad 2.E$$

where a = cross sectional area of the tube

c = concentration

F = flow rate.

2.6 Optical components.

(a) Filters.

Narrow band interference filters were used to isolate specific spectral regions of interest. The filter for isolating the atmospheric band of oxygen was supplied by Jena^{er} Glaswerk Schott and Gen, having a peak transmission of 45% at 762.9 nm. The filter was 2" square. For isolating the infra-red atmospheric band a filter supplied by Barr and Stroud was employed, having a peak transmission of 55% at 1268.0 nm. This filter, 2" in diameter, consisted of three sections, the main 1268.0 nm filter and a long and short wavelength suppressor. Other filters used for experiments had maximum transmission at 634.3 nm (Jena^{er} Glaswerk, Schott and Gen), 590 nm, 701 nm, 801 nm and 870 nm (Grubb Parsons). The transmission of each filter was checked from 300 nm to 2500 nm on a Carey 14 spectrophotometer to ensure that no sidebands or defects were present. Apart from the main band no spurious transmissions were observed. The transmission curves are shown in figure 12. In addition to the narrow band filters an OB2 + Wratten 45 filter combination was employed (see Chapter 4), and the transmission is shown in figure 12.

(b) Monochromator.

In later experiments, a Bausch and Lomb model 33-86-03 grating monochromator was used. The grating possessed 654

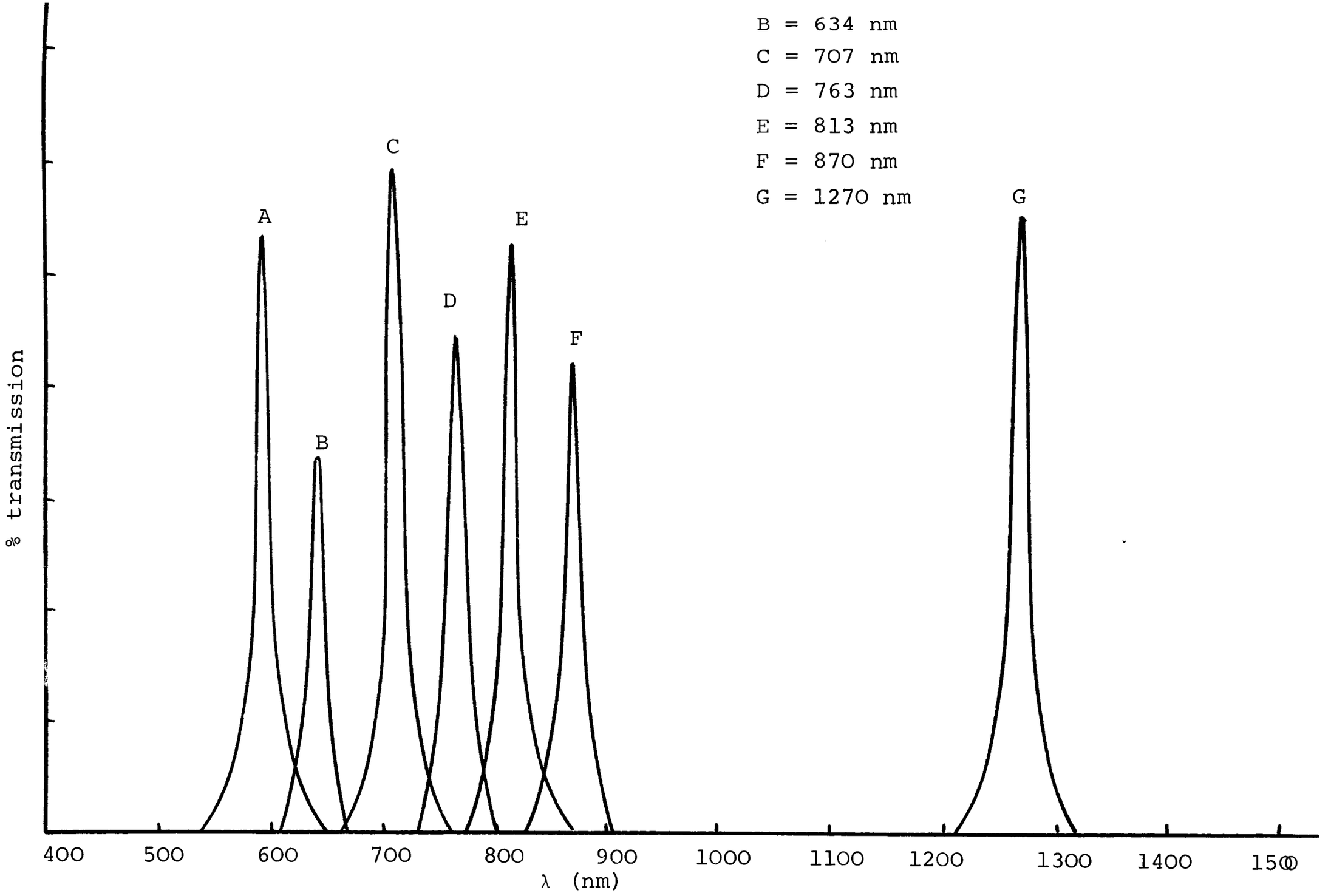


Figure 12. Transmission of interference filters between λ = 400 nm and λ = 1500 nm

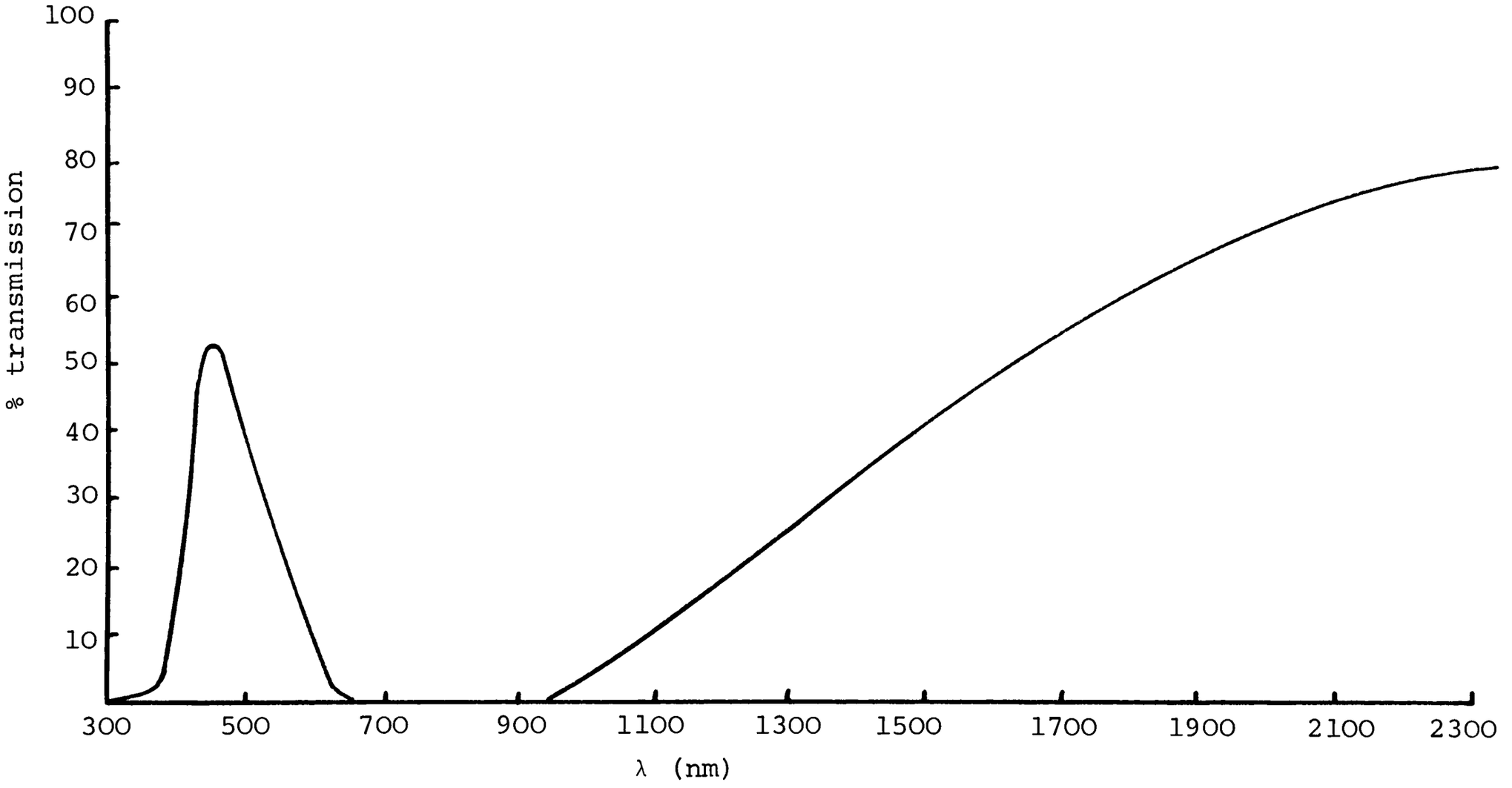


Figure 13. Spectral transmission of OB2 + Wratten 45 filter

lines mm^{-1} and a dispersion of 12$ nm.mm^{-1}. The spectral region covered was 700 nm to 1600 nm in the first order. The optical system was of the non-collimated type providing a nearly monochromatic diverging exit beam of f/3.5. The monochromator was compact, ideal for use with the flowline as the exit and entrance slits were situated at either end of the device. It was found necessary to scan slowly through a wide region of the spectrum and for this purpose an electrical motor with gear box was fitted to the grating spindle. This enabled the grating to be turned at a number of desired speeds.

(c) Detectors.

The excited singlet oxygen molecules under discussion emit at the following wavelengths:

$^1\Sigma g^+ \leftrightarrow {}^3\Sigma g^-$ (0,0) λ = 762.0 nm atmospheric band

$^1\Delta g \leftrightarrow {}^3\Sigma g^-$ (0,0) λ = 1268 nm infra-red atmospheric band.

To observe these optical transitions a number of detectors were tried and tested and are discussed below. The electronic aspect of the detection system is dealt with in section 2.7.

The atmospheric band lies in a fairly accessible spectral region for the S20 tri alkali (SbNa.K.Cs.) cathode. The EMI 9558 Q and A type photomultiplier with end on viewing window was used in all experiments involving the detection of $O_2(^1\Sigma g^+)$. The classification Q for this

photomultiplier denotes a quartz end window, whereas A indicates pyrex. In addition to this type of cathode for $O_2(^1\Sigma g^+)$ detection the 9558Q was used to detect the mercury resonance line at λ = 253.7 nm during some cross beam absorption experiments (see sections 2.8 and 2.7). The spectral distribution of the S20 cathode is shown in figure 14. The photomultiplier was housed in a brass cylinder and was operated at room temperature up to 1500 volts D.C. from a Brandenburg Model 470 regulated power supply.

The $O_2(^1\Delta g)$ optical transition lies in a more difficult spectral region. The S1 (Ag O Cs) cathode detects into the near infra-red as shown in figure 14. At 1270 nm the response is very small, in fact it is on the spectral threshold of this type of cathode [73]. It was found that the R.C.A. 7102 photomultiplier (S1 cathode) operated at -80°C gave a reasonable response at 1270 nm. However, an EMI 9684B photomultiplier with a similar cathode gave virtually no response. One concludes from this that the response of an S1 type cathode near its threshold varies greatly on the individual photomultiplier. The R.C.A. 7102 was housed in a metal case such that cardice could be packed around the tube to keep it cool and hence minimise noise. The photomultiplier was always employed with the whole end window of the tube (area 5.3 cm^2) exposed to the filtered radiating source under consideration,

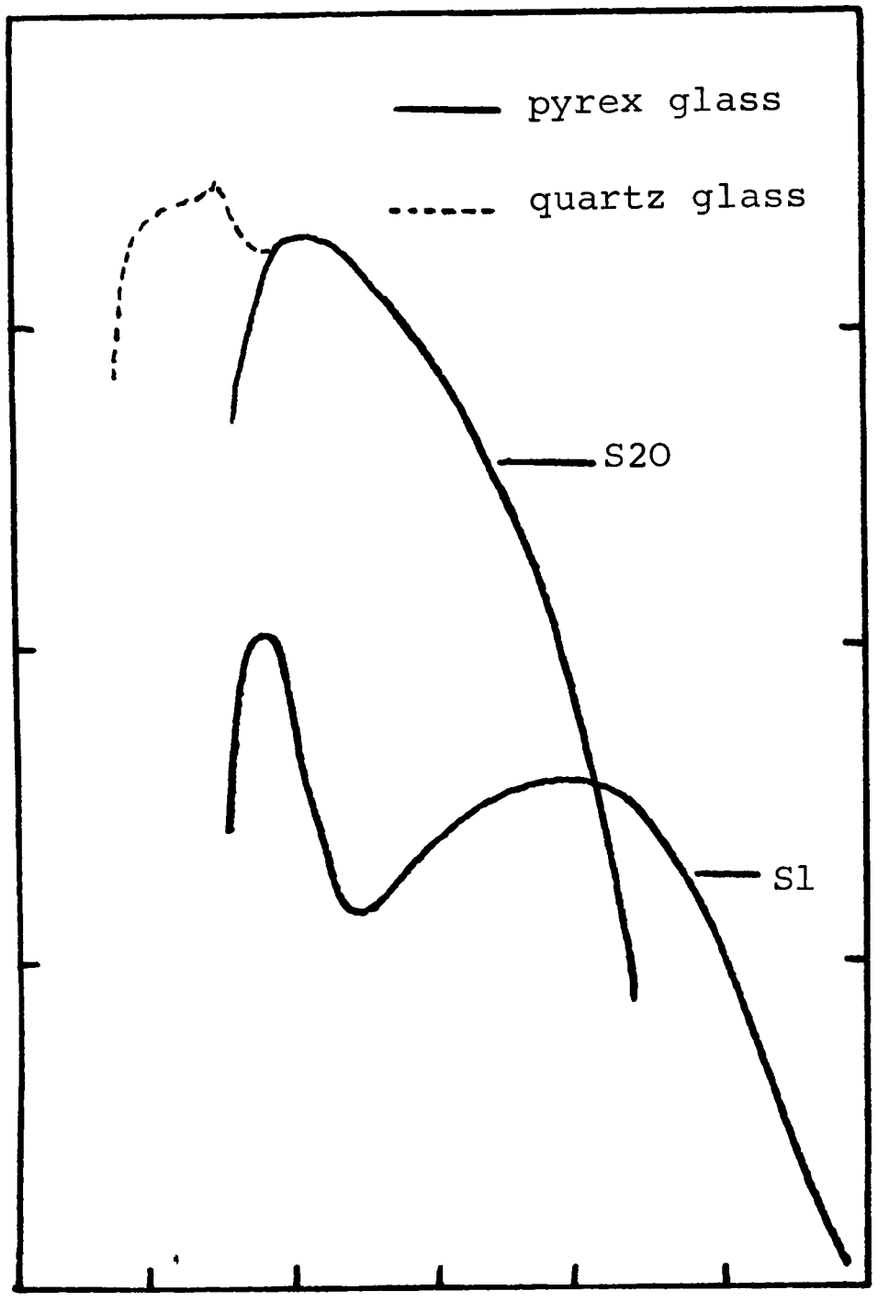


Figure 14. Spectral response of S1 and S20 cathode

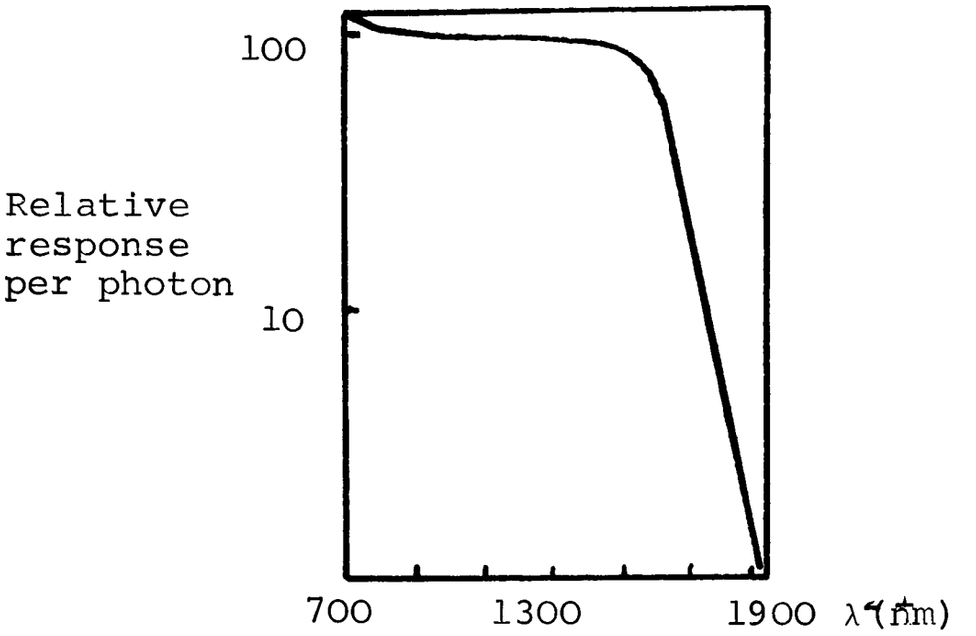


Figure 16. Spectral response of germanium crystal

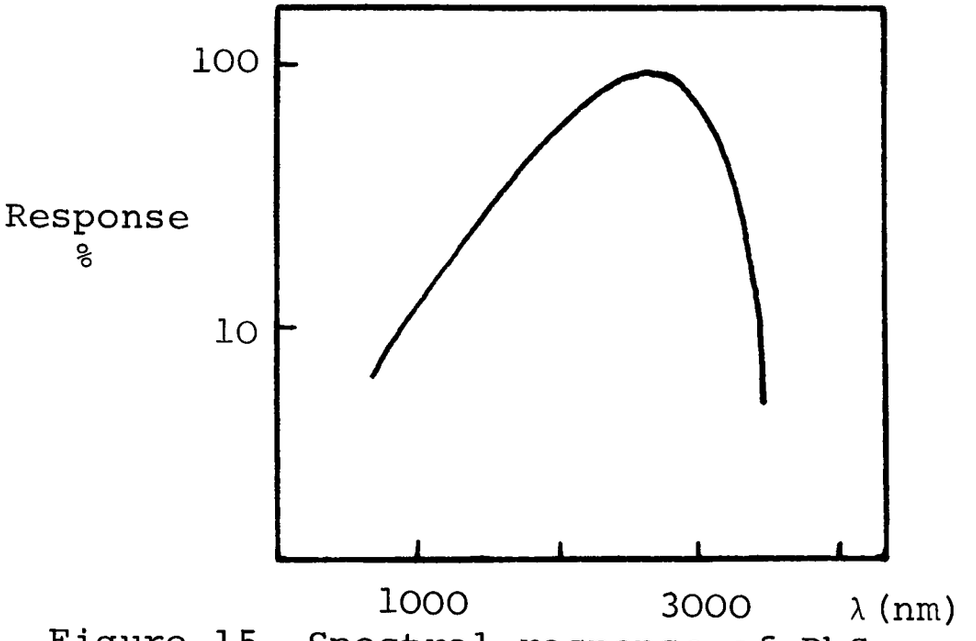


Figure 15. Spectral response of PbS cell

to collect as much light as possible. Any attempts to collimate the photomultiplier severely reduced its response at 1270 nm. The R.C.A. 7102 was energised up to 1500 volts D.C. using a Brandenburg regulated power supply.

Another type of detector often used for $O_2(^1\Delta g)$ observation [34] is the lead sulphide cell. The spectral response is shown in figure 15. A Mullard 615 V cell was tested, being operated at room temperature and energised by a 100 volt H.T. battery. The sensitive area of the cell was .68 cm^2 but it was found to be much less sensitive than the 7102 photomultiplier and was not used in any experiments.

The final detector used was a germanium photo conductor. This comprised of a small crystal of ultra-pure germanium with two electrodes soldered on using indium as an intermediate. The total surface area of the crystal was only 8 mm^2. The spectral distribution for an irradiated thin crystal of ultra-pure germanium is shown in figure 16. A review of the capabilities of this type of detector is given by Moss [74]. In the region 900 nm to 1300 nm the response is flat and it has been established by various workers that the quantum efficiency is unity in this region. The band gap for germanium is .62 eV at 300°K, the transition being indirect [75]. The photo current

density is determined by the total excess carrier concentrations and their mobilities. For a thin sample, the increase in hole concentration Δp, is related to the photon intensity I, and carrier lifetime τ by:

$$\Delta p = I\tau \qquad 2.F$$

The detector was operated at liquid nitrogen temperature to reduce noise. Initially, icing up of the container window was a problem. This was overcome by inserting the detector in a dewar type arrangement. The apparatus is shown in figure 17. The silica gel removed any water in the inner tube. The germanium detector was operated from a grid bias battery between 6 and 9 volts. It was found that the detector gave an excellent response at 1270 nm and, because of its small surface area, could be used in conjunction with the Bausch and Lomb monochromator.

The response of each detector to various incident intensities, in order to check for linearity, was required. An air afterglow was produced in the flow tube (see next section for details), and the magnitude of the glow (I) was varied by changing the nitric oxide concentration, keeping [0] constant:

$$NO + O \rightarrow NO_2 + h\nu \qquad 2.1$$

$$I = k_1[NO][O] \qquad 2.G$$

$$I \alpha [NO] \qquad 2.H$$

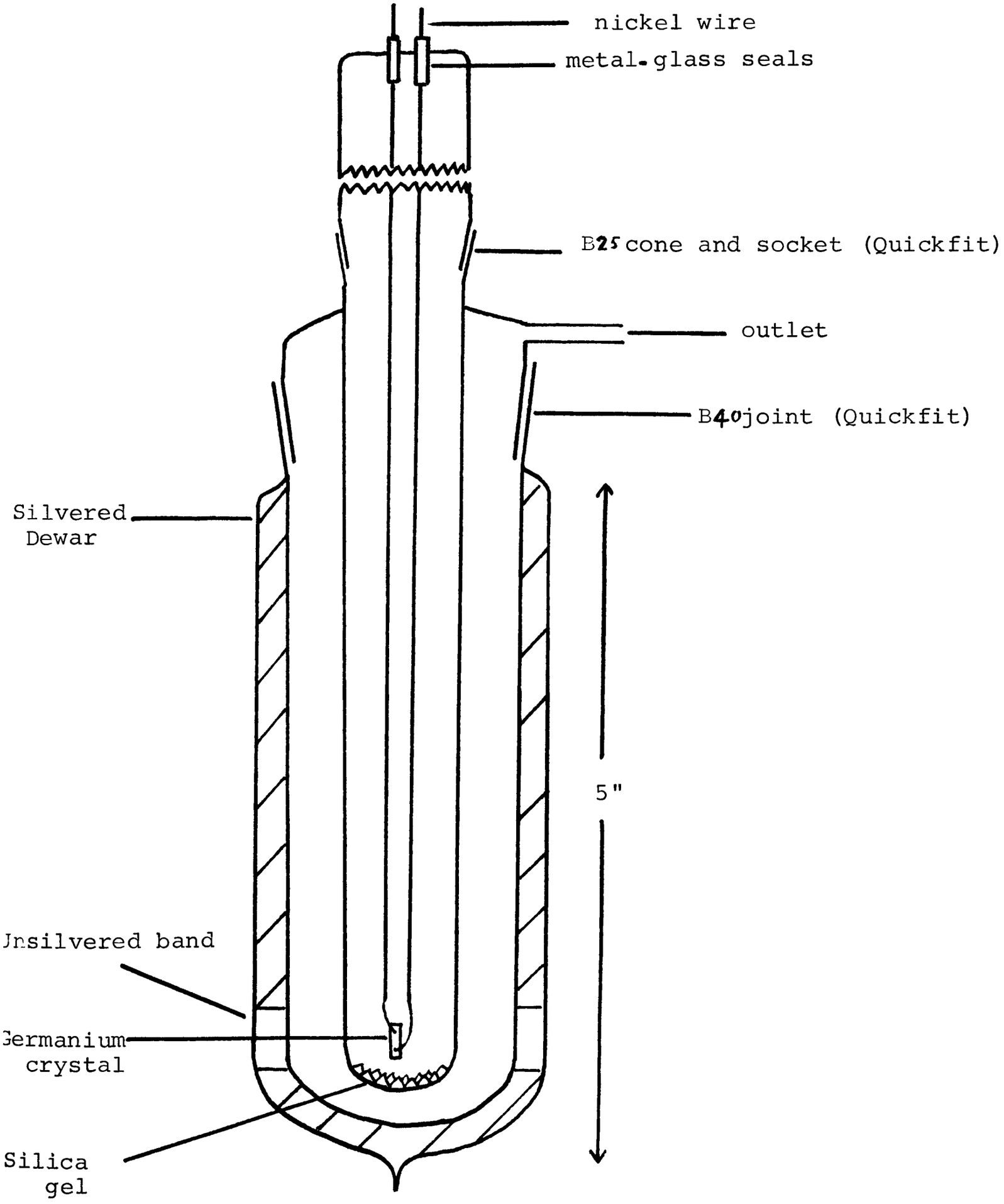


Figure 17. Germanium Detector and Dewar

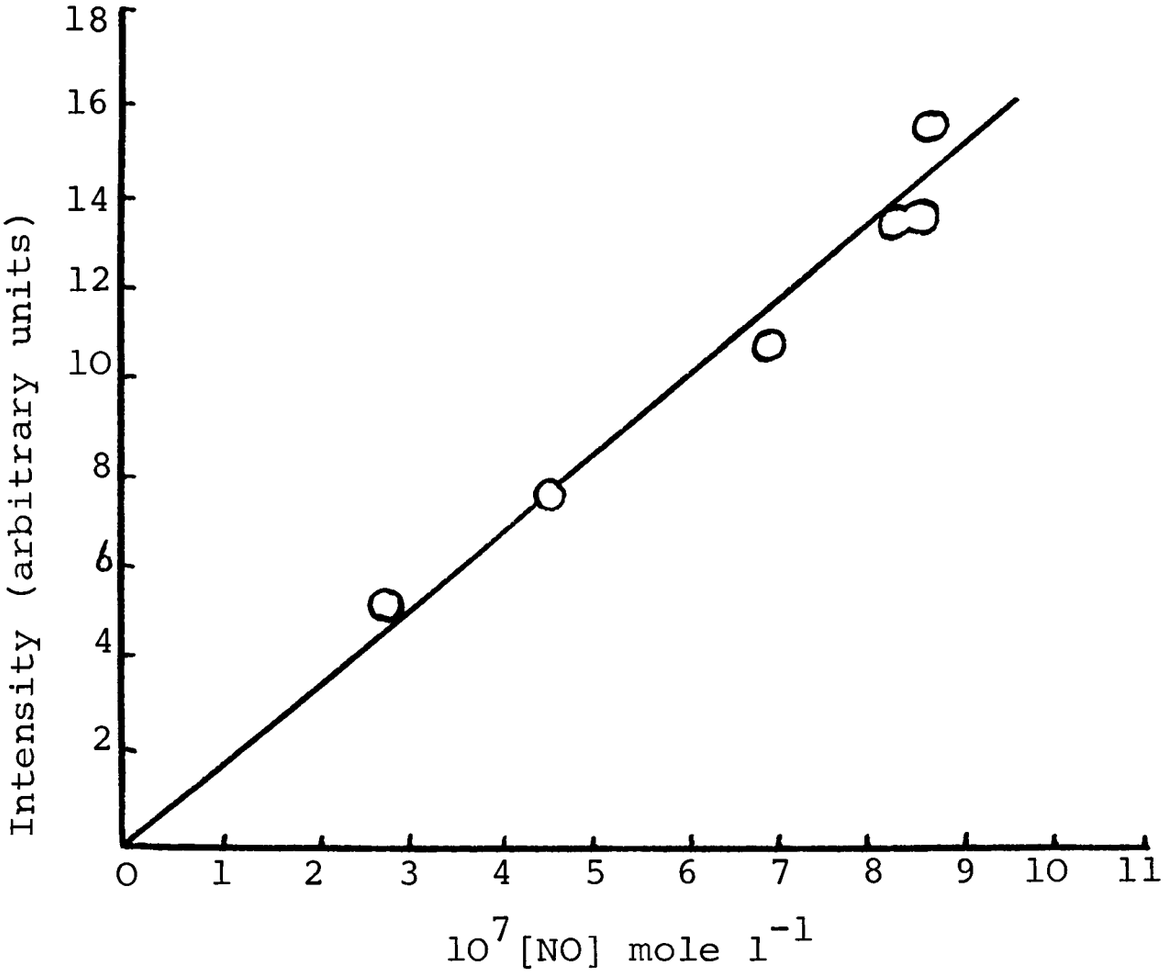


Figure 18. Linearity response of 9558A photomultiplier at 7632 nm (E.H.T. = 800 volts)

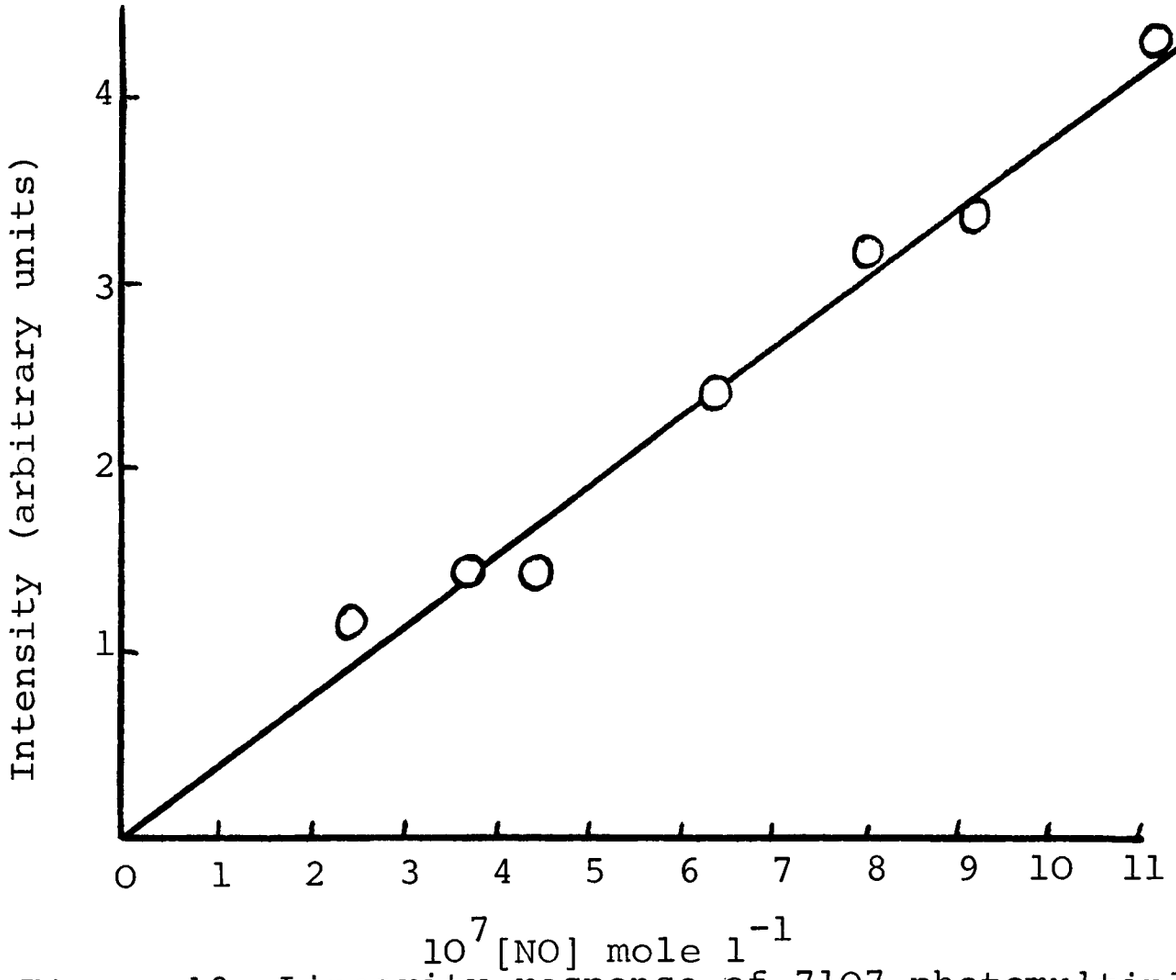


Figure 19. Linearity response of 7107 photomultiplier at 1270 nm (E.H.T. = 1000 volts)

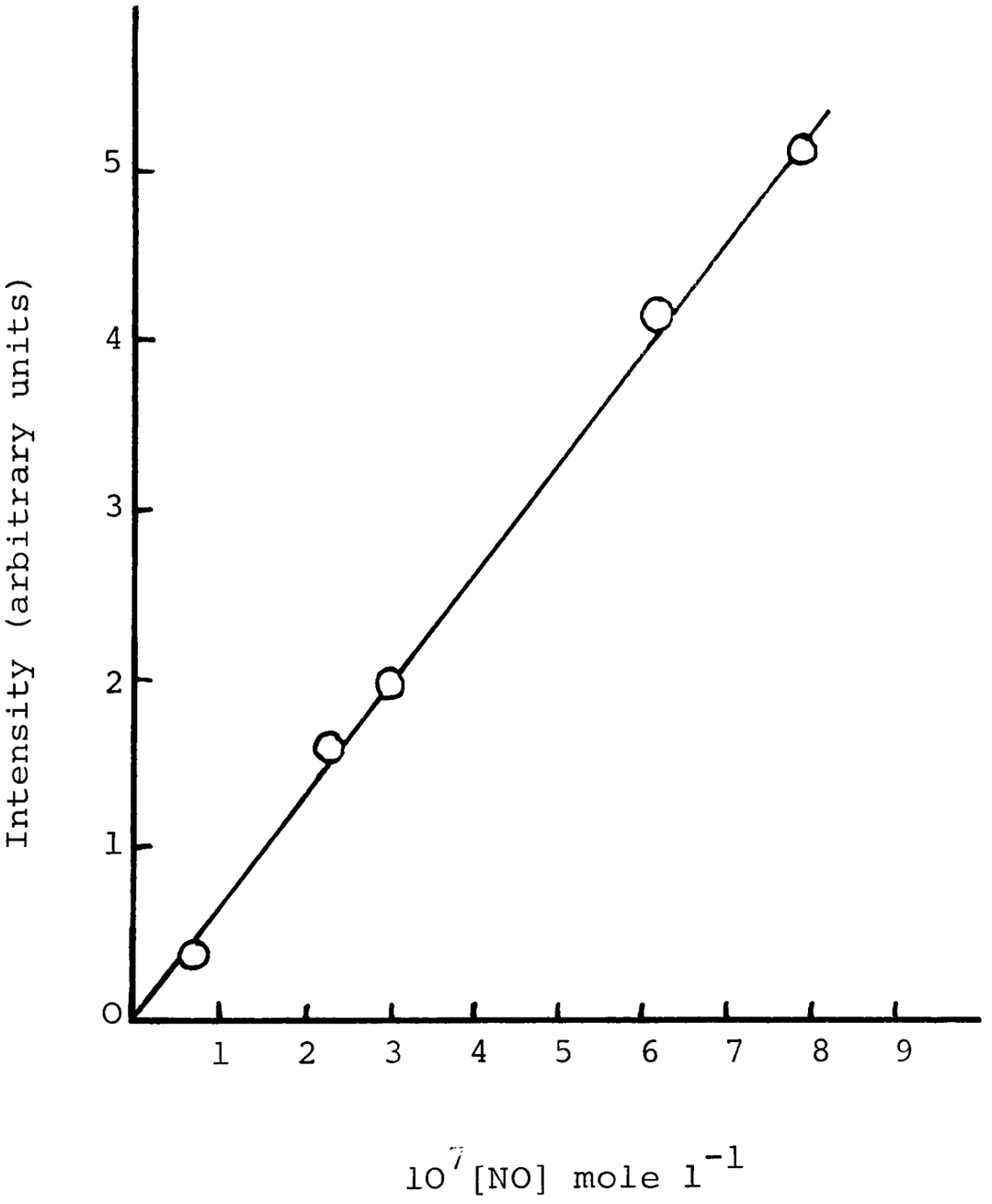


Figure 20. Linearity of response of germanium detector at 1270 nm

The response of each detector was observed with and without filters to ensure that there was no erratic behaviour at important wavelengths.

The EMI 9558Q and A photomultipliers were found to respond linearly in the first order when exposed to the air afterglow and also when viewed through the 763 nm interference filter, figure 18. The R.C.A. 7102 tube was also linear in the first order at 1270 nm, figure 19. This last observation was important since numerous workers have suggested that the S1 cathode was non-linear in response at its wavelength threshold. The germanium detector was found to have a linear first order response over a number of wavelengths, figure 20. In this instance, the monochromator was used to isolate different spectral regions.

In addition to the nature of response, the sensitivity versus applied voltage to the detector was checked. This was achieved by producing a constant air afterglow and then placing gauzes, of known transmission, between the detector and source. The increase in E.H.T. to obtain the previous signal was recorded. Figures 21 and 22 show the sensitivity versus applied voltage for the 9558A and 7102 photomultipliers respectively. These curves are essentially in agreement with the manufacturer's data. In the case of the germanium detector the variation

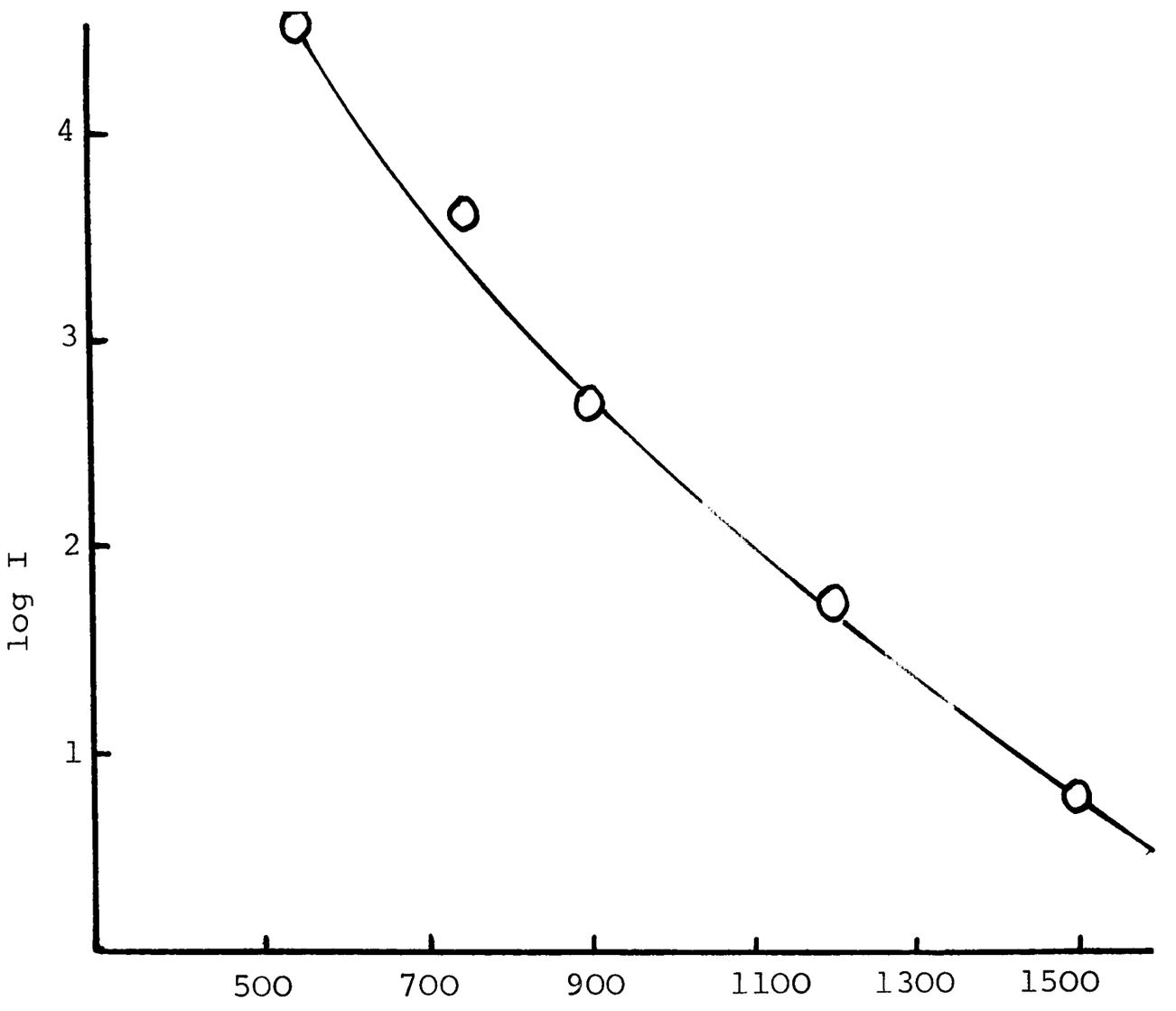


Figure 21. Sensitivity of 9558A photomultiplier

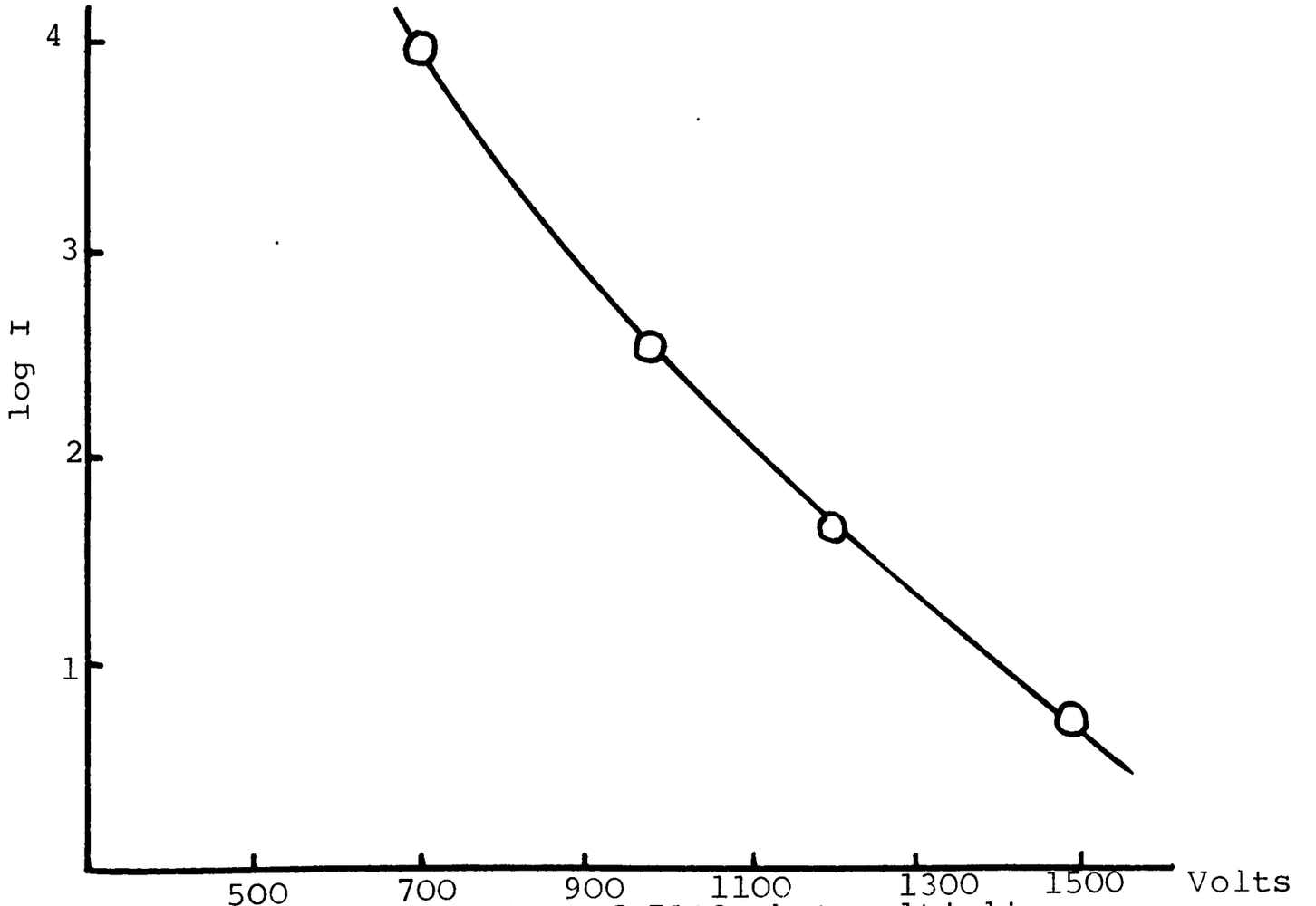


Figure 22. Sensitivity of 7102 photomultiplier.

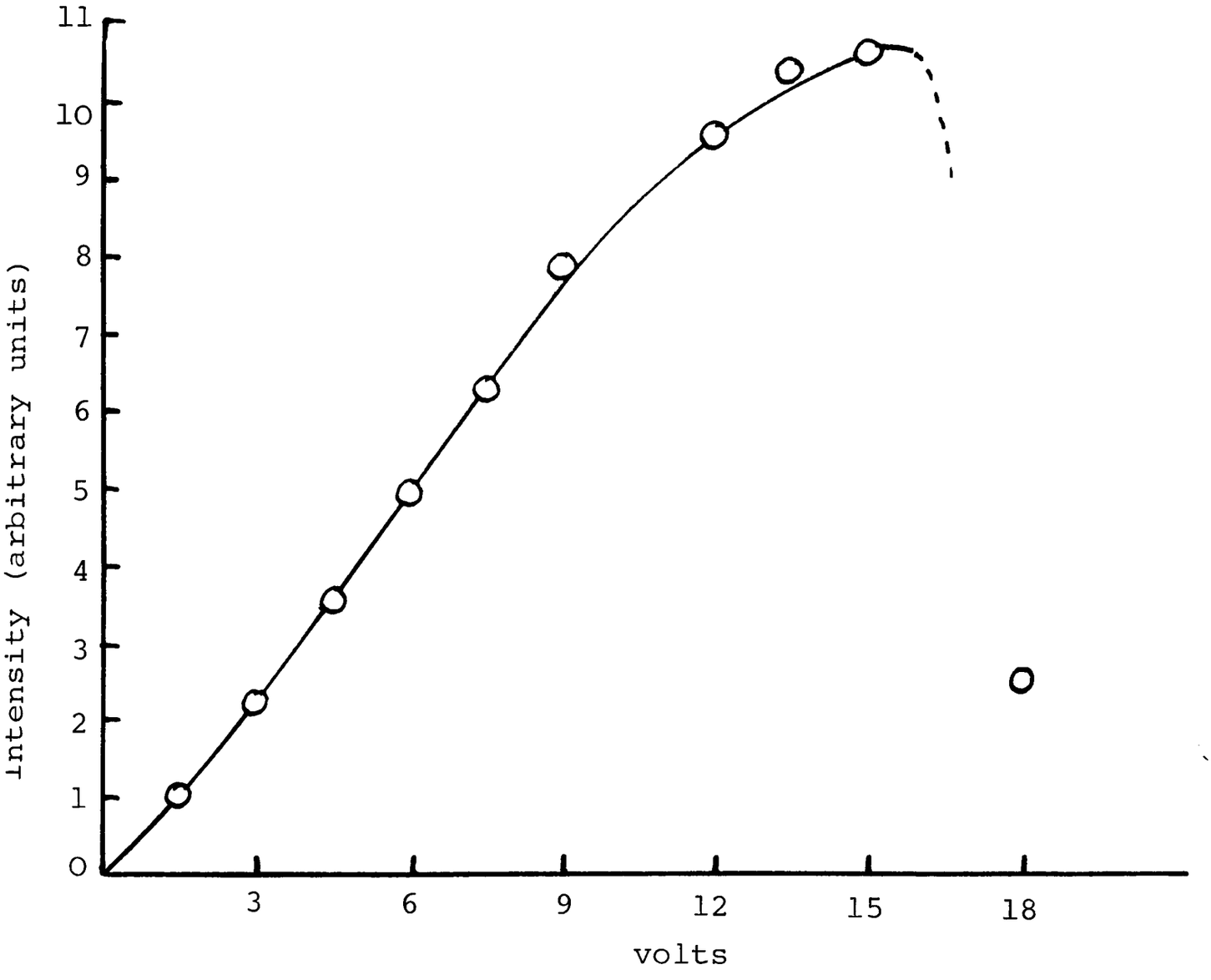


Figure 23. Variation of signal with applied voltage for germanium detector

in signal with change in the applied voltage for a constant airglow source was observed. Figure 23 shows this relationship. At high values of applied voltage there was an abrupt drop in sensitivity. It was found that operation between about 6 and 9 volts provided the most stable signal.

Calibration of detectors.

Calibration of each detector was necessary if absolute concentrations of $O_2(^1\sum g^+)$ and $O_2(^1\Delta g)$ were to be calculated. One way would be to calibrate the detector against a standard black body. However, this would involve accurate determination of the geometry and reflection characteristics of the apparatus. As the flow system was being frequently changed another calibration technique was adopted. The detectors were calibrated against the air afterglow. The glow was obtained by titrating nitrogen atoms, produced from a microwave discharge in molecular nitrogen, with nitric oxide. A null point was reached [76] when all nitrogen atoms were consumed by nitrix oxide, and the nitric oxide concentration was a measure of the oxygen atoms produced in the reaction:

$$N + NO \rightarrow N_2 + O(^3P) \qquad 2.2$$

About 1-5% nitrogen atoms were produced in the discharge. Addition of more nitric oxide develops the air afterglow:

$$NO + O(^3P) \rightarrow NO_2 + h\nu \qquad 2.1$$

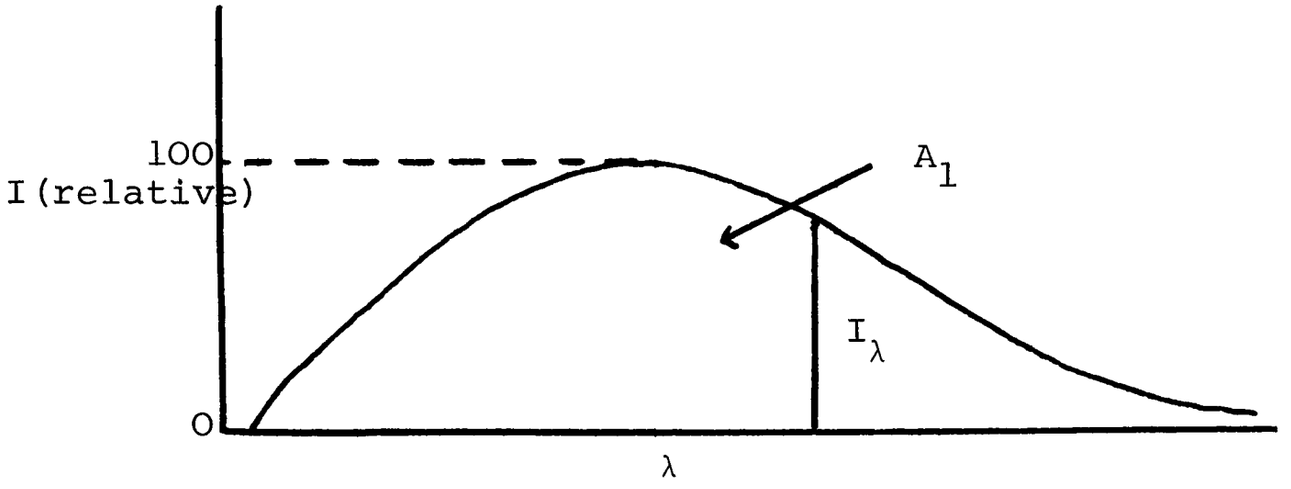
This method of producing the air afterglow was favoured to the oxygen discharge method of generating oxygen atoms and titrating with nitrogen dioxide [77]. The disadvantage being that the discharge products contain $O_2(^1\Sigma g^+)$ and $O_2(^1\Delta g)$ and thus corrections would be necessary when calibrating at these specific wavelengths.

The absolute quantum yields and spectral distribution of the air afterglow in the wavelength region 400 nm to 1400 nm were determined by Fontijn, Meyer and Schiff [78], and all values were taken from this work. Fontijn and Ellisón [79] have pointed out that care must be exercised when using NO + O afterglow intensities for atom concentration measurements in the presence of a third reactant.. However, in the present case nitrogen is unlikely to cause any problems.

In our calibrations the total pressure was about .5 torr which was above the lower limit suggested by Fontijn et al [78]. The low pressure values for the NO + O glow have been obtained by Jonathon and Petty [80]. The absolute concentration of either $O_2(^1\Sigma g^+)$ or $O_2(^1\Delta g)$ was calculated by comparing the recorded intensity, through the 763 nm or 1270 nm filters, of the air afterglow with that of a single excited oxygen band.

Consider the spectral distribution of the NO + O glow

normalised at maximum intensity by Fontijn et al [78].



The total light emitted (I_t) = $k_1[NO][O]$ quanta cc^{-1} sec^{-1}. This is distributed as shown in the diagram of area A_1. Let I_λ be the relative intensity at wavelength λ and assume that this is constant over the whole region of filter transmission. Not all the light reaches the photomultiplier and allowance is made for the filter transmission. Let the area of the filter curve be A_2. This area is scaled down by the fraction $\frac{I_\lambda}{100}$ in order to represent both filter and NO + O intensity data. Thus the integrated light (I_f) passing through the filter onto the photomultiplier tube is:

$$I_f = \frac{I_\lambda}{100} \cdot \frac{A_2}{A_1} \cdot I_t \text{ quanta } cc^{-1} \text{ } sec^{-1} \qquad 2.I$$

$$\equiv \frac{I_\lambda}{100} \cdot \frac{A_2}{A_1} \cdot I_t \text{ V quanta } sec^{-1} \qquad 2.J$$

where V = emitting volume.

The light received by the photomultiplier tube is measured

as current i_f and $i_f = g_\lambda I_f$ where g_λ is a sensitivity factor of the photomultiplier at wavelength λ.

Now consider an emitter at λ producing a line. If the concentration of the emitter is c, then the total intensity I_ℓ is:

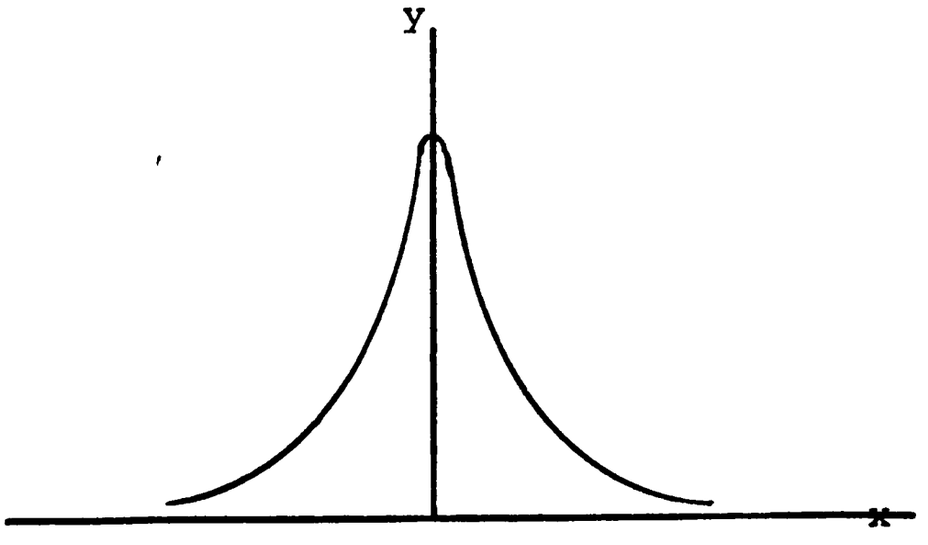
$$I_\ell = k_2 cV \text{ quanta sec}^{-1} \qquad 2.K$$

where k_2 = transition probability for the line.
At the photomultiplier a fraction T (% transmission of the filter at λ) is received and current i_ℓ measured:

$$\frac{i_f}{i_f} = \frac{TI\ g_\lambda}{I_f \cdot g_\lambda} = \frac{Tk_2 cVg_\lambda}{\frac{I_\lambda}{100} \cdot \frac{A_2}{A_1} \cdot I_t Vg_\lambda} \qquad 2.L$$

$$c = \frac{i_\ell I_\lambda A_2}{i_f 100 A_1} \frac{k_1[NO][O]}{T\ k_2} \qquad 2.M$$

For this calculation to be carried out the area of the filter A_2 is required. The filter was regarded as a Gaussian distribution as shown below.



$$y = e^{-a^2x^2} \qquad 2.N$$

for what values of x is $y = \frac{1}{2}$

$$\frac{1}{2} = e^{-a^2x^2} \qquad 2.O$$

$$\ln\frac{1}{2} = -a^2x^2 \qquad 2.P$$

$$x_{\frac{1}{2}} = \pm\sqrt{.694.\frac{1}{a^2}} \qquad 2.Q$$

The halfwidth (HW) is between $x_{\frac{1}{2}}$ and $-x_{\frac{1}{2}}$

$$HW = 2\sqrt{.694.\frac{1}{a^2}} \qquad 2.R$$

$$a = \frac{2}{H.W}\sqrt{.694} \qquad 2.S$$

$$\text{Area of filter } A_2 = \int_{-\infty}^{\infty} e^{-a^2x^2} = \frac{\sqrt{\pi}}{a} \qquad 2.T$$

$$= \frac{\sqrt{\pi}}{2\sqrt{.694}} \qquad 2.U$$

$$= 1.06 \times HW. \qquad 2.V$$

If the maximum transmission of the filter is Tmax then the area $A_2 = 1.06 \times HW \times Tmax.$ 2.W

When using the Bausch and Lomb monochromator the spectral area for a given slit opening was calculated using the manufacturer's data. The image of the entrance slit at the exit slit was 56% the size of the entrance slit [81]. It was therefore necessary to multiply the width of the exit slit by the factor 1.78 to obtain the proper width of the entrance slit. Using this ratio only a single wavelength can pass through the system at full

intensity. The monochromator used had a dispersion of 12.8 nm. mm^{-1}. In order to pass a band of 10 nm the exit slit was set at 0.78 mm, i.e. $\frac{10\ nm}{12.8\ nm.mm^{-1}}$. The entrance slit was set at 1.39 (i.e. 0.78 x 1.78). The monochromator grating was set at 762.0 nm. With the above slit settings the wavelength at 762.0 nm passed through at full intensity. Wavelengths at 757.0 nm and 767.0 nm appeared at 50% intensity and wavelengths at 753.0 nm and 771.0 nm appeared at 10%. The limiting wavelengths were 752.0 nm and 772.0 nm. The area of this band pass was calculated by assuming the above wavelength distribution as a gaussian distribution. The same formula derived for the area of the interference filters was used. The overall transmission of the monochromator is not known, but as calibrations comparing the air afterglow and a line source were carried out at the same wavelength this factor was common to numerator and denominator in equation 2.M and its value was not required.

An example of a calibration carried out for $[O_2(^1\Sigma g^+)]$ determination in Chapter 4 is presented below to bring together all the points arising from the above discussion. An E.M.I. 9558A photomultiplier operated at 1310 volts D.C. was employed. The monochromator entrance slit was set at 1.3 mm and the exit slit at 0.78 mm. This was

equivalent to filter band pass of half width 10 nm. From equation 2.W the area is given by:

$$\text{Area}(A_2) = T \times 1.06 \times 10,$$

where T is the transmission factor of monochromator. At λ = 762.0 nm, I_λ = 81 from Fontijn, Meyer and Schiff [78]. An air afterglow was produced by titrating a discharged nitrogen flow of 3.6×10^{-5} moles l^{-1} with nitric oxide and then developing the glow with more nitric oxide. This yielded values of $[O] = 3.4 \times 10^{-7}$ mole l^{-1} and $[NO] = 9.6 \times 10^{-8}$ mole l^{-1}. The glow produced a reading on the pen recorder equivalent to 41 cms on the range 1 setting of the recorder. Fontijn et al [78] give the value of $k_1 = 3.85 \times 10^4$ mole^{-1} l sec^{-1} and the Total area $A_1 = 4.7(\pm .6) \times 10^4$. k_2 is taken as .14 sec^{-1}. Applying equation 2.M, the concentration of $O_2(^1\Sigma g^+)$ equivalent to a recorded signal i_ℓ is:

$$[O_2(^1\Sigma g^+)] = \frac{i_\ell \times 81 \times T \times 1.06 \times 10 \times 3.85 \times 10^4 \times 9.6 \times 10^{-8} \times 3.4 \times 10^{-7}}{41 \times 100 \times 4.7 \times 10^4 \times T \times 0.14} \text{ mole } l^{-1} \text{ cm}^{-1}$$

$$= i_\ell \times 4 \times 10^{-14} \text{ mole } l^{-1} \text{ cm}^{-1}$$

Thus a recorded signal of 2 cms is equivalent to

$$[O_2(^1\Sigma g^+)] = 8 \times 10^{-14} \text{ mole } l^{-1}$$

In the case of $O_2(^1\Delta g)$ calibration a means of checking the value from the above techniquewas available. This was by measuring the $O_2(^1\Delta g)$ signal produced by a microwave

discharge through molecular oxygen. The percentage of $O_2(^1\Delta g)$ is reported as being between 1 and 10% of the total gas flow [46,47]. The germanium detector-monochromator was calibrated with the air afterglow for experiments described in section 5.1. The exit slits were set at 1.56 mm and the entrance slits at 1.39 mm. This allowed radiation at 1270 nm passing through at full intensity, with a half width band of 20 nm. Using the procedure described above the concentration of $O_2(^1\Delta g)$ was found to be:

$$[O_2(^1\Delta g)] = i_\ell x 3 \times 10^{-10} \text{ mole } l^{-1} \text{ cm}^{-1}$$

where i_ℓ was the observed signal on the pen recorder in cms. This value was checked using an oxygen discharge. The same observation system was employed. Oxygen was discharged using a Microton 200 microwave supply. The oxygen concentration was 2×10^{-5} mole l^{-1}. The recorded signal was 19.5 cms on the pen recorder with the amplifier on the lowest gain. All experiments described above used the amplifier at maximum gain, so a scaling amplification factor was required to bring the oxygen discharge signal into relation with the other calibrations. The amplification factor was obtained by observing an NO + O glow at low gain and then at full gain. The amplification factor was 49. If the percentage of $O_2(^1\Delta g)$ in the discharge is about 2% then the $[O_2(^1\Delta g)] = 4 \times 10^{-7}$ moles l^{-1}. In

this system the flow was fast, about 3.5 meters sec^{-1}, so it was assumed that there was no decay of $O_2(^1\Delta g)$. The smallest meaningful measurement on the pen recorder was 1 cm. This meant that 1 cm scale on the full gain was about 4×10^{-10} mole l^{-1}. In the other method of calibration the minimum detectable $[O_2(^1\Delta g)]$ was 3×10^{-10} mole l^{-1}. This shows that the air afterglow calibration technique was fairly reliable. However, there are some errors which must be considered, The errors become larger at longer wavelengths, which is due to the relative intensities (I_λ) being far from certain at wavelengths greater than λ = 1000 nm. For example, the relative intensity at 1270 nm could be any value between 1 and 10 according to Fontijn et al [78]. Thus at λ = 1270 nm an overall error factor of ten would be reasonable. This clearly underlines the need for accurate relative intensity measurements at the doubtful wavelengths. At λ = 762 nm the relative intensity is well established and an error factor of two or three is expected.

2.7 Electronics.

(a) Phase sensitive detector.

In all experiments the radiation was mechanically chopped at 300 Hz before entering the detector and the output amplified by means of a phase sensitive detector amplifier.

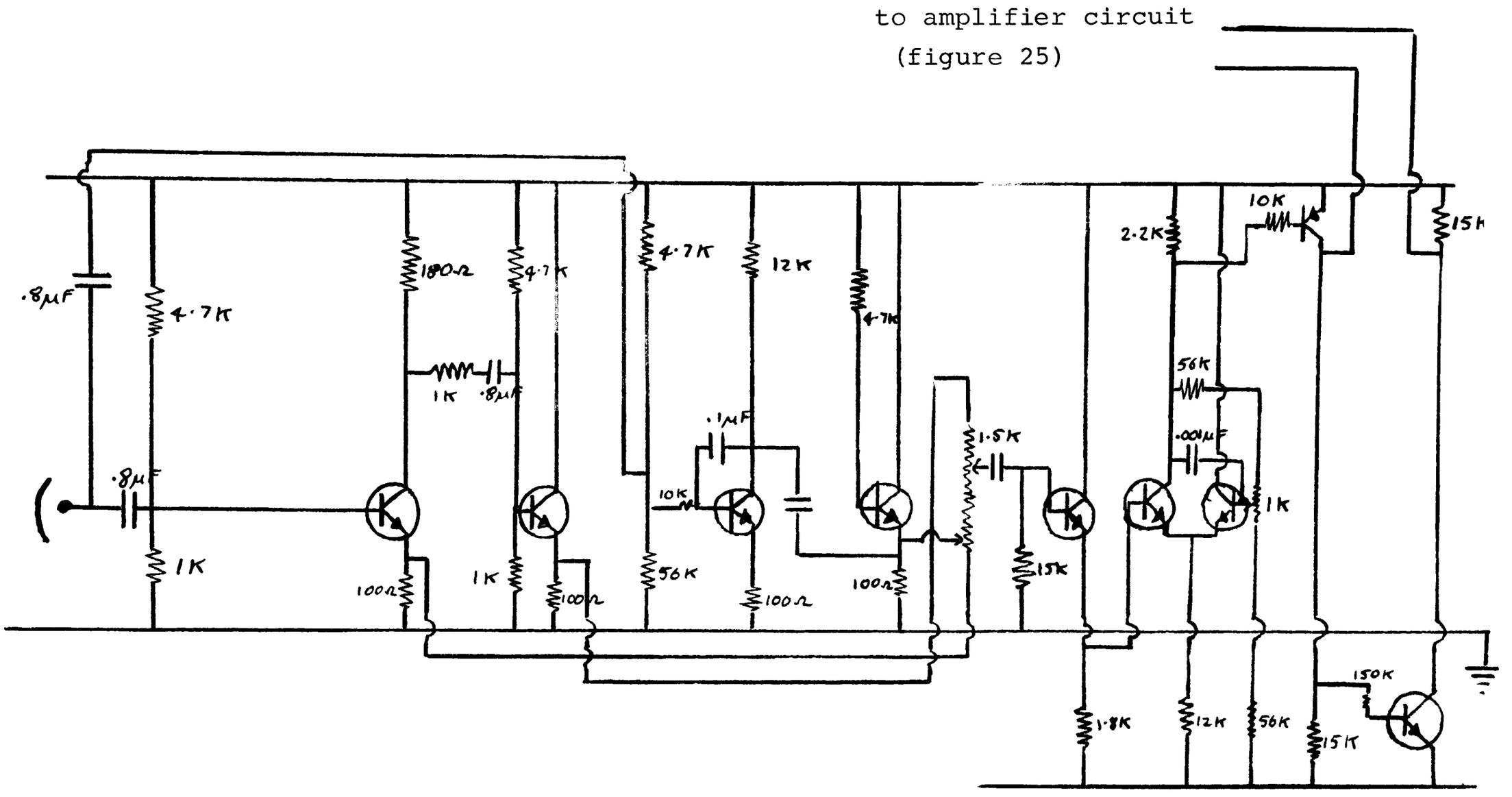


Figure 24. Reference circuit

The principle of phase sensitive detection is that a signal is rectified, by mixing with a reference square wave of the same frequency and observing the resulting D.C. output [82]. The reference voltage must have a definite phase relationship to the signal.

The reference input was produced in the form of a sine wave at the frequency of the mechnical chopper (300 Hz), from a variable reluctance winding positioned next to the chopper. The circuit for the reference section is shown in figure 24. The phase detector was a fully transistorised, half wave type, operated from a built in 15-0-15 volts stabilised power supply. At each half cycle the transistors were switched on or off by the reference voltage, and a phase control adjusted the point in time at which the transistors switch. The low impedance reference input was connected to a Schmitt trigger. This is a bistable circuit which triggers in one direction when the input exceeds a certain level and triggers back again when the input returns to the same level. This level was set at 3 volts and produced a reference square wave from the input sine wave. The reference and input waveforms were monitored on an oscilloscope. This facilitated the setting of the phase shift control.

The input signal from the photomultiplier was

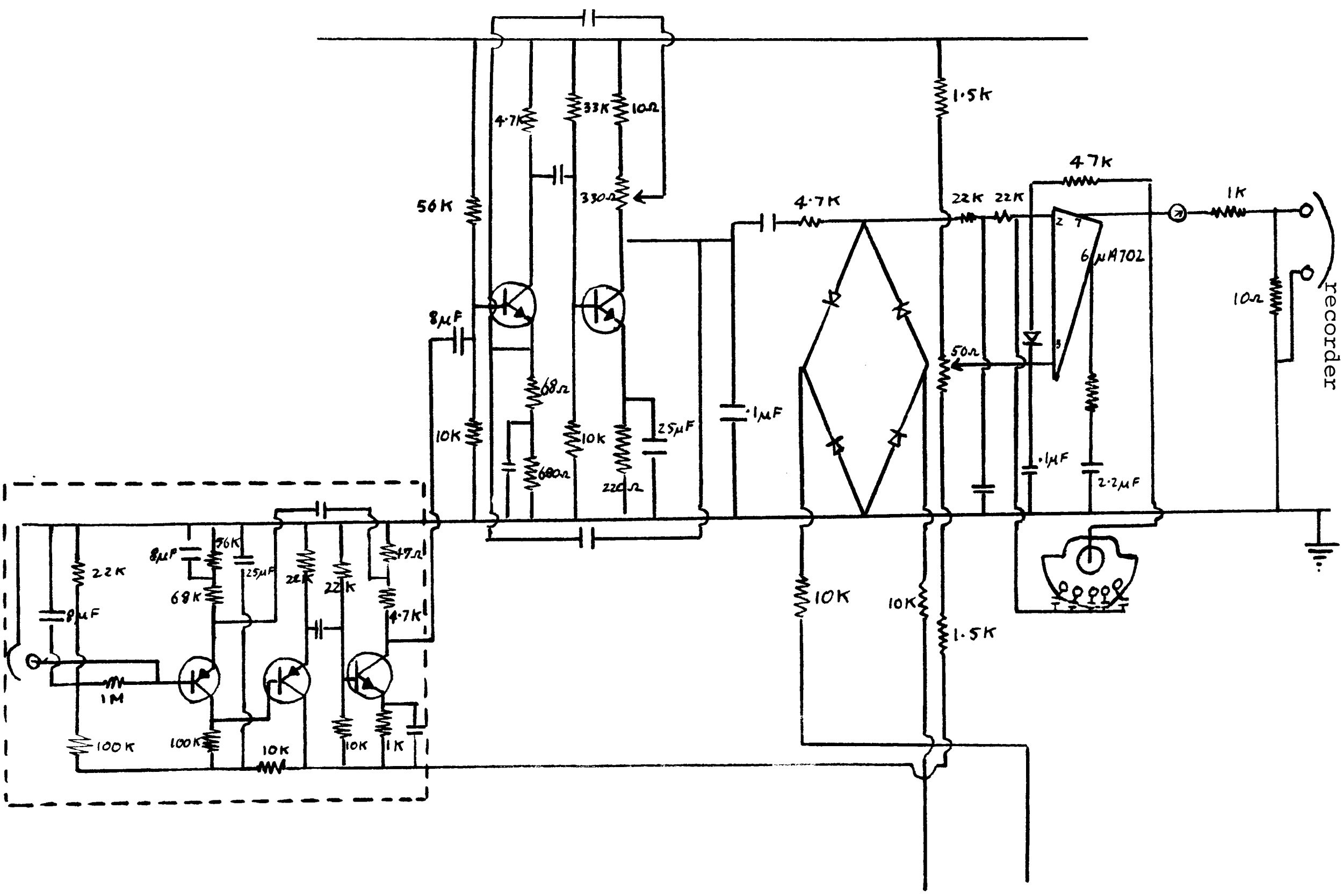


Figure 25. Amplifier circuit

to reference circuit
(figure 24)

developed over a 22 MΩ resistor. This was amplified by a broadly tuned (damped **LC**) transistorised amplifier, figure 25, and detected by mixing with the reference square wave produced from the circuit in figure 24. Integration times of 1 to 10 seconds were used, according to the degree of amplification and the output signal was recorded on an A.E.I.-Sunvic pen recorder.

(b) D.C. amplifier.

In a number of experiments, see Chapter 3.7, the percentage decomposition of photolysed ozone was required. To measure this a cross beam device was set up, using a mercury resonance line at 253.7 nm as the cross beam. The system is described in detail in section 3.7. The intensity of the cross beam was measured by a 9558Q photomultiplier operated at 400 volts D.C. and the output fed into a D.C. amplifier. The circuit is shown in figure 26. The principle behind the type of amplifier being that the very small current produced develops a voltage across the 10^8Ω resistor. This acts as a gate leak into a pair of F.E.T's balanced to minimise drift. The F.E.T's have high input impedance. One of the F.E.T's acts as a reference and the difference in D.C. levels was amplified by an operational amplifier, incorporating an integrated circuit. The amplifier was used with 100% feedback for stability. A 10 KΩ helipot enabled the

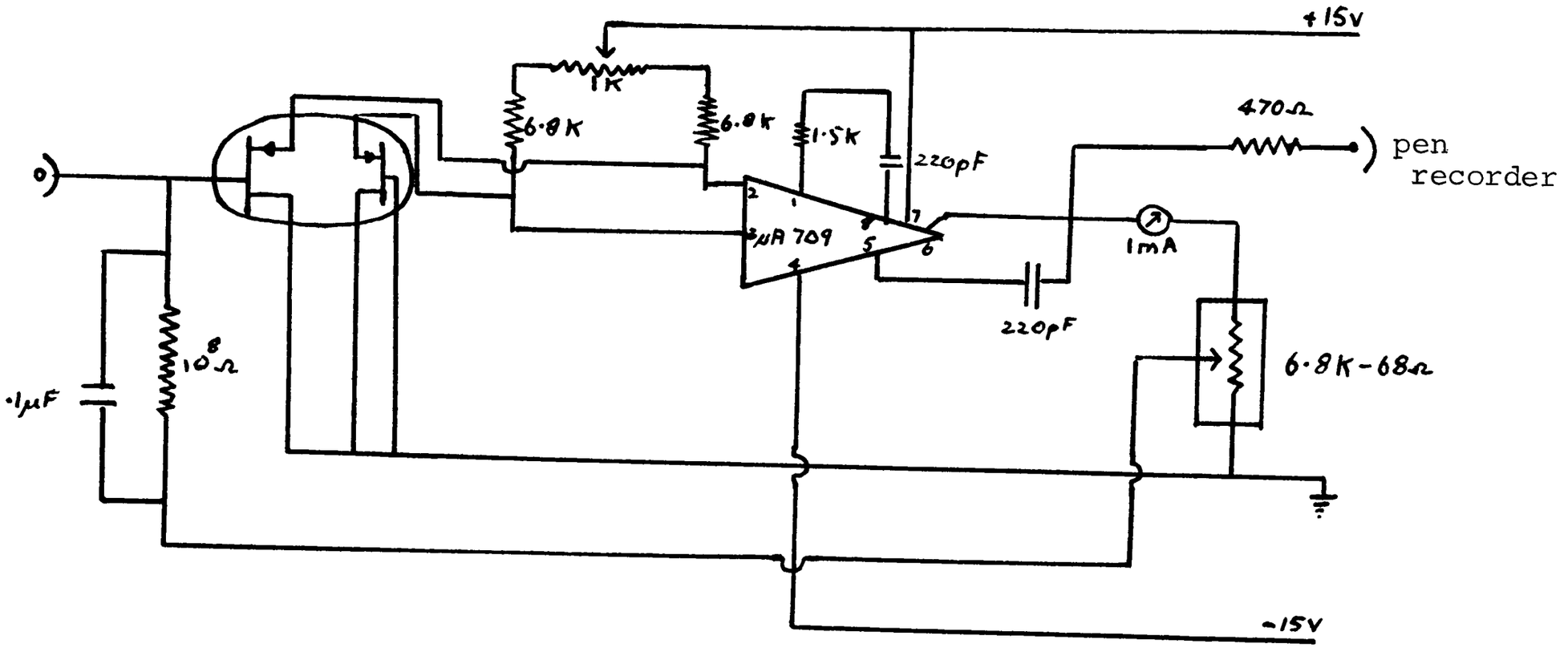


Figure 26. D.C. Amplifier circuit

signal to be backed off against the negative supply, so small differences in current caused appreciable deflections on the pen recorder.

CHAPTER 3

THE ULTRA VIOLET PHOTOLYSIS OF OZONE

2.1 Summary.

Circumstantial evidence has accumulated which suggests that singlet excited oxygen is produced in the ultra-violet photolysis of ozone [21,22]:

$$O_3 + h\nu \longrightarrow O_2(^1\Sigma g^+) + O(^1D) \quad [266\ nm] \qquad 3.1a$$

$$O_3 + h\nu \longrightarrow O_2(^1\Delta g) + O(^1D) \quad [310\ nm] \qquad 3.1b$$

A system was devised to try to detect excited oxygen produced via reaction 3.1a or 3.1b. None was observed.

$O_2(^1\Delta g)$ was, however, observed in the photolysis of oxygen-ozone mixtures at $\lambda = 253.7$ nm [32], and was attributed to the energy transfer process:

$$O_2(^3\Sigma g^-) + O(^1D) \rightarrow O_2(^1\Delta g) + O(^3P) \qquad 3.2$$

Kinetic studies were carried out on this system and the rate constant for reaction 3.2 was found to be $3.5 \pm 2 \times 10^8$ moles^{-1} l sec^{-1}.

In addition, the rate constant for the reaction:

$$O_3 + O(^1D) \rightarrow O_2 + O_2 \qquad 3.4$$

was evaluated as $k_4 = 3.5(\pm .6) \times 10^{11}$ moles^{-1} l sec^{-1}.

The rate constant for reaction 3.5 was measured approximately:

$$O_2(^1\Delta g) + O_3 \rightarrow 2O_2 + O(^3P) \qquad 3.5$$

and found to be $4.1 \pm 1.5 \times 10^6$ mole^{-1} l sec^{-1}.

Experiments are also described to establish whether excited oxygen molecules were produced in ozone photolysis at $\lambda > 266$ nm.

3.2 Flow apparatus and Materials.

The initial experiments adopted a flow system which is diagramatically represented in figure 27. The gases entered through needle valve N, through cold traps into the quartz irradiation tube Q, 50 cms long and 2.8 cms in diameter. After the irradiation tube the gases passed through a Rayleigh horn R, which acted as a light trap, into the main observation area G. This was a large, internally gold plated 5 litre bulb. Reactant gases could be added before and after irradiation into the main flow line through jets J_1 and J_2. The flow rates were measured with conventional capillary flow meters using di-butyl phthalate as a measuring fluid (see section 2.5). The total pressure in the flow system was measured with a silicone oil manometer.

Ozone was prepared by silent discharge of oxygen and collected on silica gel at $-80^{\circ}C$ (see section 2.1a). The ozone was generally about 80% pure, oxygen being the only major impurity. B.O.C. cylinder oxygen, nitrogen and argon was dried by passing through P_2O_5 tubes and cold traps.

3.3 Optical components.

The photolysis source L consisted of three Hanovia

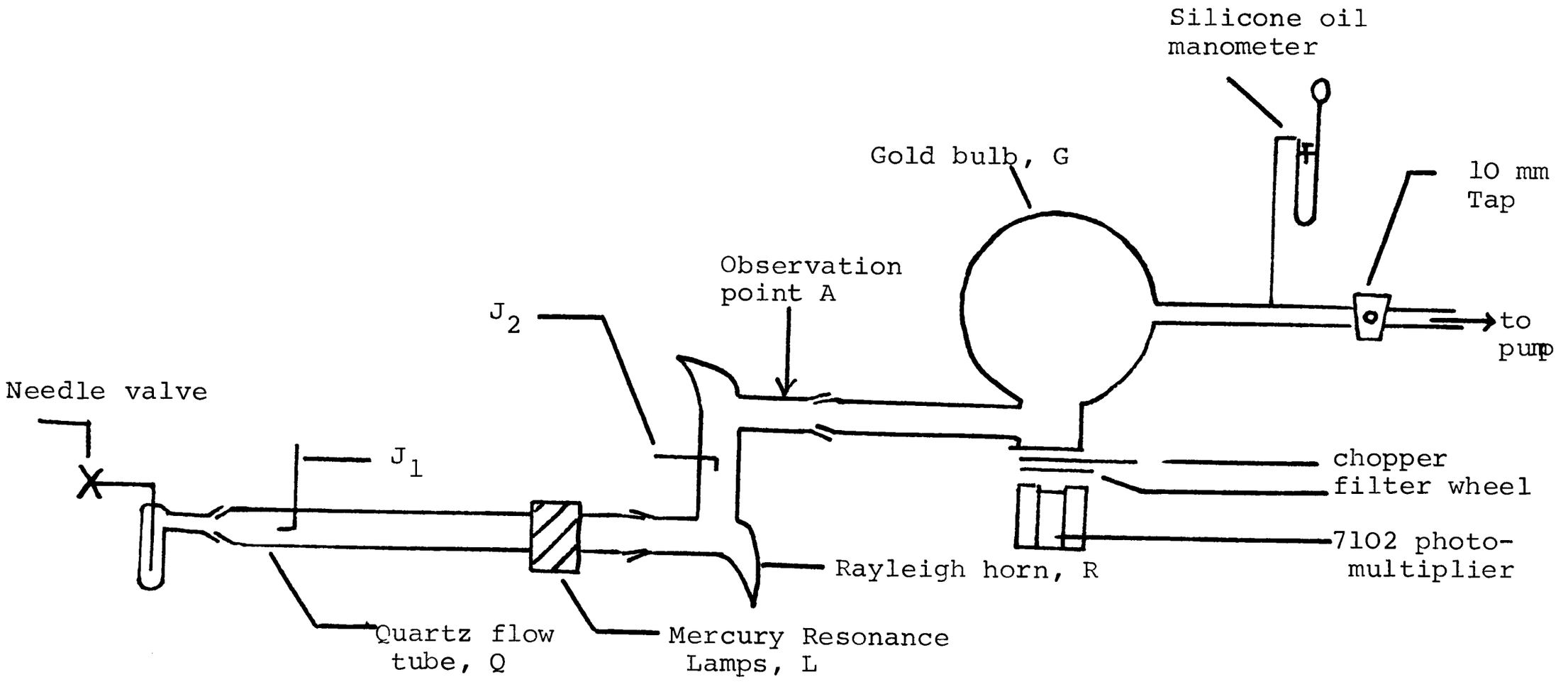


Figure 27. Schematic diagram of flow system for studying ozone photolysis at λ = 253.7 nm

"U" type mercury resonance lamps producing a strong line at λ = 253.7 nm. These were placed symmetrically and close to the irradiation tube Q. These lamps were enclosed by aluminium foil to act as a reflector, and were operated from a 2000 volt transformer.

To detect any emitted radiation from the $O_2(^1\Delta g)$ species an R.C.A. 7102 photomultiplier, operated at -80^oC was used. This was energised by a Brandenburg regulated power supply. The radiation was mechanically chopped and the photomultiplier output amplified by means of a phase sensitive amplifier described in section 2.7a. For observing the $O_2(^1\Sigma g^+)$ species an E.M.I. 9558A photomultiplier operated at room temperature was used involving the same circuitry described above.

Because of its low intensity, the spectral distribution of any emission was examined by the use of narrow band interference filters (see section 2.6a), placed in front of the photomultiplier. To enable rapid observation over a number of spectral regions during an experimental run a rotating disc device was used. This had ten holes punched symmetrically around the edge. A filter was placed across each hole. The disc could be turned by means of a spring catch till any desired filter was in front of the photomultiplier tube.

3.4 Nitrogenous impurities.

Earlier experiments of Wayne [83] on ozone photolysis at λ = 253.7 nm were complicated by the observation of emission from the reaction:

$$NO + O_3 \rightarrow NO_2 + O_2 \qquad 3.13$$

resulting from traces of nitrogen pentoxide present in the ozone. The nitrogen pentoxide was formed by a series of reactions initiated by nitrogen atoms (from the small nitrogen impurity in B.O.C. oxygen) formed in the silent discharge of the ozoniser:

$$N + O_3 \rightarrow NO + O_2 \qquad 3.14$$

$$NO + O_3 \rightarrow NO_2 + O_2 \qquad 3.13$$

$$2NO_2 + O_3 \rightarrow N_2O_5 + O_2 \qquad 3.15$$

The ozone used in the experiments discussed in this chapter was extensively purified but still it was found that an impurity emission was present. To check if the impurity was indeed due to reaction 3.13, an $NO + O_3$ glow was produced in the flow system by adding small amounts of Nitric oxide at J_2 to the ozone. The intensities through a series of filters were recorded and the results are listed in Table 2 as percentage intensities relative to one of the filters.

3.5 Ozone photolysis.

Ozone was photolysed at various concentrations and

the weak emission through each filter was recorded. The results are presented in Table 2 together with the experimental conditions. It is clear from Table 2 that the background impurity emission present in ozone photolysis has the same relative intensity distribution as that of the NO + O_3 reaction. This demonstrated that the background emission was due to the NO + O_3 reaction, thus confirming Wayne's observations [83].

Over the ozone concentration range employed there was no real variation at 762 nm and 1270 nm, which suggests that $O_2(^1\Sigma g^+)$ and $O_2(^1\Delta g)$ <u>are not</u> produced in the primary photolytic step.

Experiments were carried out in which foreign gases were introduced to the ozone flow through either jets J_1 or J_2. When nitrogen or argon were added before and after irradiation the impurity background emission was reduced, although the relative intensities through various filters remained identical with those listed in Table 2. Thus addition of nitrogen and argon only reduced the intensity of the background emission.

Addition of oxygen upstream of the irradiation unit caused a reduction of the background emission through all filters except at 1270 nm where an <u>increase</u> in emission was observed. Addition of more oxygen decreased the background to an immeasurable amount, while the emission

Table 2. Relative intensities through various filters of the emission from the NO + O_3 glow and ozone photolysis at λ = 253.7 nm.

10^7 [NO] mole l^{-1}	10^6 [O_3] mole l^{-1}	634 nm	701 nm	762 nm	801 nm	1270 nm	Detector	EHT. volts
		←——relative intensities——→						
2.0	5.0	28	45	49	100	7.0	7102	1000
2.0	1.0	29	45	50	100	7.8	"	1000
2.0	1.4	26	46	48	100	6.5	"	1000
	0.5	28	45	50	100	7.0	"	1500
	0.92	26	45	50	100	6.0	"	1400
	2.0	26	46	48	100	6.4	"	1400
1.7	3.0	16	100	50	19	-	9558A	1080
1.7	1.2	17	100	52	20	-	"	1080
1.7	0.7	17	100	51	20	-	"	1080
	0.55	20	100	48	18	-	"	1350
	1.32	19	100	48	20	-	"	1350
	2.10	20	100	50	20	-	"	1350

through the 1270 nm filter increased. This increase was not observed if oxygen was added after the irradiation unit, or if only oxygen (in the absence of ozone) was irradiated by λ = 253.7 nm.

The intensity of the 1270 nm emission could be corrected for the background emission since the relative intensities were known from Table 2. The variation of corrected 1270 nm emission with oxygen concentration at various ozone concentrations is shown in figure 28. For some experimental conditions the intensity observed at 1270 nm was more than 100 times that which could be accounted for by the residual NO + O_3 photochemiluminescent glow. The emission at 1270 nm is thus consistent with the production of $O_2(^1\Delta g)$.

Attempts were made to detect $O_2(^1\Sigma g^+)$ in the irradiated oxygen-ozone system at λ = 253.7 nm, but none was observed.

The preliminary observations suggest that $O_2(^1\Delta g)$ is formed in the ultra violet photolysis of oxygen-ozone mixtures. The necessity of the presence of molecular oxygen for the appearance of the $O_2(^1\Delta g)$ emission leads, at this stage, to certain conclusions about the mode of excitation of the $O_2(^1\Delta g)$. It is clear from the results that the primary photolytic step does not produce significant quantities of $O_2(^1\Delta g)$. Badger et al [14]

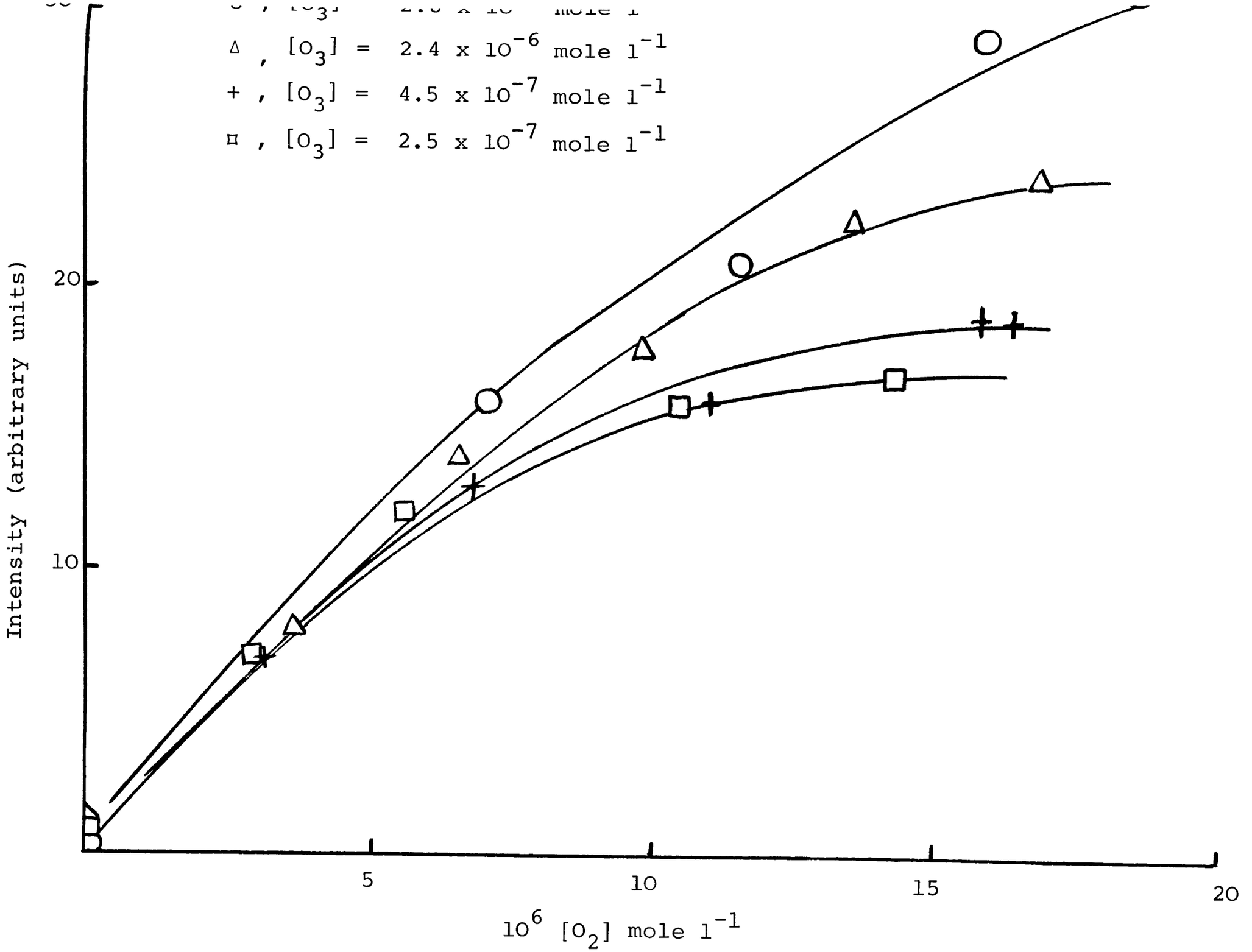


Figure 28. Variation of emitted intensity with oxygen concentration

have shown that the rate of spontaneous emission from $O_2(^1\Delta g)$ is increased in the presence of molecular oxygen, although their results suggest that a much greater pressure of oxygen than those employed in the present experiments would be necessary to give a marked enhancement of the transition probabilities. An alternative explanation is that the overall process represented by equation 3.1 is inefficient at the low ozone pressures employed and becomes increasingly more efficient with increasing pressure [84]. For example, the photolysis mechanism might proceed via an excited ozone molecule, O_3^*, which is then deactivated by excess carrier [M] to $O_2(^1\Delta g)$ and $O(^1D)$:

$$O_3 + h\nu \xrightarrow{u/v} O_3^* \xrightarrow{[M]} O_2(^1\Delta g) + O(^1D) \qquad 3.1c$$

If equation 3.1c is the correct mechanism then addition of nitrogen or argon should have the same effect as addition of oxygen. However, the effect was not observed. The only explanation to account for this is that the efficiency of deactivation of the excited ozone molecule to $O_2(^1\Delta g)$ and $O(^1D)$ by nitrogen is much less than that of oxygen. Consideration of the magnitude of the corrected signal at 1270 nm suggests that the efficiency of reaction 3.1c when nitrogen or argon is the carrier would be at least ten times less than that when oxygen is the carrier.

A more plausible source of the $O_2(^1\Delta g)$ which is consistent with the results involves energy transfer in the secondary process. It has been well substantiated that $O(^1D)$ atoms are formed in the primary step in the ultra violet photolysis of ozone [23] and one of the simplest excitation mechanisms would be:

$$O(^1D) + O_2(^3\Sigma g^-) \rightarrow O_2(^1\Delta g) + O(^3P) \qquad 3.2$$

as suggested by Vallence-Jones and Gattinger [35] for the formation of $O_2(^1\Delta g)$ in the atmosphere. This reaction is directly analogous to the energy transfer process yielding $O_2(^1\Sigma g^+)$ [33,37]:

$$O(^1D) + O_2(^3\Sigma g^-) \rightarrow O_2(^1\Sigma g^+) + O(^3P) \qquad 3.9$$

3.6 Use of the monochromator for $O_2(^1\Delta g)$ isolation.

One of the major disadvantages of the experiments described in section 3.5 was the use of the 7102 photomultiplier in conjunction with interference filters. Since the 7102 photomultiplier has low sensitivity at 1270 nm the whole end face of the tube was exposed to the emitting source. Clearly with this optical set up the light acceptance angle and area was large, so it was possible that wavelengths other than those defined by the filter transmission curves might be detected. Although an increase in intensity was observed at 1270 nm, there was still some small scope for doubting whether the

emitting species was $O_2(^1\Delta g)$. Indeed the increase in intensity could be due to some spurious impurity emission occurring near 1270 nm. It was thought desirable to use a monochromator to isolate the $O_2(^1\Delta g)$ band under the experimental conditions described in section 3.5.

A Bausch and Lomb high intensity grating monochromator was employed (see section 2.6b for a complete description of this instrument). The monochromator had small exit and entrance slits thus making the use of the 7102 photomultiplier impractical. A liquid nitrogen cooled germanium photo conductor was used which is discussed in section 2.6c. This was kindly made by Mr. A.C. Mears of the Clarendon Laboratory, Oxford. The detector was used in conjunction with a chopper, pre-amplifier and basic phase sensitive detector amplifier described in section 2.7. The optical set up was: gold bulb - chopper - monochromator - detector. Because of the small area of the germanium detector, about 6 mm^2, great difficulty was encountered mounting it in front of the monochromator exit slits. This was overcome by producing a source of $O_2(^1\Delta g)$ by means of a microwave discharge in oxygen and moving the detector around to achieve maximum signal at 1270 nm. The entrance slit was set at 1.4 mm and the exit slit at 1.6 mm. The relevance of these values is

discussed in section 2.6c. The spectral region between 800 nm and 1500 nm could be scanned by means of a geared, variable speed, electric motor coupled to the grating spindle.

The presence of $O_2(^1\Delta g)$ in photolysis of pure ozone at λ = 253.7 nm was checked with the monochromator-germanium detector, but none was observed.

Figure 29 shows a scan of an ozone-oxygen mixture photolysed at λ = 253.7 nm. The instrument was at maximum gain, hence the noise in the base line. Figure 30 shows a scan of the products from an oxygen microwave discharge which contains $O_2(^1\Delta g)$ in concentrations of about 5% of the total gas flow. Comparison of figures 29 and 30 clearly indicates that $O_2(^1\Delta g)$ was produced in the ultra violet photolysis of ozone-oxygen mixtures. It thus appears that the mechanistic conclusions drawn in section 3.5 are reasonable and that the excited molecule is produced by energy transfer:

$$O(^1D) + O_2(^3\Sigma g^-) \rightarrow O_2(^1\Delta g) + O(^3P) \qquad 3.2$$

One would also expect $O_2(^1\Sigma g^+)$ to be produced since the analogous reaction:

$$O(^1D) + O_2(^3\Sigma g^-) \rightarrow O_2(^1\Sigma g^+) + O(^3P) \qquad 3.9$$

does occur [33,37]. Attempts were made to isolate the $O_2(^1\Sigma g^+)$ band with the aid of a 9558A photomultiplier

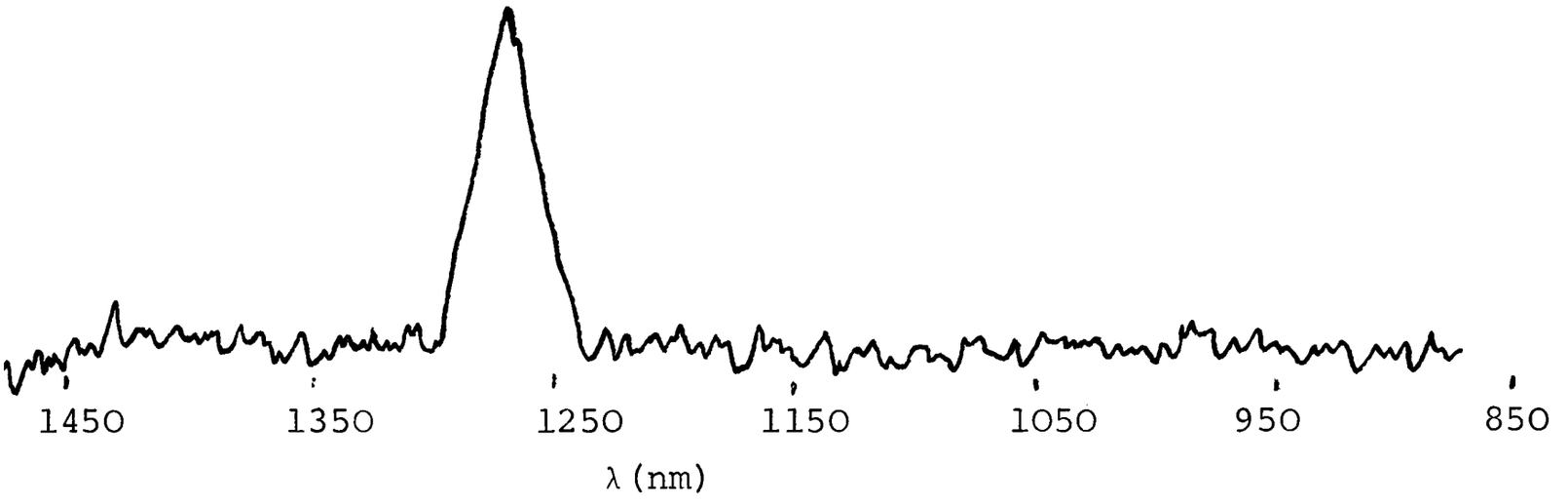


Figure 29. Scan of oxygen-ozone mixture photolysed at λ = 253.7 nm using germanium detector. $[O_2]$= 2.8 x 10^5mole l^{-1}. $[O_3]$= 8 x 10^7 mole l^{-1}.

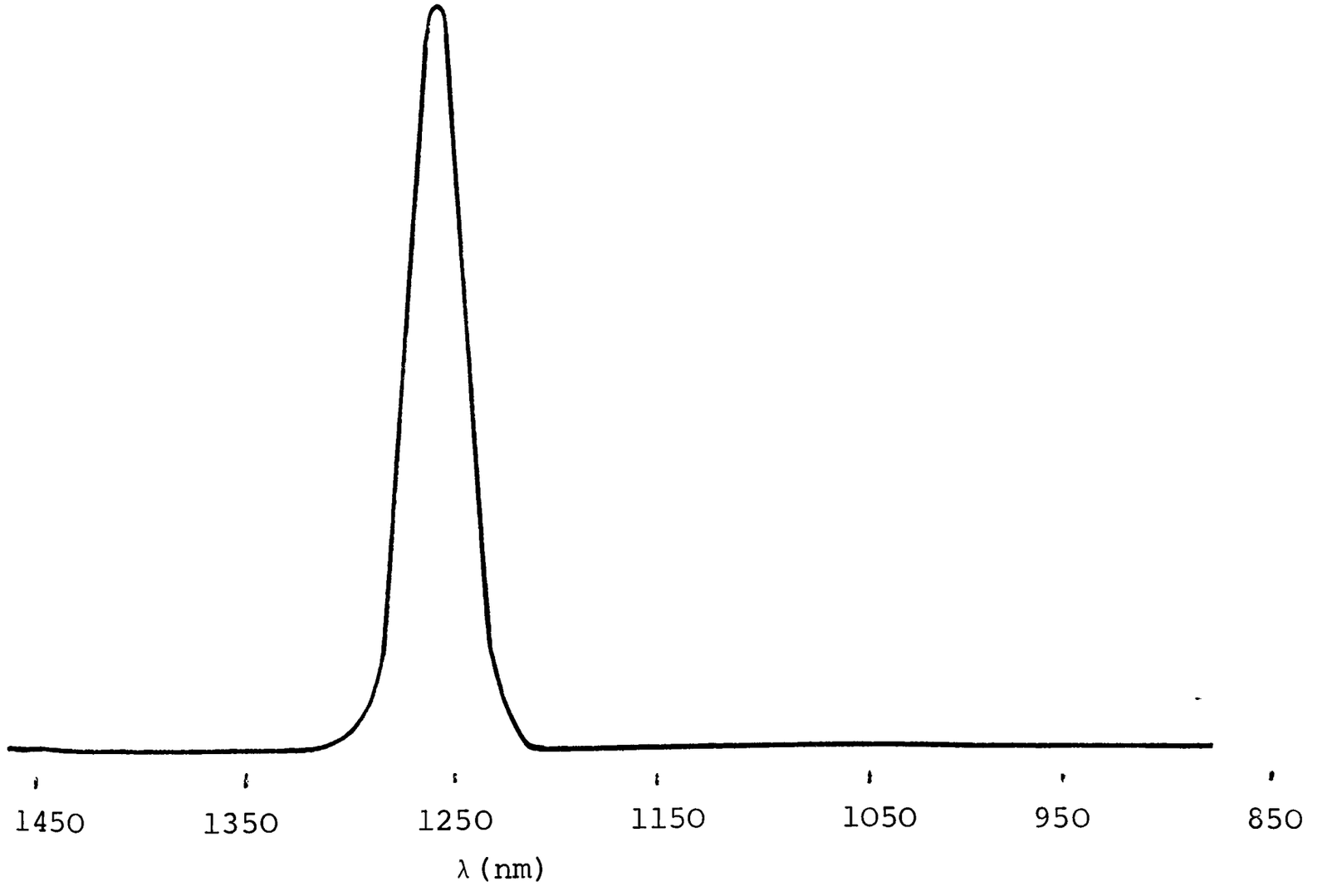


Figure 30. Scan of discharge products of microwave discharge through oxygen using germanium detector. $[O_2]$ = 4 x 10^{-5} mole l^{-1}

and monochromator. No $O_2(^1\Sigma g^+)$ was observed. The absence, however, can be explained by the very high reaction rate of 3.10 [33, Chapter 4], $k_{10} = 4 \times 10^9$ mole^{-1} l sec^{-1}:

$$O_3 + O_2(^1\Sigma g^+) \rightarrow 2O_2 + O(^3P) \qquad 3.10$$

The decay of $O_2(^1\Sigma g^+)$ is given by $\frac{[O_2(^1\Sigma g^+)]}{[O_2(^1\Sigma g^+)]_o} = e^{-k_{10}[O_3]t}$

where $[O_2(^1\Sigma g^+)]_o$ is the concentration of the species in the irradiation area. For the lowest $[O_3]$ value of about 3×10^{-7} mole l^{-1} employed, and a residence time of 0.1 sec, the ratio $\frac{[O_2(^1\Sigma g^+)]}{[O_2(^1\Sigma g^+)]_o} = e^{-120}$, which is vanishingly small.

Indeed this first deactivation also explains why no $O_2(^1\Sigma g^+)$ was observed from the primary step (see section 3.5) in our system where the lowest concentration employed was about 5×10^{-7} moles l^{-1}.

3.7 Kinetic measurements.

For kinetic experiments it is ideally desirable to observe the $O_2(^1\Delta g)$ emission directly across the flow tube, since this simplifies a number of the kinetic measurements. The apparatus was set up with the monochromator and germanium detector viewing across the flow tube at point A in figure 27. However, although the signal at 1270 nm was measurable, it was too small to carry out numerous kinetic runs. Thus the original system, incorporating the gold

bulb, was adopted. The final flow apparatus was identical to that used for the preliminary observations except that the irradiation unit consisted of two Hanovia "U" tube mercury lamps and one spiral low pressure mercury lamp (see section 2.4) surrounded by aluminium foil.

Experimental runs were carried out in which the oxygen concentration was kept constant and the ozone concentration varied. The maximum signal observed at 1270 nm was recorded. The oxygen concentration was then changed and the same procedure repeated. The linear flow velocities varied between 4.4 and 4.85 meters sec^{-1}. The results are listed in Table 3. Absolute calibrations using the air afterglow (see section 2.6c) were performed after a set of runs in order to calculate the $O_2(^1\Delta g)$ concentration at the observation point. These are presented in Table 3. In order to calculate the concentration of $O_2(^1\Delta g)$ formed in the irradiation area, $[O_2(^1\Delta g)]_o$, it was necessary to know the time of residence of the species in the system, i.e. the time taken for the gas to pass from the irradiation area through the observation point. This was complicated by having a large gold bulb as part of the flow line, since the geometry of the bulb made the mathematical calculation of the residence time difficult. An indirect method was thus

Table 3. Variation of $[O_2(^1\Delta g)]$ in the photolysis of ozone-oxygen mixtures at λ = 253.7 nm.

Run No. and Legend	$10^5[O_2]$ moles l^{-1}	$10^7[O_3]$ moles l^{-1}	Pen recorder (I) signal cms.	Calibration factor x moles l^{-1}	$10^{10}[O_2(^1\Delta g)]$ mole l^{-1}
A (+)	4.5	16.5	3.9	I x 3 x 10^{-10}	11.8
		11.2	3.6	"	10.8
		8.7	3.1	"	9.3
		4.7	1.8	"	5.4
		1.9	1.0	"	3.0
B. O	2.9	15.7	2.65	I x 3 x 10^{-10}	7.9
		10.4	2.3	"	6.8
		6.2	1.6	"	4.8
		3.0	0.9	"	2.7
C Δ	1.85	16.4	1.7	I x 3 x 10^{-10}	5.1
		12.9	1.65	"	5.0
		9.2	1.4	"	4.2
		3.0	0.7	"	2.2
D. ■	3.4	12.5	4.8	I x 1.9 x 10^{-10}	9.1
		7.3	3.75	"	7.1
		5.1	3.3	"	6.3
		3.0	2.7	"	5.1
		1.7	1.25	"	2.4

Table 3 (contd.)

E X	2.2	8.2	3.0	I x 1.9 x 10^{-10}	5.7
		9.8	2.6	"	5.0
		6.6	2.55	"	4.8
		4.4	2.2	"	4.2
		2.0	1.2	"	2.3
F .	1.4	9.5	2.35	I x 1.9 x 10^{-10}	4.5
		6.3	2.0	"	3.8
		3.6	1.35	"	2.6
		1.1	0.51	"	1.0

adopted. It was assumed that the major source of decay of $O_2(^1\Delta g)$ in our system was by reaction 3.5:

$$O_2(^1\Delta g) + O_3 \rightarrow 2O_2 + O(^3P) \qquad 3.5$$

Using a microwave discharge in oxygen the difference in signal at 1270 nm between observation at the gold bulb and observation upstream at point A, figure 27, was measured. The ratio of signals was 7.2. Decay of $O_2(^1\Delta g)$ in this case is very small since the concentration of ozone produced in the microwave discharge is low and the flow velocity is high, about 4 meters sec^{-1}. The same procedure was adopted when photolysing a known ozone concentration in oxygen. The ratio of the signals obtained at point A and at the gold bulb was obtained. Any deviation from the value of 7.2 could be attributed to decay of $O_2(^1\Delta g)$ by reaction with ozone. The rate constant for reaction 3.5 is about 2×10^6 $moles^{-1}$ 1 sec^{-1} [93,94]. The decay of $O_2(^1\Delta g)$ by reaction with ozone is given by the equation:

$$\frac{[O_2(^1\Delta g)]_{t_1}}{[O_2(^1\Delta g)]_o} = e^{-k_5[O_3]_{t_1}}$$

where $[O_2(^1\Delta g)]_o$ is the concentration of the excited species in the irradiation area and $[O_2(^1\Delta g)]_{t_1}$ the concentration of the species in the observation area. In a typical run the value $[O_3] = 7 \times 10^{-7}$ mole l^{-1}, and the ratio

$\frac{[O_2(^1\Delta g)]_{t_1}}{[O_2(^1\Delta g)]_o} = 0.7$. Thus the residence time (t_1) was calculated as about 0.25 secs. Using this value, $[O_2(^1\Delta g)]_o$ was evaluated for each run and the results presented in Table 4. The errors using this value for the residence time are discussed in the concluding sections of this chapter.

The amount of ozone decomposed by the irradiation unit was required to obtain a fuller understanding of the kinetics. To measure the decomposition a cross beam device was set up, using the mercury resonance line at λ = 253.7 nm as the source. A cell with two quartz windows was inserted into the flow line a few centimeters downstream of the Rayleigh horn. Radiation, produced from the low pressure mercury lamp, was passed through a colimating hole of ⅛" diameter, through a $NiSO_4/Cl_2$/OX7 [85] filter system before the cell and a $NiSO_4$/OX7 filter after the cell. This combination of filters ensures a pure 253.7 nm line [86] reaching the E.M.I. 9558Q detector (see section 2.7c for discussion of the electronics employed). The lamp was cooled by an air blast. Figure 31 shows a diagram of the complete cross beam unit.

The Beer Lambert law states that

$$I = I_o e^{-\varepsilon cd}$$

where the symbols have their usual meaning.

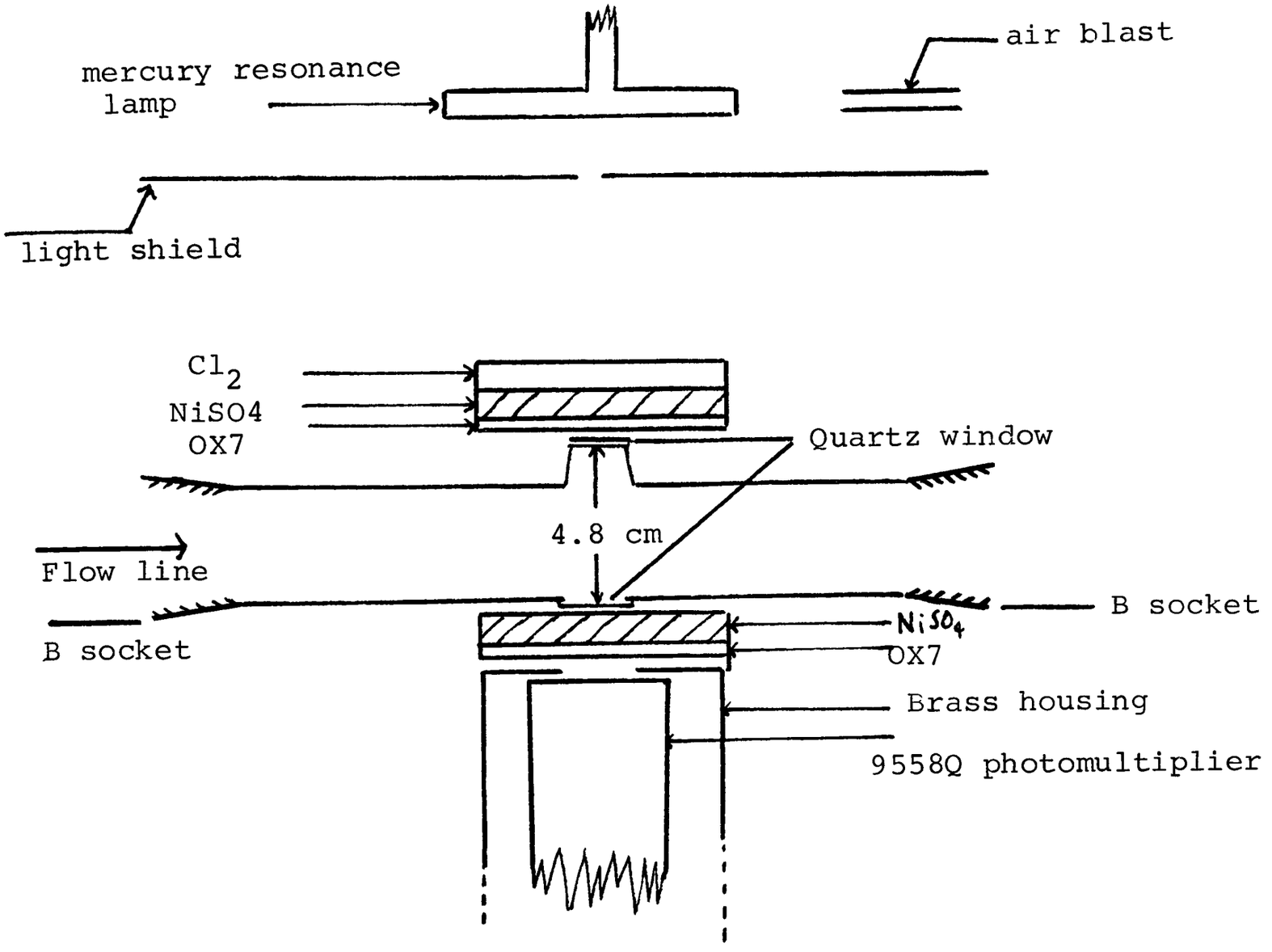


Figure 31. Cross beam apparatus

Table 4.

Run No. and Legend	fraction of $(O_2(^1\Delta g)$ decay	$10^{10}[O_2(^1\Delta g)]o$ mole l^{-1}	$10^3 \frac{[O_2(^1\Delta g)]o}{[O_3]}$	slope 10^7 mole l^{-1}	intercept 10^9 mole l^{-1}	$10^7[O_2]t$ mole l^{-1} sec.
A +	0.66	18.0	1.09	32.5	5.4	13.9
	0.77	14.0	1.25			
	0.80	11.5	1.33			
	0.86	6.2	1.33			
	1.00	3.0	1.58			
B O	0.68	11.5	0.7	27.5	3.1	9.7
	0.77	8.9	0.85			
	0.86	5.6	0.9			
	0.92	3.0	1.0			
C Δ	0.66	7.7	0.47	16.5	1.5	6.15
	0.73	8.9	0.53			
	0.79	5.5	0.58			
	0.93	2.4	0.8			
D ■	0.72	12.8	1.0	27.5	4.1	10.9
	0.84	8.5	1.15			
	0.89	7.0	1.35			
	0.93	5.5	1.8			
	1.00	2.4	1.4			

Table 4 (contd.)

E X	0.82	7.0	0.85	19	2.4	7.25
	0.77	6.5	0.7			
	0.86	5.7	0.93			
	0.90	4.7	0.95			
	1.00	2.3	1.15			
F .	0.77	5.8	0.6	16	1.55	4.75
	0.85	4.5	0.7			
	0.90	2.8	0.75			
	1.00	1.0	0.9			

$$I = I_o - I_{abs}$$

$$\therefore \quad I = I_o[1 - e^{-\varepsilon cd}]$$

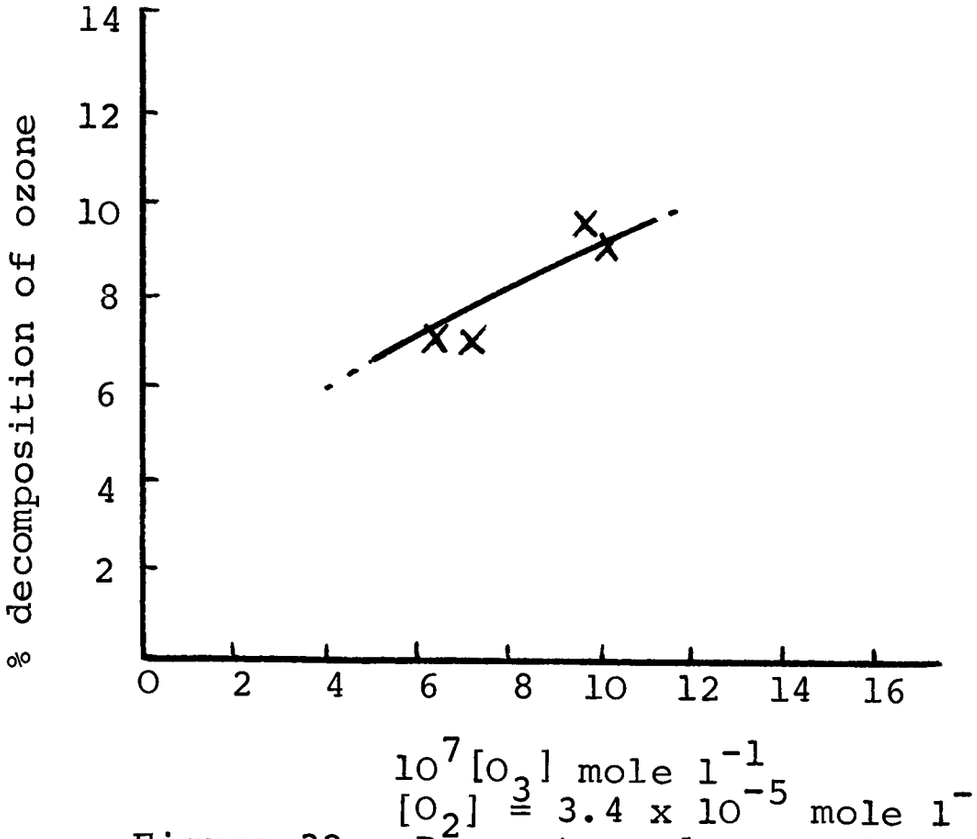
$$I_{abs} = I_o[1 - e^{-\varepsilon cd}]$$

$$I_{abs} = I_o[\varepsilon cd - \tfrac{1}{2}(\varepsilon cd)^2 .....]$$

There is little observed deviation from linearity up to 10% absorption, and in our system where d = 4.8 cms, the maximum ozone concentration about 0.1 torr, so the maximum absorption is about 9%. Hence, the response in our system was linear.

In an experiment the same oxygen concentrations as in the kinetic measurements were employed. The absorption when the photolysing lamp was on and then off was recorded. Turning the lamp off caused an increase in absorption. The difference in the "light on", "light off" signals was a measure of the amount of ozone decomposed by the lamp. Care was taken to ensure that the lamp was fully warmed up before taking any measurements. The results are listed in Table 5 and figures 32 show the % decomposition at various ozone concentrations at a constant oxygen concentration. The response to added ozone was checked and in each case it was linear.

It was assumed that the measured decomposition was a result only of the photolysis and not due to subsequent reactions outside the irradiation area. The only main



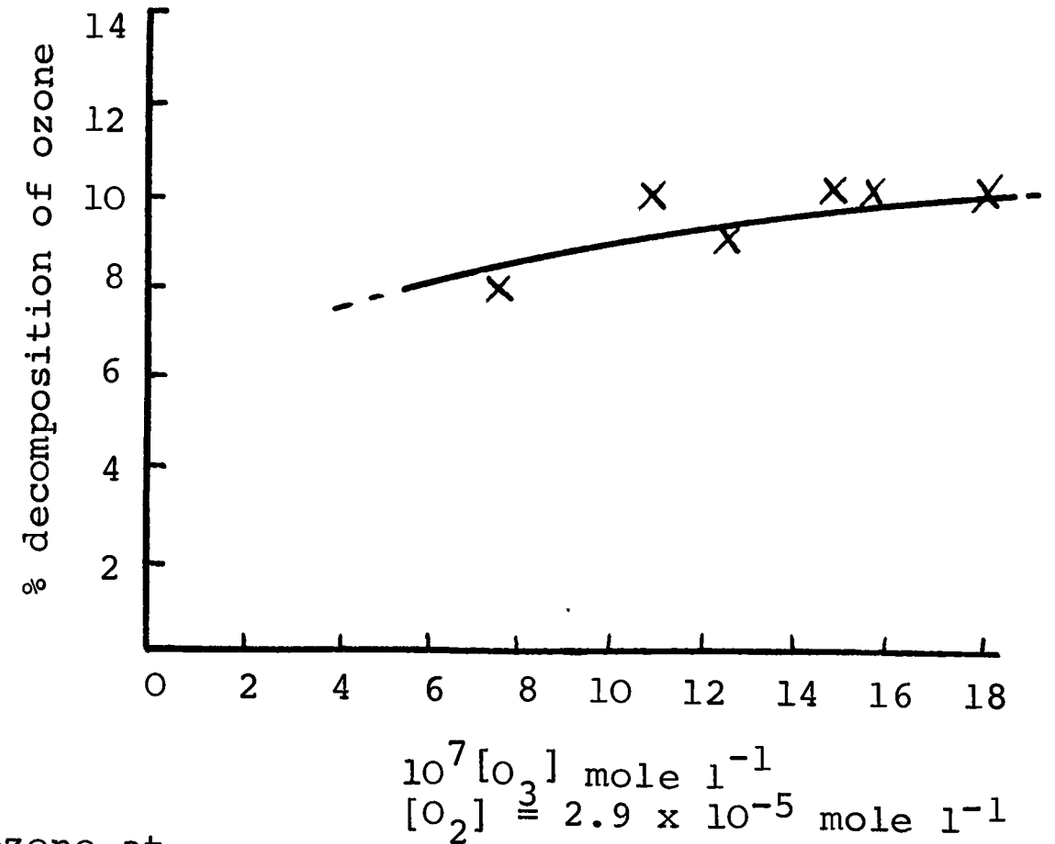
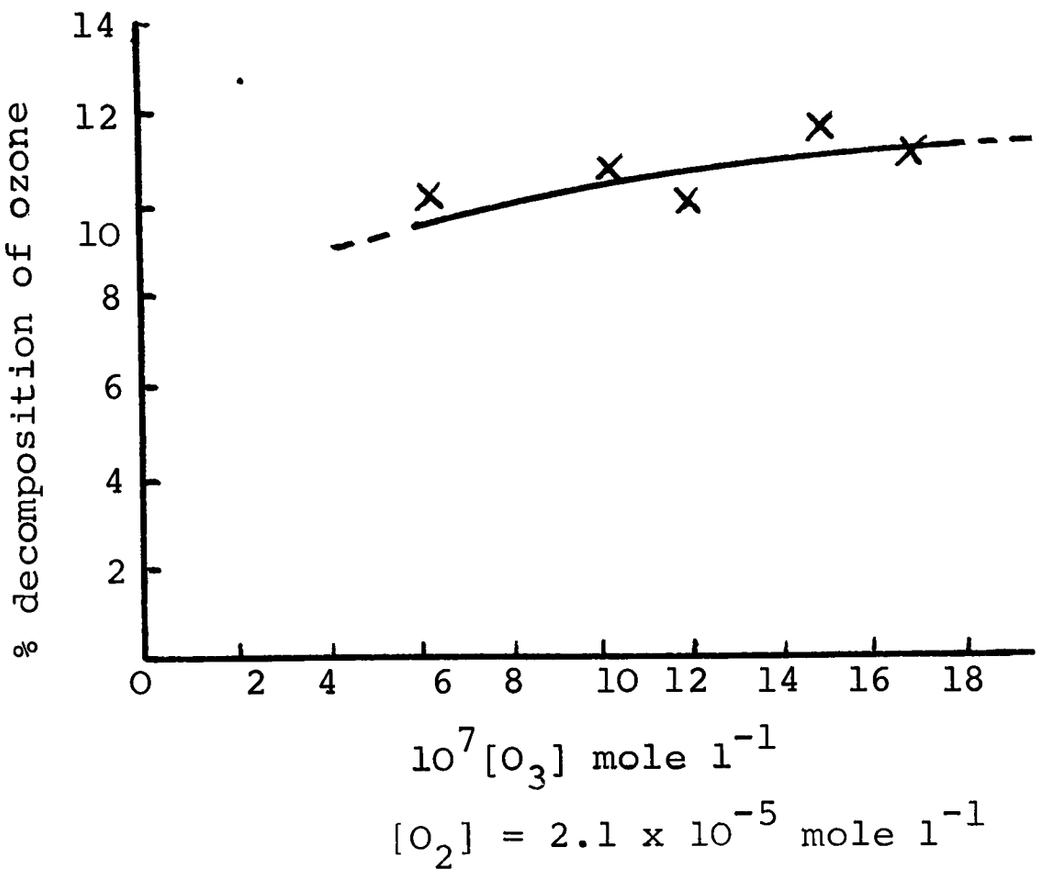


Figure 32. Percentage decomposition of ozone at various oxygen concentrations.



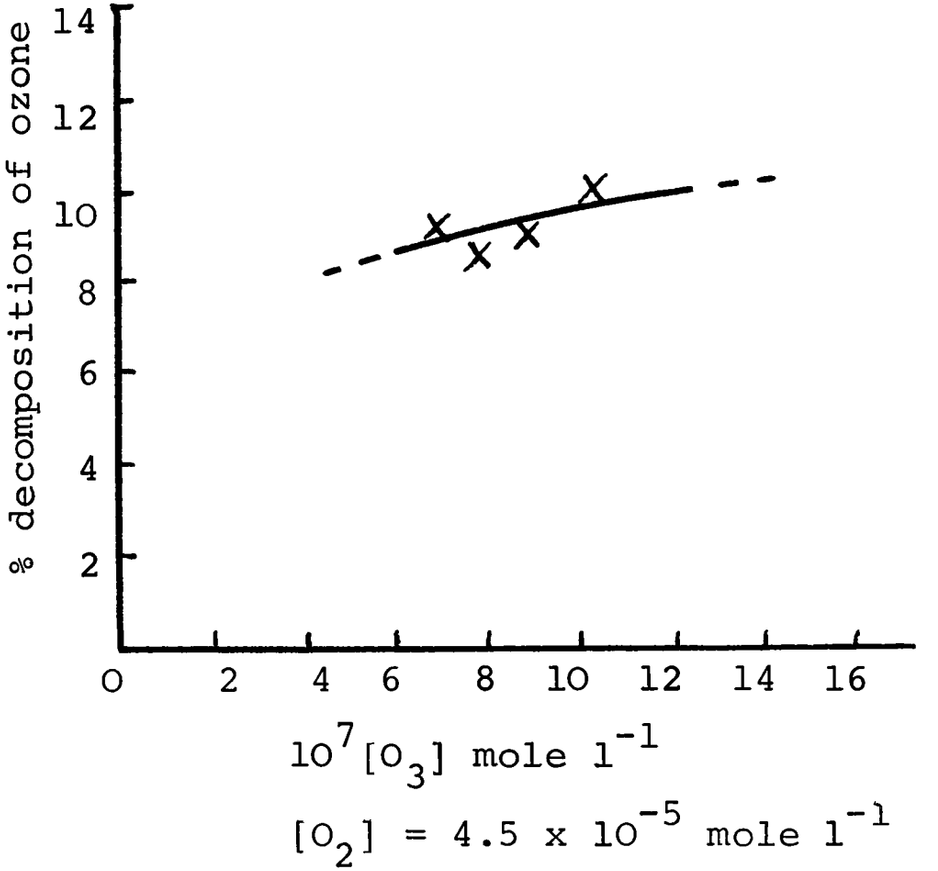


Figure 32 (continued)

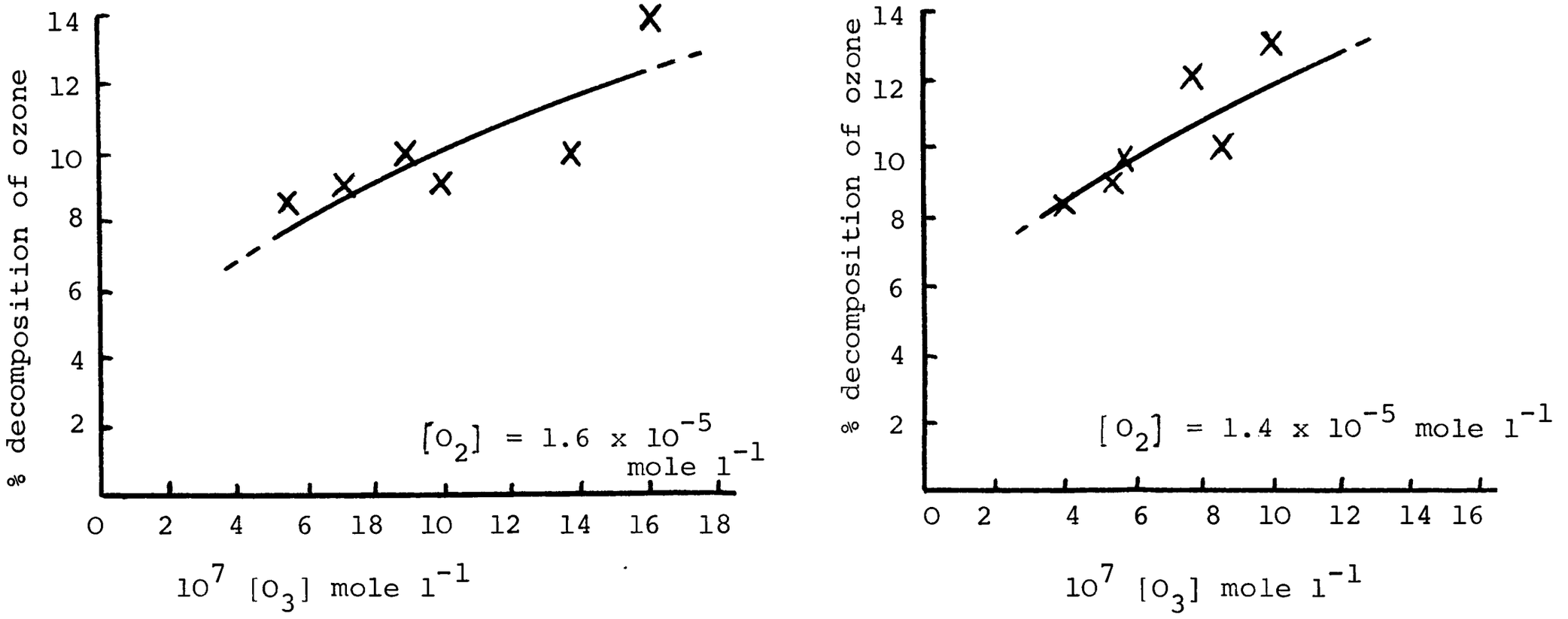


Figure 32 (continued)

Table 5. Percentage decomposition of ozone due to photolysis at λ = 253.7 nm for various oxygen concentrations

Run No.	$[O_3]$ $\times 10^{7}$ mole l^{-1}	$[O_2]$ $\times 10^{5}$ mole l^{-1}	Lamp on cms.	Lamp off cms.	% decomposition
16	13.7	1.6	9.75	10.7	10.0
17	16.0		11.0	12.8	14.0
19	10.0		7.7	8.45	9.0
20	7.3		5.9	6.5	9.0
21	5.4		3.95	4.3	8.5
30	10.1	1.40	9.6	11.0	13.0
31	8.7		8.4	9.35	10.0
32	7.7		7.2	8.2	12.0
39	5.5		5.05	5.55	9.0
35	4.3		3.35	3.65	8.5
43	15.5	2.9	9.85	10.9	10.0
44	18.5		11.4	12.8	11.0
45	12.7		8.05	8.8	9.0
46	11.0		7.0	7.75	10.0
48	15.2		9.0	10.0	10.0
49	7.5		4.70	5.0	8.0
51	17.2	2.2	9.9	11.1	11.0
52	15.0		9.4	10.6	11.5
53	12.1		7.75	8.5	10.0
54	10.2		6.7	7.5	10.5
56	6.6		3.65	4.05	10.0
58	10.4	4.5	7.45	8.3	10.0
60	8.8		6.2	6.8	9.0
61	7.2		4.9	5.4	9.0
62	8.05		5.2	5.7	8.5

Table 5 (contd.)

64	10.1	3.4	6.1	6.8	10.0
65	9.75		6.2	6.85	8.5
67	6.55		4.35	4.7	7.0
69	7.2		4.7	5.05	7.0

source of decomposition outside the irradiation area would be by reaction 3.11:

$$O(^3P) + O_3 \rightarrow 2O_2 \qquad 3.11$$

The rate constant for 3.11 is about $2\text{-}3\times10^6$ mole^{-1} l sec^{-1} [87] and with a time scale of about 2.5×10^{-1} secs and with $[O(^3P)] \lesssim 10^{-8}$ mole l^{-1} there is very little decay of ozone due to reaction 3.11.

3.8 Kinetic analysis.

The following reaction scheme was proposed:

$$O_3 + h\nu \rightarrow O_2 + O(^1D) \qquad 3.1$$

$$O(^1D) + O_2 \rightarrow O_2(^1\Delta g) + O(^3P) \qquad 3.2$$

$$O(^1D) + O_2 \rightarrow O_2 + O(^3P) \qquad 3.3$$

$$O(^1D) + O_3 \rightarrow 2O_2 \qquad 3.4$$

$$O_2(^1\Delta g) + O_3 \rightarrow 2O_2 + O(^3P) \qquad 3.5$$

$$O_2(^1\Delta g) + O_2 \rightarrow 2O_2 \qquad 3.6$$

$$O_2(^1\Delta g) + \text{Wall} \rightarrow O_2 \qquad 3.7$$

$$O_2(^1\Delta g) \rightarrow O_2 + h\nu \qquad 3.8$$

It is not apparent whether, in the irradiation area,

$O(^1D)$ atoms can be treated by a steady state approximation. Thus a non-steady state analysis was carried out first. In the irradiation section only:

$$\frac{d[O(^1D)]}{dt} = k_1 I_o [O_3] - k_2 [O(^1D)][O_2] - k_3 [O(^1D)][O_2] - k_4 [O(^1D)][O_3] \qquad 3.A$$

now when $t = 0$, $[O(^1D)] = 0$

$$\therefore [O(^1D)] = \frac{k_1 I_o [O_3]}{(k_2+k_3)O_2 + k_4[O_3]} \left\{1 - e^{-[(k_2+k_3)O_2 + k_4[O_3]]t}\right\} \qquad 3.B$$

The major source of deactivation of $O_2(^1\Delta g)$ is by ozone. However, the maximum concentration of ozone was about 2×10^{-6} mole l^{-1} and the residence time in the irradiation area was about 3×10^{-2} secs, so the deactivation of $O_2(^1\Delta g)$ by ozone was clearly going to be very small. Therefore, in the irradiation zone no deactivation reactions of $O_2(^1\Delta g)$ were considered.

$$\frac{d[O_2(^1\Delta g)]}{dt} = k_2 [O(^1D)][O_2] \qquad 3.C$$

Introducing B into C

$$\frac{d[O_2(^1\Delta g)]}{dt} = \frac{k_1 k_2 I_o [O_2][O_3]}{a} [1 - e^{-at}] \qquad 3.D$$

where $a = [(k_2 + k_3)[O_2] + k_4[O_3]]$

when $t = 0$, $[O_2(^1\Delta g)] = 0$

$$\therefore O_2(^1\Delta g) = \frac{k_1 k_2 I_o [O_2][O_3]}{a} [t - \frac{1}{a}(1-e^{-at})] \qquad 3.E$$

Consider now the steady state approach for $[O(^1D)]$

$$0 = \frac{d[O(^1D)]}{dt} = k_1 I_o [O_3] - k_2 [O(^1D)][O_2] - k_3 [O(^1D)][O_2] - k_4 [O(^1D)][O_3] \qquad 3.F$$

$$[O(^1D)] = \frac{k_1 I_o [O_3]}{a} \qquad 3.G$$

and

$$\frac{d[O_2(^1\Delta g)]}{dt} = k_2 [O(^1D)][O_2] \qquad 3.H$$

$$\therefore \int_o^{\Delta_o} d[O_2(^1\Delta g)] = \int_o^t \frac{k_1 k_2 I_o [O_2][O_3] dt}{a} \qquad 3.I$$

$$[O_2(^1\Delta g)]_o = \frac{k_1 k_2 I_o [O_2][O_3] t}{a} \qquad 3.J$$

In our system for a typical run $[O_3] \approx 10^{-6}$ mole l^{-1}, $[O_2] \approx 3 \times 10^{-5}$ mole l^{-1}, $[k_2 + k_3] \approx 3 \times 10^{10}$ mole^{-1} l sec^{-1} [39,52], $k_4 \approx 2 \times 10^{11}$ mole^{-1} l sec^{-1} [90] and $t = 3 \times 10^{-2}$ secs. Hence $a \approx 10^6$ sec^{-1}.

Using these values it is clear that equations E and J, B and G are virtually identical, and it seems reasonable to adopt the steady state approach for the kinetic analysis of our results.

Consider equation J:

$$[O_2(^1\Delta g)]_o = \frac{k_1 k_2 I_o [O_2][O_3] t}{(k_2+k_3)[O_2] + k_4 [O_3]} \qquad 3.K$$

If $[O_2]$ is kept constant during a run and only $[O_3]$ is varied then:

$$[O_2(^1\Delta g)]_o \left((k_2+k_3)[O_2] + k_4 [O_3]\right) = k_1 k_2 I_o [O_2][O_3] t \qquad 3.L$$

therefore:

$$[O_2(^1\Delta g)]_o = \frac{-[O_2(^1\Delta g)]_o (k_2+k_3)[O_2]}{[O_3]} \frac{}{k_4} + \frac{k_2 k_1 I_o [O_2] t}{k_4} \qquad 3.M$$

For a given run in which $[O_2]$ is kept constant, then $k_1 I_o [O_2]$ will be constant and a plot of $[O_2(^1\Delta g)]_o$ against $\frac{[O_2(^1\Delta g)]_o}{[O_3]}$ should give a straight line. This was done for runs A - F and the plots are shown in figure 33. From equation 3.M, the slope of these plots is $\frac{(k_2+k_3[O_2]}{k_4}$. The slopes are listed in Table 4. A plot of these slopes against the relevant oxygen concentration gives a straight line, the slope of which is $\frac{(k_2+k_3)}{k_4}$, (see figure 34). The value of $\frac{k_2+k_3}{k_4}$ is 8.6×10^{-2}. The value of k_3 has been recently established as about 3×10^{10} moles^{-1} l sec^{-1} although as pointed out later in chapter 4 (section 4.11), there is still some uncertainty about its value [38,39], and if it is assumed that $k_2 << k_3$, then (k_2+k_3) is 3×10^{10} moles^{-1} l sec^{-1} and k_4 is therefore 3.5×10^{11} mole^{-1} l sec^{-1}. This result is in fairly good agreement with the results of Snelling [90] and Katakis [91] and is discussed together with the likely errors later in the chapter.

From equation 3.M the intercept of the straight line in figure 33 is $\frac{k_2 k_1 I_o [O_2]t}{k_4}$. The values of the intercepts are listed in Table 4. A plot of the intercept against $[O_2]t$ gives a straight line, figure 35, of slope $\frac{k_2}{k_4} k_1 I_o$. In order to obtain the value of $\frac{k_2}{k_4}$ it is necessary to know $K_1 I_o$. From figure 32 it can be seen that the percentage

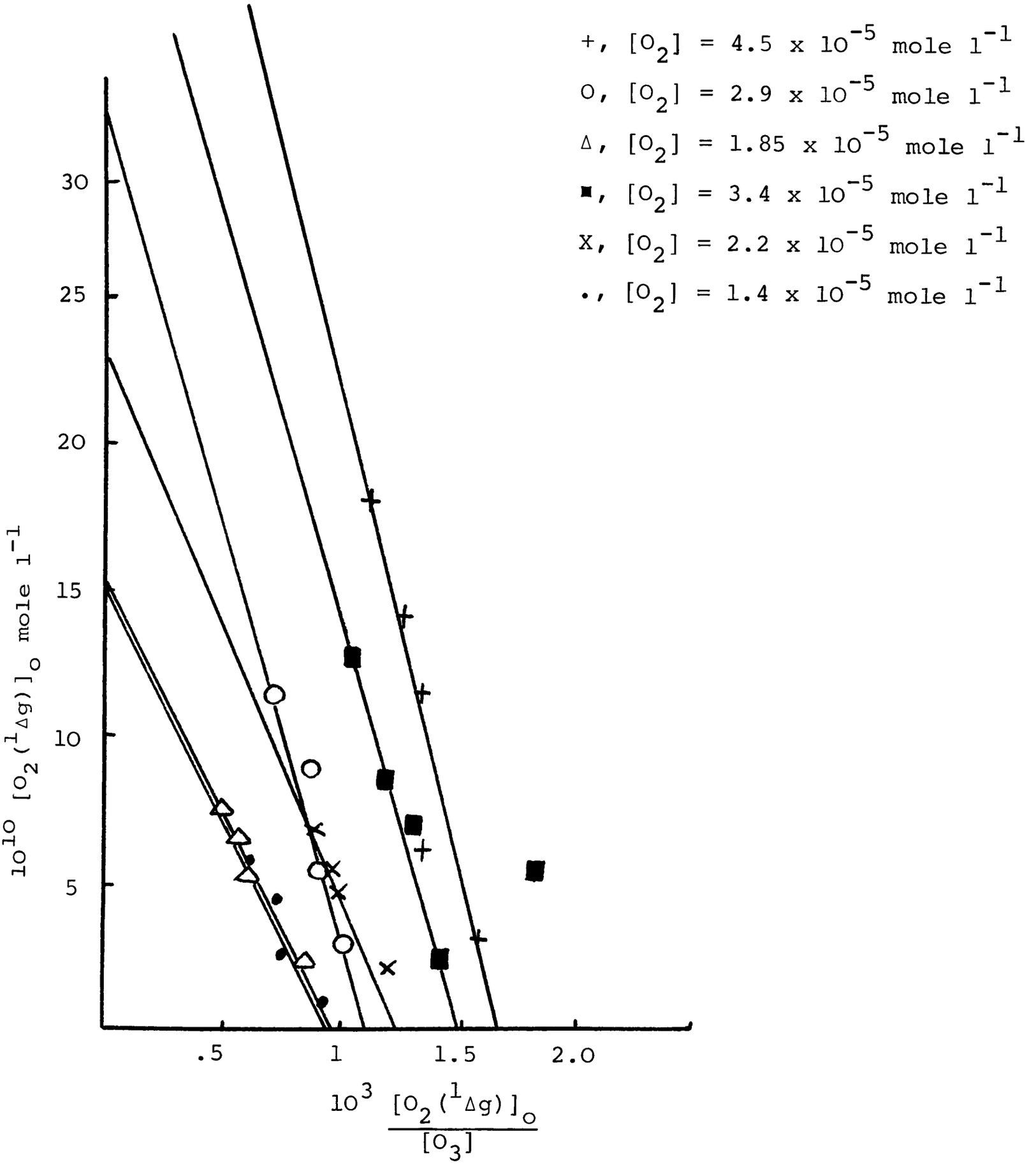


Figure 33. Dependence of $[O_2(^1\Delta g)]_o$ on $\frac{[O_2(^1\Delta g)]_o}{[O_3]}$ for various oxygen concentrations

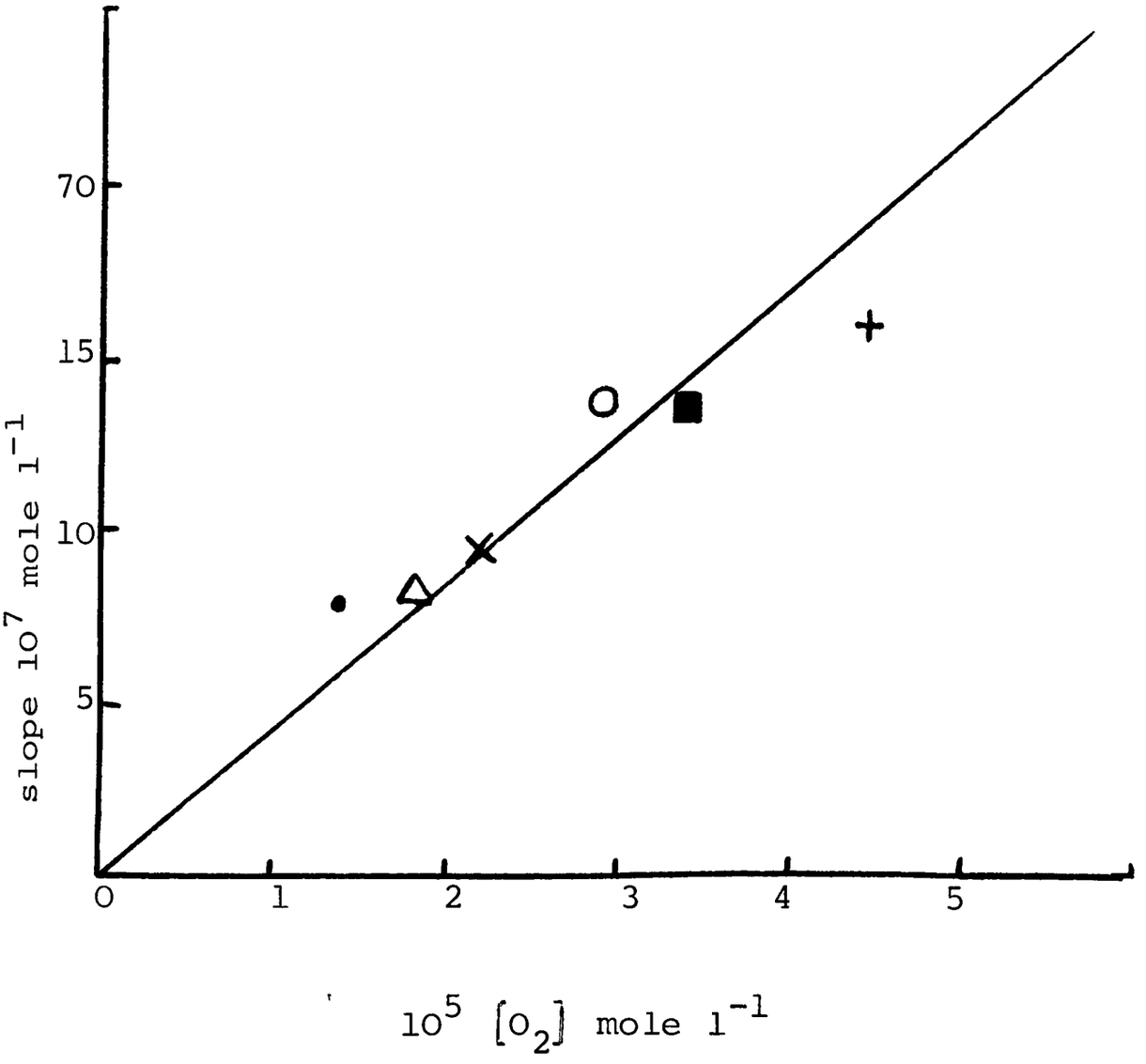


Figure 34. Dependence of slope of plots in figure 33 with oxygen concentration

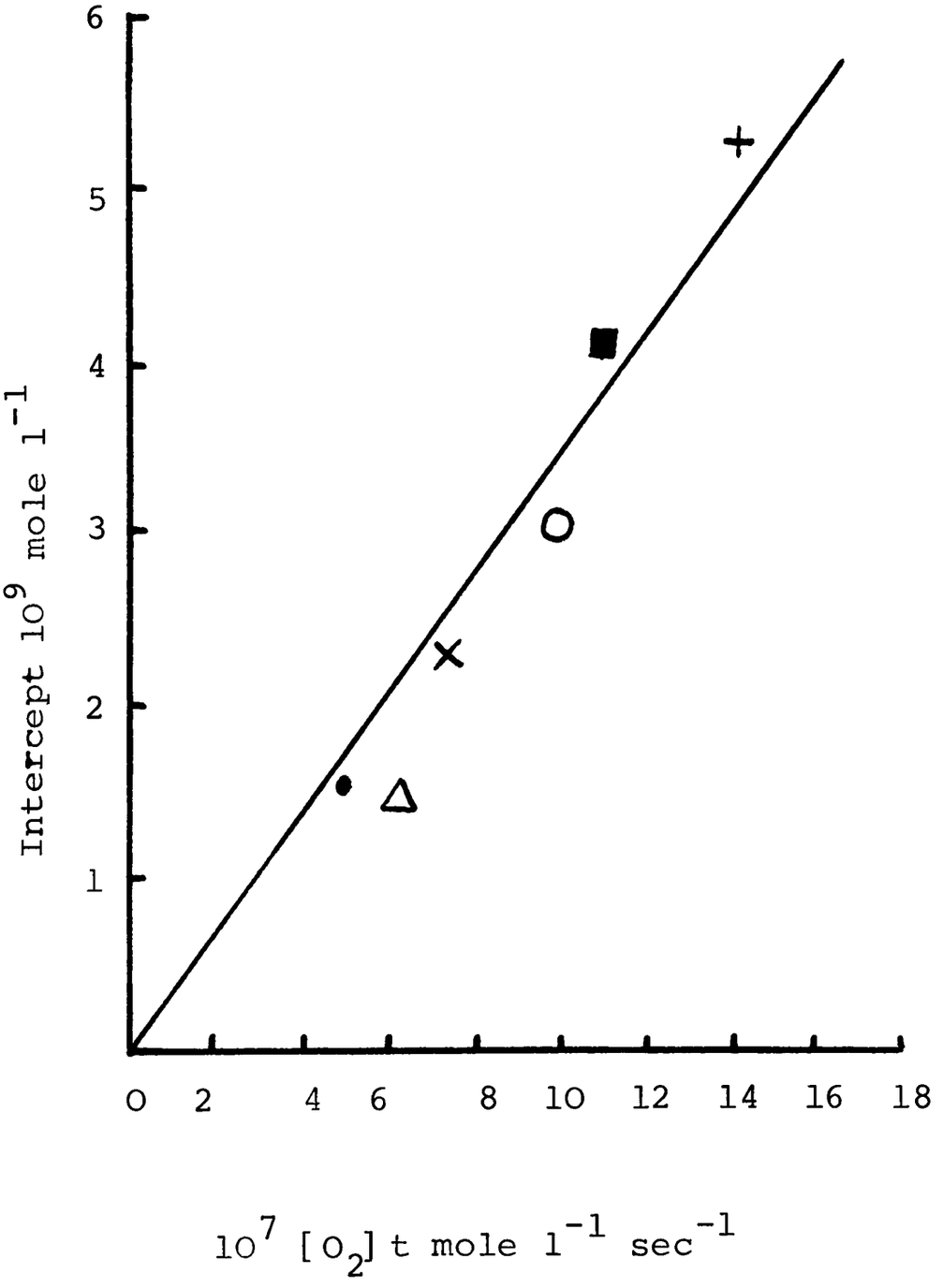


Figure 35. Dependence of intercept plots in figure 33 on [O_2]t

decomposition of ozone varies with oxygen concentration. At lower oxygen concentrations when the residence time is longer the decomposition is more pronounced. To evaluate $k_1 I_o$ the complete ozone decomposition differential equation was considered:

$$\frac{d[O_3]}{dt} = -k_1 I_o [O_3] - k_4 [O(^1D)][O_3] \qquad 3.N$$

Substituting G in N

$$\frac{d[O_3]}{dt} = -k_1 I_o [O_3] - \frac{k_4 k_1 I_o [O_3]^2}{(k_2+k_3)[O_2]+k_4[O_3]} \qquad 3.O$$

Putting $\alpha = k_1 I_o$, $\beta = k_4$ and $\gamma = (k_2+k_3)[O_2]$

$$\frac{d[O_3]}{dt} = -\alpha[O_3] - \frac{\alpha\beta[O_3]^2}{(\gamma+\beta[O_3])} \qquad 3.P$$

rearranging the equation,

$$\frac{d[O_3]}{dt} = \frac{(-\alpha\gamma[O_3] - 2\alpha\beta[O_3]^2)}{(\gamma + \beta[O_3])} \qquad 3.Q$$

Integrating between $[O_3]_t$ and $[O_3]_o$

$$\int_{[O_3]_o}^{[O_3]_t} \left(\frac{1}{\alpha[O_3]} - \frac{\beta/\alpha}{\gamma+2\beta[O_3]}\right) d[O_3] = \int_o^t -dt \qquad 3.R$$

$$\therefore \frac{(\gamma+ 2\beta[O_3]_o)^{\frac{1}{2}}}{(\gamma+ 2\beta[O_3]_{t_1})^{\frac{1}{2}}} \cdot \frac{[O_3]_t}{[O_3]_o} = e^{-\alpha t} \qquad 3.S$$

In full form S becomes

$$\frac{[O_3]_t}{[O_3]_o} = \left\{ \frac{\left(\frac{k_2+k_3}{k_4}\right)[O_2] + 2[O_3]_o}{\left(\frac{k_2+k_3}{k_4}\right)[O_2]+2[O_3]_t} \right\}^{-\frac{1}{2}} e^{-k_1 I_o t} \qquad 3.T$$

$$\therefore k_1 I_o = \frac{2.303}{t} \log \frac{O_3\ t}{O_3\ o} \left(\frac{(\frac{k_2+k_3}{k_4})[O_2] + 2[O_3]_o}{(\frac{k_2+k_3}{k_4})[O_2] + 2[O_3]_t} \right)^{\frac{1}{2}} \qquad 3.U$$

The values of $[O_3]_t$ and $[O_3]_o$ are presented in Table 6, using the value of $\frac{k_2+k_3}{k_4}$, taken from figure 34, as 8.6×10^{-2}.

The value of $k_1 I_o$ was calculated for each run and the results presented in Table 6. The values obtained are substantially constant and give confidence in the validity of this approach for obtaining $k_1 I_o$. An average value of $k_1 I_o$ was taken as 3.25 sec^{-1}. From figure 35, the slope of the plot, i.e. $\frac{k_2}{k_4} k_1 I_o$, is 3.5×10^{-3} secs, thus giving $\frac{k_2}{k_4} = 1.05 \times 10^{-3}$. It has been established earlier in the kinetic analysis (from figure 34) that the value of $k_4 = 3.5 \times 10^{11}$ $mole^{-1}$ l sec^{-1}. Taking this value, the rate constant for reaction 3.2 is 3.5×10^{8} $mole^{-1}$ l sec^{-1}.

Before reaching any definite value of k_2 and k_4 the likely errors must be considered. The major error is probably in the measurement of the residence time t_1, since this does involve movement of the detection apparatus. The residence time used in the above kinetic analysis was 0.25 secs. It was thought worthwhile to take residence times of 0.4 secs and 0.1 secs and compare the resulting values of k_2 and k_4 with those obtained using $t_1 = 0.25$ secs. When the residence time was 0.1 secs, $k_2 = 2.5 \times$

Table 6.

Run No.	$10^7[O_3]_o$ mole l^{-1}	$10^7[O_3]_t$ mole l^{-1}	$10^2 t$ sec.	$\left\|\frac{.086[O_2]+2[O_3]_o}{.086[O_2]+2[O_3]_t}\right\|^{\frac{1}{2}}$	$k_1 I_o$ sec^{-1}
16	13.7	12.3	3.4	.328	3.20
17	16.0	13.7		.333	3.10
19	10.0	9.1		.325	3.21
20	7.3	6.65		.324	3.18
21	5.4	4.95		.323	3.20
30	10.1	8.8	3.4	.329	3.15
31	8.7	7.8		.327	3.17
32	7.7	6.8		.327	3.11
34	5.5	5.0		.323	3.17
35	4.3	4.05		.321	3.19
43	15.5	14	3.3	.325	3.24
44	18.5	16.5		.327	3.31
45	12.7	11.5		.327	3.29
46	11.0	9.9		.324	3.24
48	15.2	13.7		.326	3.25
49	7.5	6.9		.321	3.28
51	17.2	15.3	3.3	.328	3.25
52	15.0	13.3		.328	3.25
53	12.1	10.9		.327	3.25
54	10.2	9.1		.327	3.25
56	6.6	5.95		.323	3.22
58	10.4	9.35	3.1	.321	3.49
60	8.8	8.0		.321	3.45
61	7.2	6.55		.321	3.45
62	8.00	7.35		.319	3.51
64	10.1	9.1	3.2	.323	3.32
65	9.75	8.8		.323	3.32
67	6.55	6.1		.321	3.40
69	7.2	6.7		.320	3.40

10^8 mole^{-1} l sec^{-1} and $k_4 = 3 \times 10^{11}$ mole^{-1} l sec^{-1}. When the residence time was 0.4 secs, $k_2 = 5.5 \times 10^8$ mole^{-1} l sec^{-1} and $k_4 = 4.1 \times 10^{11}$ mole^{-1} l sec^{-1}. Consideration of the values gives an idea of the likely error of k_2 and k_4 expected in an experiment of this nature. The final values were taken as:

$$k_2 = 3.5\ (\pm\ 2) \times 10^8 \text{ mole}^{-1} \text{ l sec}^{-1}$$

$$k_4 = 3.5\ (\pm\ .6) \times 10^{11} \text{ mole}^{-1} \text{ l sec}^{-1}$$

The rate constant for reaction 3.2 cannot be compared as yet with any other workers, although it compares favourably with an upper limit of $k_2 < 6 \times 10^8$ mole^{-1} l sec^{-1} set by Izod and Wayne [33], from experiments carried out on the photolysis of oxygen (see Chapter 4).

The most recent determination of k_4 is that of Snelling, who obtained a value of $2(\pm\ 1)\ 10^{11}$ mole^{-1} l sec^{-1} which is in good agreement with the present result. Katakis [91] has obtained a value for the ratio of $\frac{k_4}{k_{12}} = 4 \pm 1$ where k_{12} is the rate constant for the following reaction:

$$O(^1D) + H_2O \rightarrow OH^+ + OH \qquad 3.12$$

The most reliable value of k_{12} is that given by Schofield [59] (from comparison of results obtained by Dixon-Lewis et al [114]) as $k_{12} = 8.4 \times 10^{10}$ mole^{-1} l sec^{-1}, which suggests that $k_4 = 3.4\ (\pm 1) \times 10^{11}$ mole^{-1} l sec^{-1}, a value in good agreement with that obtained from our

experiments.

3.9 Deactivation of $O_2(^1\Delta g)$ by reaction with ozone.

The monochromator and germanium detector combination proved conclusively that the observed emission in irradiated ozone-oxygen mixtures, with λ = 253.7 nm, was due to $O_2(^1\Delta g)$. However, between the time of receiving the apparatus (May, 1969) and the preliminary observations (February, 1968), the following experiment to be described in this section was carried out in an attempt to prove indirectly that $O_2(^1\Delta g)$ was present.

If $O_2(^1\Delta g)$ was the observed emission, then it should be possible to measure the decay of the species by reaction with ozone and so obtain a rate constant for reaction 3.5:

$$O_3 + O_2(^1\Delta g) \rightarrow 2O_2 + O(^3P) \qquad 3.5$$

Comparison of this value with generally accepted values of k_5 should indicate whether or not the species could be $O_2(^1\Delta g)$.

The flow system adopted is shown in figure 36. It was found that the cooled 7102 photomultiplier, operated at 1500 volts D.C., with the end window fully exposed to the flow line did detect measurable amounts of radiation through the 1270 nm interference filter. Thus the gold bulb was not required, and hence the kinetic analysis was more straightforward. The actual detection area was by necessity large (see figure 37), and no attempt was made to collimate the beam reaching the detector.

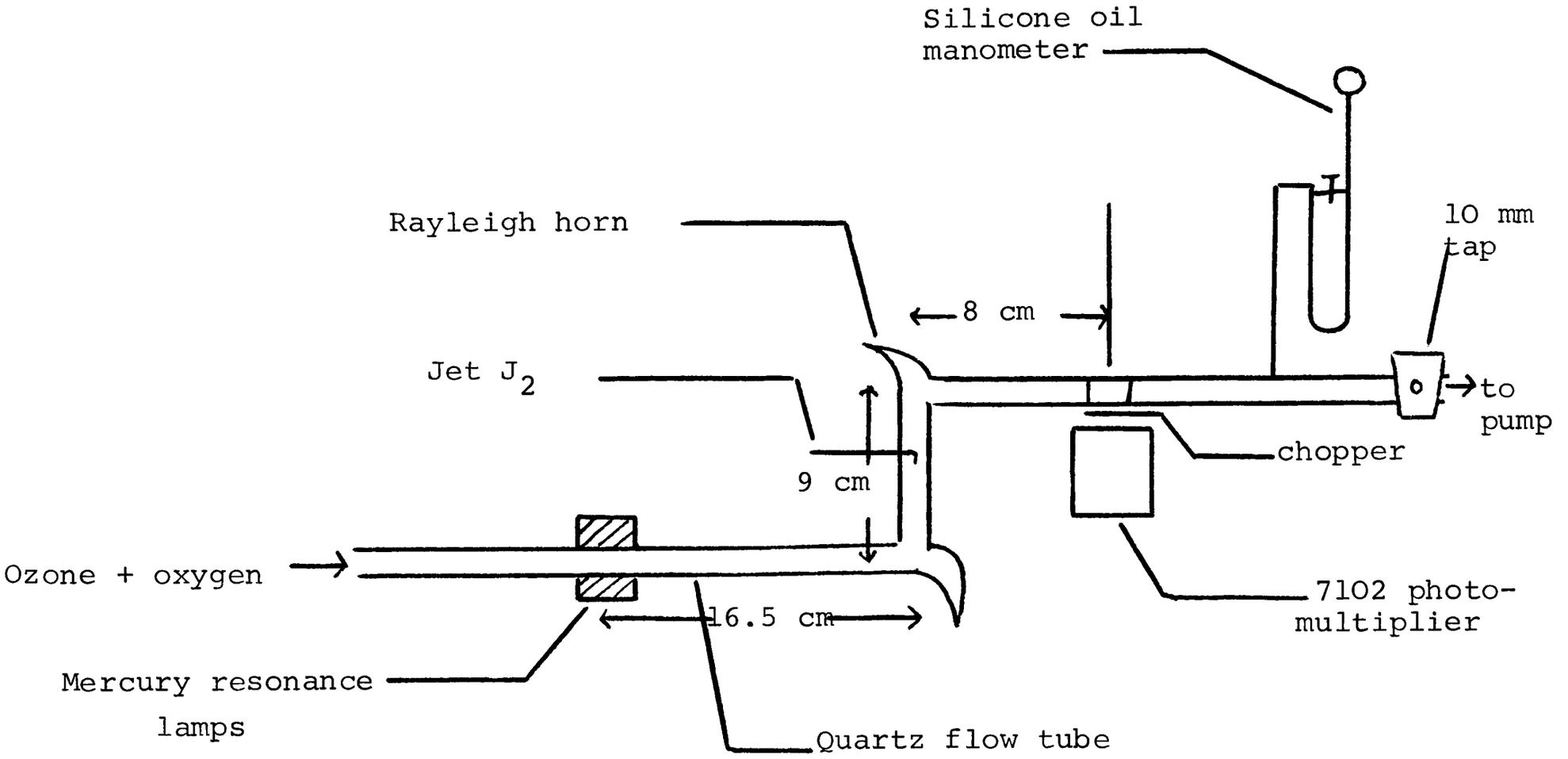


Figure 36. Flow system for measuring the deactivation of $O_2(^1\Delta g)$ by reaction with ozone

Ozone could be introduced, after irradiation, to the ozone-oxygen mixture through Jet J_2. The concentrations employed were typically $\sim 10^{-6}$ mole l^{-1}, so that the flow conditions in the main tube were not disturbed. Linear flow velocities of about 2 meters sec^{-1} were used.

As pointed out in the discussion of the preliminary experiments, a background impurity signal was present, which decreased with increasing oxygen concentration. Clearly, a correction has to be made to any signal at 1270 nm for this background emission. Figure 38 shows the percentage change in background signal, viewed through a 700 nm interference filter for given ozone concentrations, when oxygen was added. When $[O_2]$ is about 2×10^{-5} moles l^{-1} the background is in the region of a few percent, and so most experiments were carried out with $[O_2] \geq 2 \times 10^{-5}$ moles l^{-1}. A small correction was made for each signal as described in section 3.4.

In an experimental run the main ozone-oxygen flow was kept constant and the signal at 1270 nm recorded. Known concentrations of ozone were then added at J_2 and the decrease in signal recorded. The main flow was then altered and the same procedure repeated.

The loss reactions for $O_2(^1\Delta g)$ taking place after irradiation are as follows:

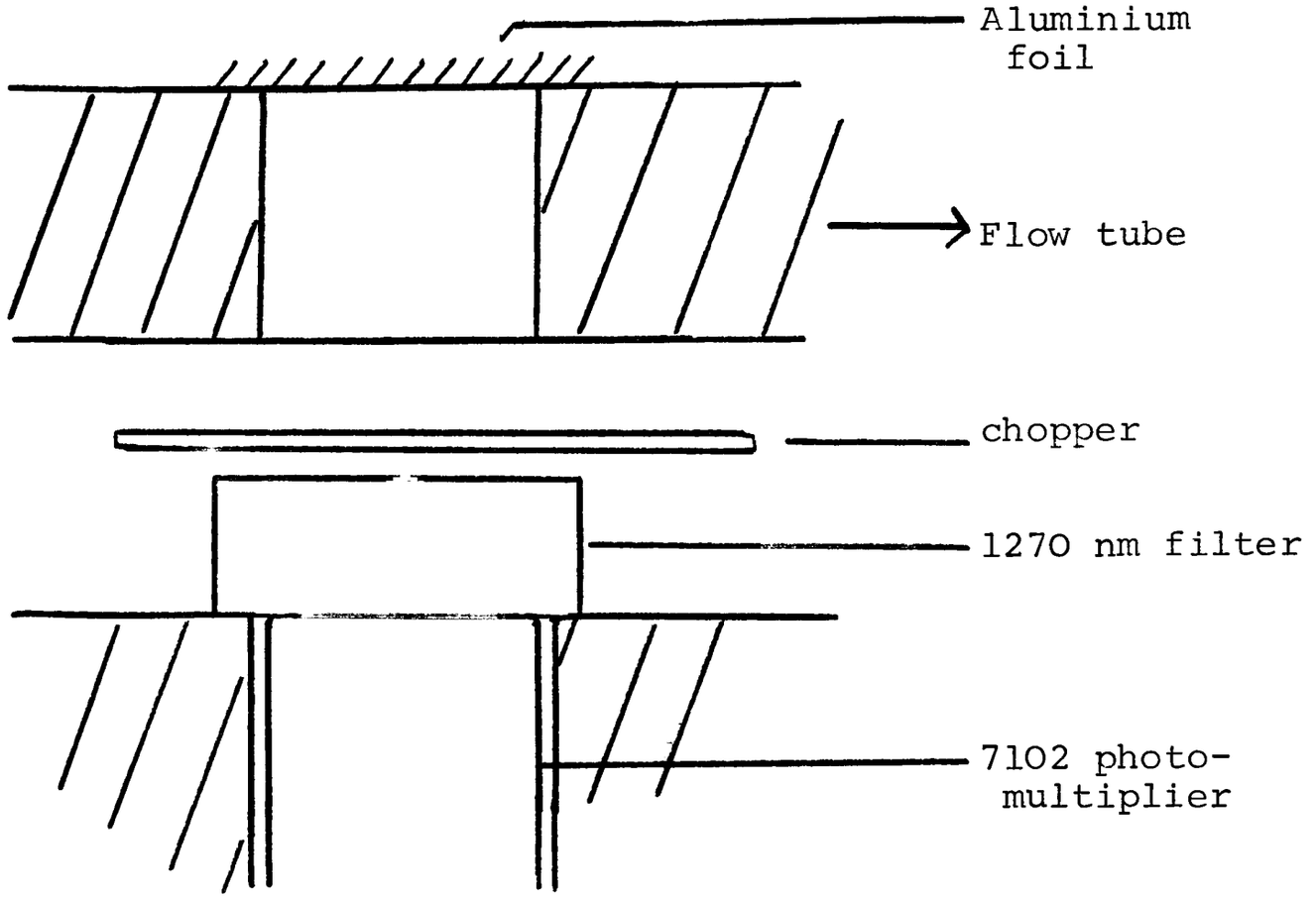


Figure 37. Diagram of the observation area (to scale) to experiments described in section 3.9

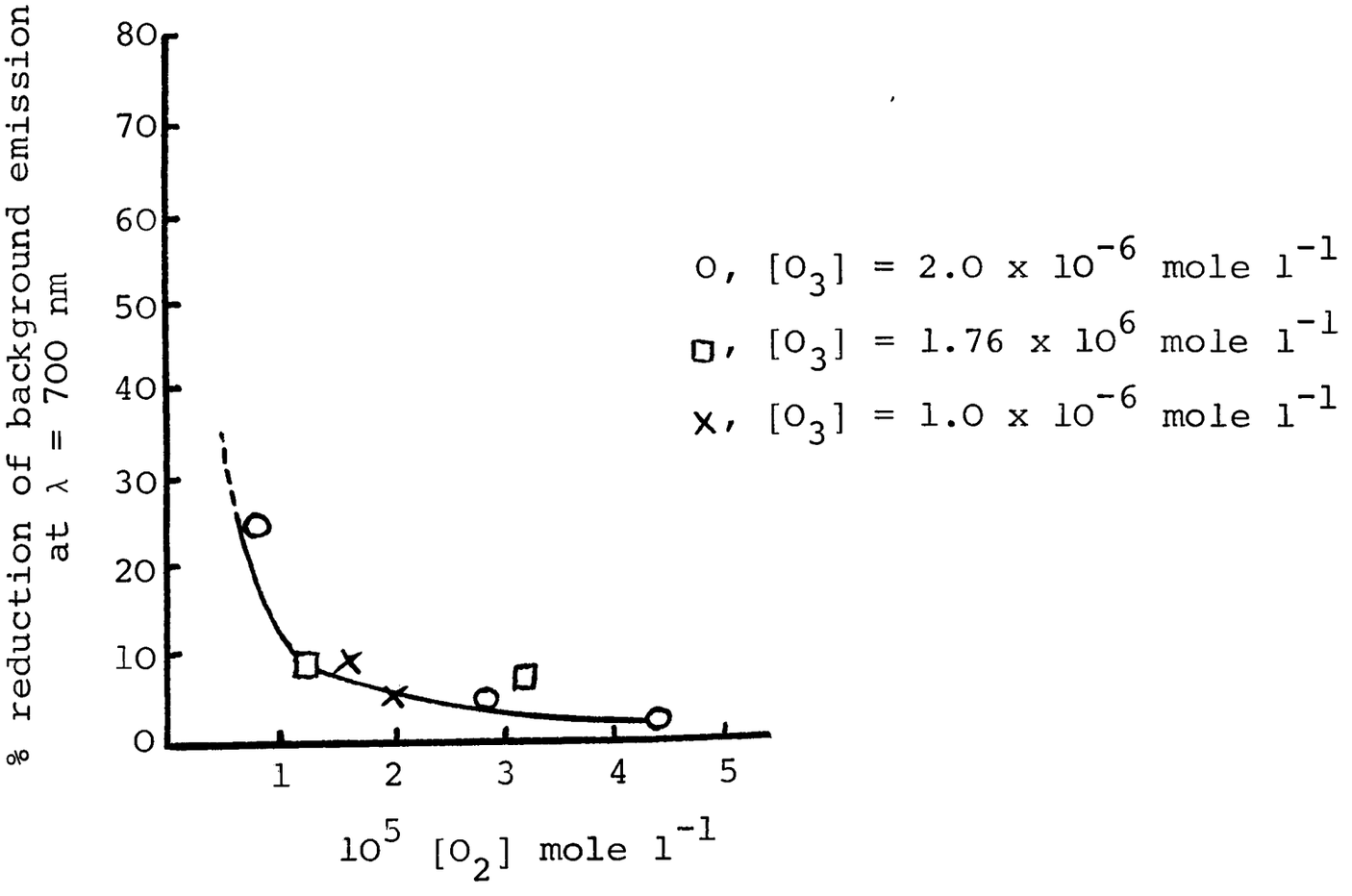


Figure 38. Percentage variation of the background emission at λ = 700 nm with increasing oxygen concentration

$$O_2(^1\Delta g) + O_3 \rightarrow 2O_2 + O(^3P) \qquad 3.5$$

$$O_2(^1\Delta g) + O_2 \rightarrow 2O_2 \qquad 3.6$$

$$O_2(^1\Delta g) \xrightarrow{wall} O_2 \qquad 3.7$$

$$O_2(^1\Delta g) \rightarrow O_2 + h\nu \qquad 3.8$$

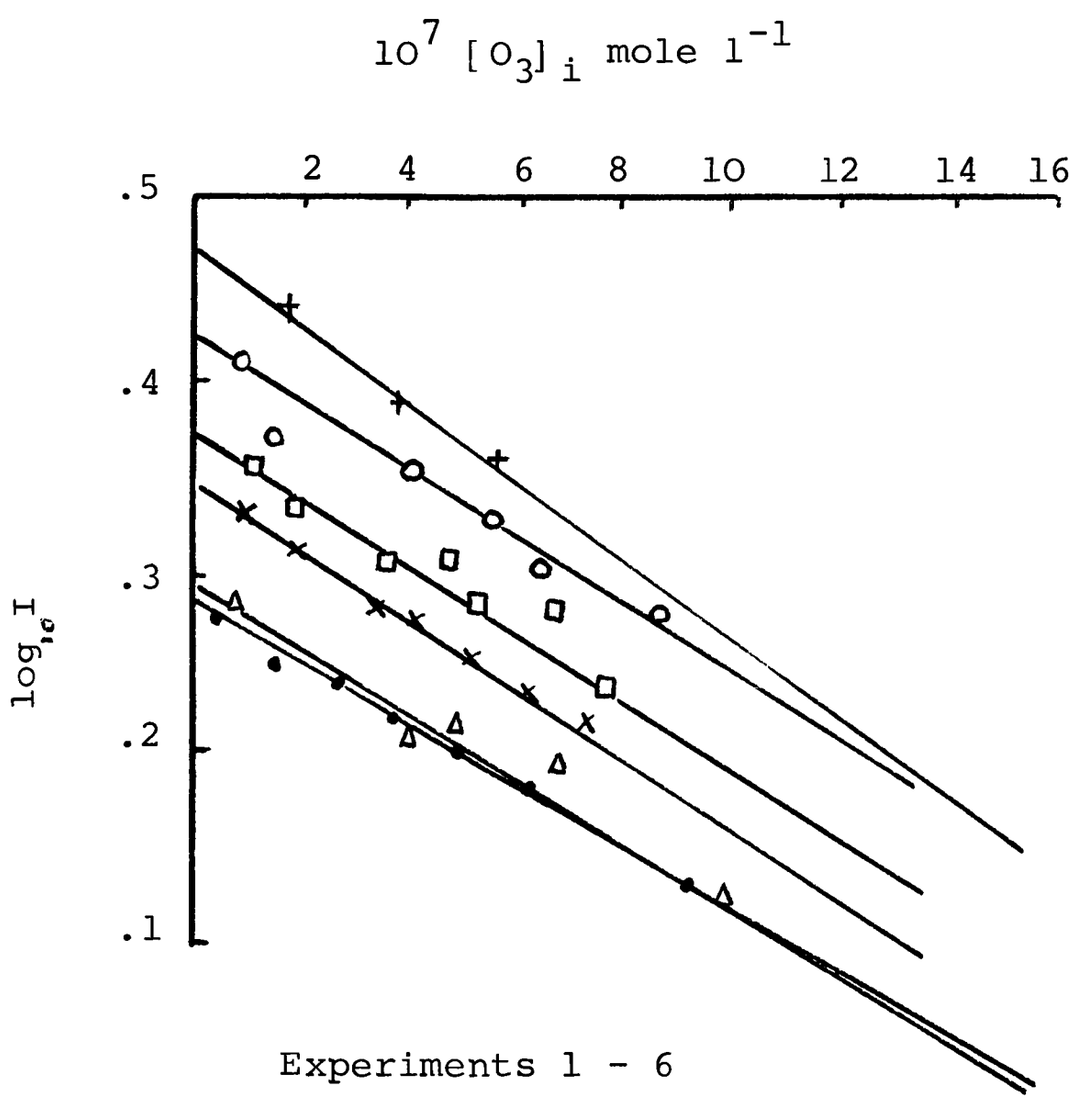
If the ozone $[O_3]_c$ + oxygen $[O_2]$ irradiation mixture is kept constant, and only the ozone concentration $[O_3]_i$ introduced at J_2 is varied, then the intensity I of the $O_2(^1\Delta g)$ signal in arbitrary units is given by:

$$\ln I = -k_5[O_3]_i t_2 - k_5[O_3]_c t_2 - k_6[O_2]t_2 - k_7[t_2] - k_8 t_2 \qquad 3.V$$

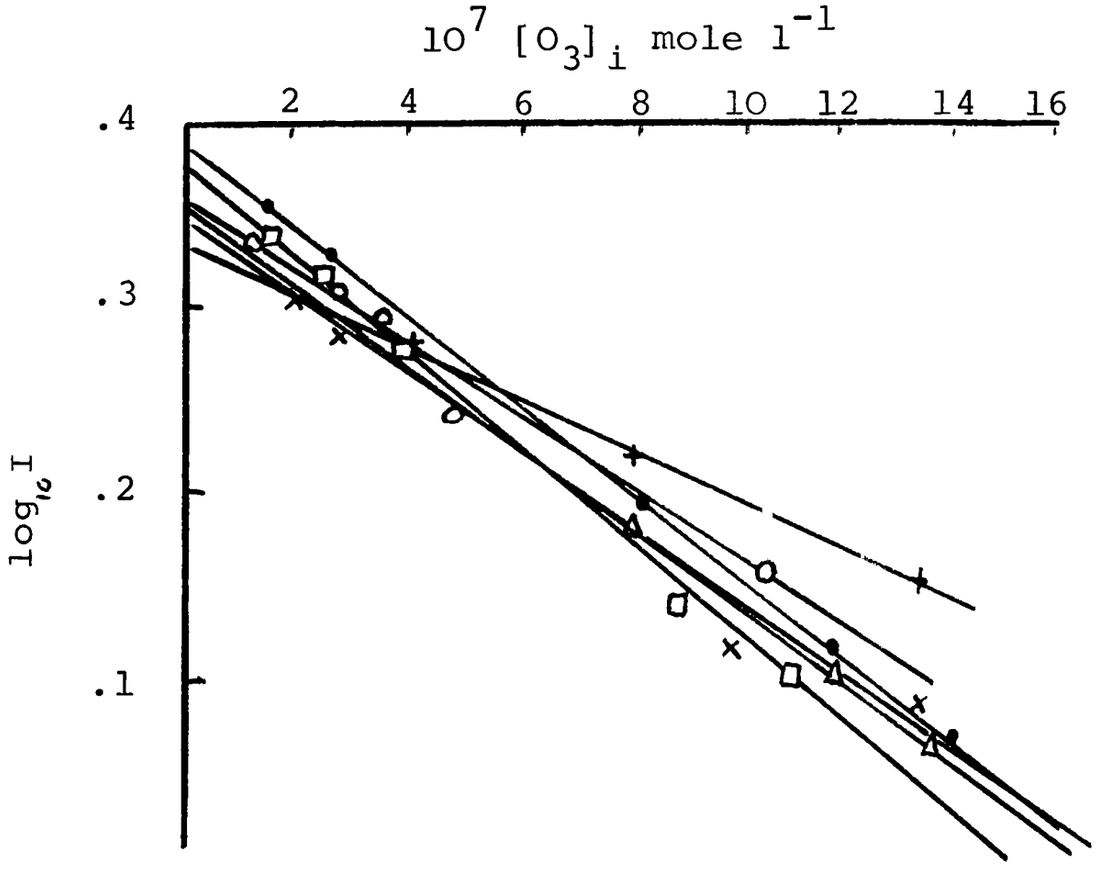
$$= - k_5[O_3]_i t_2 - \text{constant.} \qquad 3.W$$

where t_2 is the time from J_2 to the centre of the observation area. If the above conditions hold true then a plot of lnI against $[O_3]_i$ should give a straight line of slope $-k_5t_2$. Figure 39 shows the plots of logI against $[O_3]_i$ for a number of ozone-oxygen mixtures. Table 7 lists the conditions and the value of k_5 obtained from each slope from figure 39.

The major error in these experiments was in the value adopted of t_2. From figure 37 it is apparent that the light acceptance area of the photomultiplier is large. In fact there is about a 6 cm emitting source along the flow tube, which leads to a possible error in the measurement of t_2 of about 35%. The average value of k_5 taken from

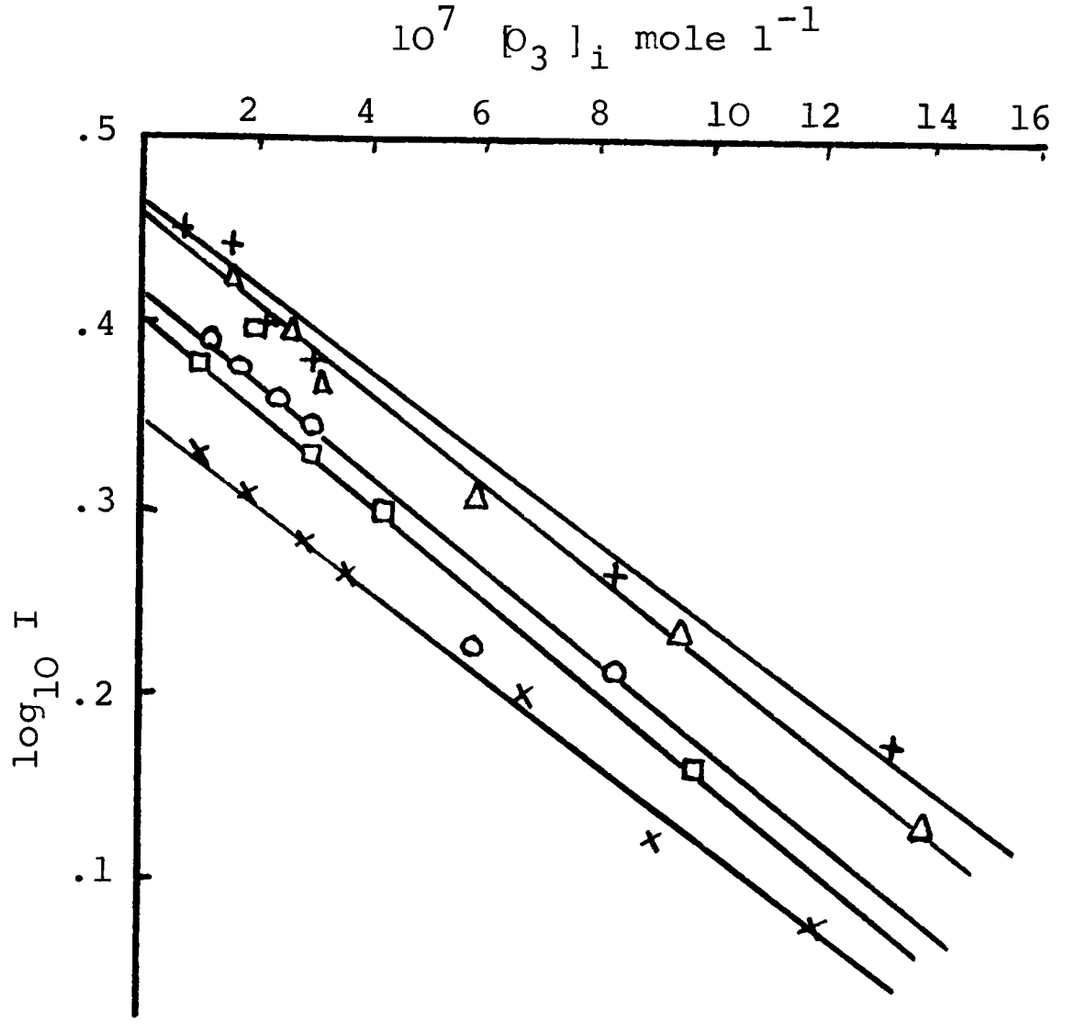


Experiments 1 - 6

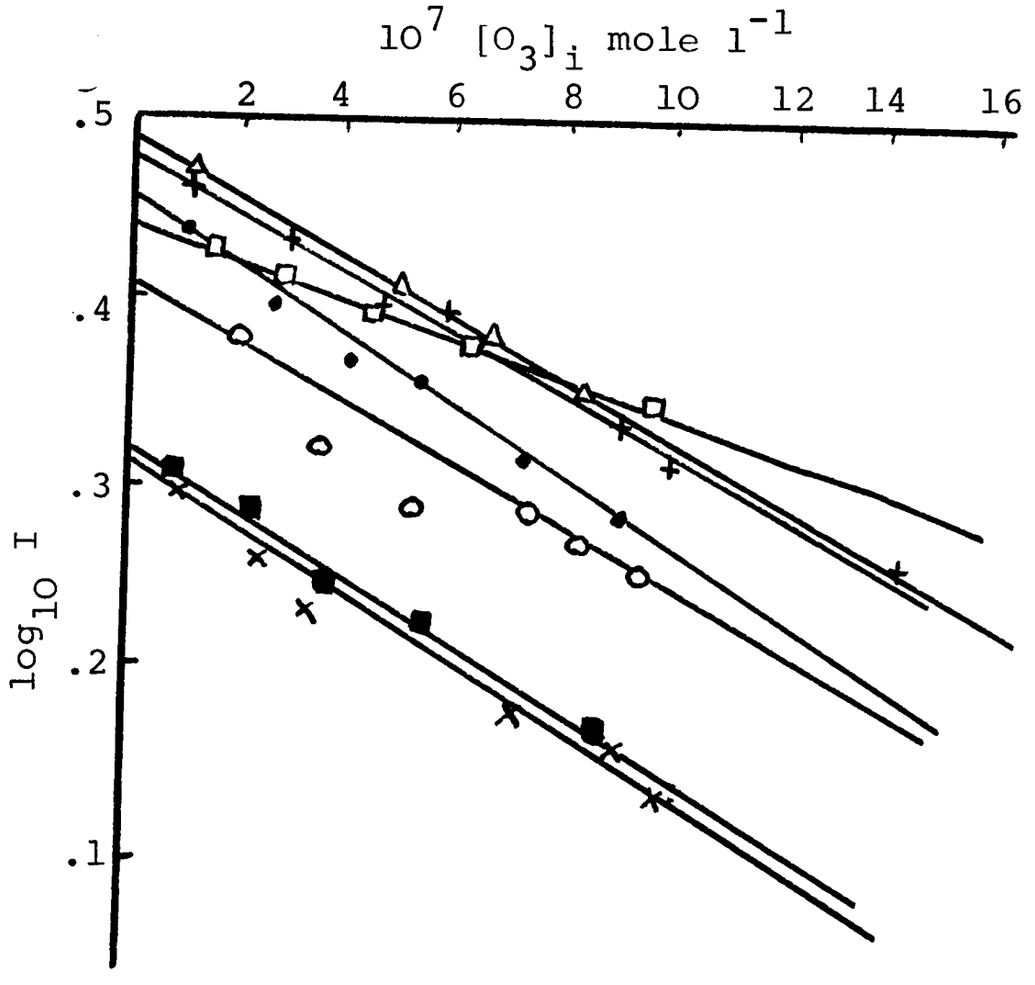


Experiments 7 - 12

Figures 39. Variation of $\log_{10} I$ with added ozone



Experiments 13 - 17



Experiments 18 - 24

Figure 39. (continued)

Table 7. Values of k_5 obtained from the slopes in figure 39 at various ozone and oxygen concentrations

Run No. and Legend	$10^5[O_2]$ mole l^{-1}	$10^6[O_3]$ mole l^{-1}	10^6 k_5 mole^{-1} l sec^{-1}	flow velocity cm sec^{-1}
1 O	2.4	2.05	4.3	150
2 □		1.82	4.25	"
3 X		1.53	4.5	"
4 Δ		1.33	4.0	"
5 .		1.55	4.1	"
6 +		2.58	4.15	"
7 +	2.0	1.43	2.95	135
8 O		1.17	4.0	"
9 X		1.04	4.2	"
10 □		0.87	5.3	"
11 Δ		1.00	4.35	"
12 .		1.20	4.4	"
13 +	2.2	1.48	4.0	140
14 O		1.11	4.3	"
15 X		0.89	4.1	"
16 □		1.38	4.4	"
17 Δ		1.92	4.25	"
18 +	3.35	2.00	3.65	162
19 O		1.40	4.05	"
20 X		1.06	3.95	"
21 □		1.57	2.70	"
22 ▲		2.19	3.65	"
23 .		2.26	4.15	"
24 ■		1.12	4.45	"

table was k_5 = 4.1 (± 1.5) x 10^6 $mole^{-1}$ l sec^{-1}.

The values quoted by other workers are k_5 = 2-3 x 10^6 $mole^{-1}$ l sec^{-1} [92], 1.7(± .5) x 10^6 $mole^{-1}$ l sec^{-1} [93] and 2 x 10^6 $mole^{-1}$ l sec^{-1} [94]. Thus the value obtained lies fairly close, within the experimental error, to the values quoted above, and is consistent with the production of $O_2(^1\Delta g)$ during photolysis of ozone-oxygen mixtures at λ = 253.7 nm.

3.10 Photolysis of ozone at $\lambda \geq 266$ nm.

It has been suggested that $O_2(^1\Delta g)$ may be formed in the primary step of ozone photolysis at $\lambda \geq 266$ nm [34], but not at shorter wavelengths. Attempts were made to detect $O_2(^1\Delta g)$ using two medium pressure mercury lamps (Ediswan) as the photolytic source. These lamps yield most intense lines around 303 nm and 366 nm, although there were contributions from 253.7 nm [10]. The two lamps were operated separately from a Philips 400 watt and 125 watt choke. An air blast was employed to cool the lamps which become very hot during operation. The flow apparatus was similar to that in figure 27. No $O_2(^1\Delta g)$ was observed, with either the germanium detector or the 7102 photomultiplier, over the concentration range (5 x 10^{-7} mole l^{-1} to 10^{-5} mole l^{-1}) of ozone employed.

However, this experiment does not provide unequivocal evidence for the non-production of $O_2(^1\Delta g)$ at $\lambda \geq 266$ nm

for a number of technical reasons. Firstly, the intensity from the lamps was not high and, secondly, the small absorption coefficient of ozone at $\lambda \sim 300$ nm, figure 3, suggests that at the concentrations employed very little reaction would occur. A more refined apparatus is needed to test this idea.

CHAPTER 4

PHOTOLYSIS OF OXYGEN BY ULTRA VIOLET RADIATION

4.1 Summary.

This chapter describes experiments to study the kinetic reactions of $O_2(^1\Sigma g^+)$. The source of excited oxygen was obtained from the ultra violet photolysis of oxygen at λ = 147 nm and the merits of this mode of production over other methods is discussed. A time resolved flow system is described which was used to evaluate the rate constants of the following reactions:

$$O_2(^1\Sigma g^+) + O_3 \rightarrow 2O_2 + O(^3P) \qquad k_3 = 4.3 \times 10^9 \text{ mole}^{-1}\ 1\ \text{sec}^{-1} \qquad 4.3$$

$$O_2(^1\Sigma g^+) + N_2 \rightarrow O_2 + N_2 \qquad k_2 = 1.4 \times 10^6 \text{ mole}^{-1}\ 1\ \text{sec}^{-1} \qquad 4.2$$

$$O_2(^1\Sigma g^+) + O_2 \rightarrow 2O_2 \qquad k_2 = < 6 \times 10^4 \text{ mole}^{-1}\ 1\ \text{sec}^{-1} \qquad 4.2$$

$$O_2(^1\Sigma g^+) - \overset{\text{wall}}{\rightarrow} O_2 \qquad \gamma \sim 10^{-2} \qquad 4.8$$

An estimate of the energy pooling process, 4.1:

$$O_2(^1\Delta g) + O_2(^1\Delta g) \rightarrow O_2(^1\Sigma g^+) + O_2(^3\Sigma g^-) \qquad 4.1$$

rate constant of $k_1 = 1.4 \times 10^3$ mole^{-1} 1 sec^{-1} was obtained. Estimates of the energy transfer reactions and the deactivation reactions of $O(^1D)$ atoms were obtained:

$$O(^1D) + O_2 \rightarrow O_2(^1\Sigma g^+) + O(^3P) \qquad k_5 = 4 \times 10^7 \text{ mole}^{-1}\ 1\ \text{sec}^{-1} \qquad 4.5$$

$$O(^1D) + O_2 \rightarrow O_2(^1\Delta g) + O(^3P \qquad k_{14} < 6 \times 10^8 \text{ mole}^{-1}\ 1\ \text{sec}^{-1} \qquad 4.14$$

$$O(^1D) + N_2 \rightarrow O(^3P) + N_2 \qquad k_{12} = 7 \times 10^{10} \text{ mole}^{-1}\ 1\ \text{sec}^{-1} \qquad 4.12$$

$$O(^1D) + Ar \rightarrow O(^3P) + Ar \qquad k_{12} = 8 \times 10^9 \text{ mole}^{-1}\ 1\ \text{sec}^{-1} \qquad 4.12$$

These results are discussed and compared with those of other workers, and suggestions for further work are discussed.

4.2 Choice of system.

Experiments performed in Chapter 3 demonstrated that the electronic energy transfer reaction does give rise to $O_2(^1\Delta g)$. In the photolysis of ozone-oxygen with $\lambda = 253$ nm $O_2(^1\Delta g)$ was observed but not $O_2(^1\Sigma g^+)$, although this latter species is certainly produced by an energy transfer process [37]. This lack of observation suggested that some other reactions in our system were removing $O_2(^1\Sigma g^+)$ rapidly and clearly a kinetic study of the reactions of $O_1(^1\Sigma g^+)$ was necessary.

Laboratory studies of $O_2(^1\Sigma g^+)$ have generally used a flow technique and have relied on the electric discharges through molecular oxygen to produce small concentrations of the excited species [50,95,96,97]. However, relatively large proportions of $O_2(^1\Delta g)$ are produced by the electric discharge, and it now appears [96] that much of the $O_2(^1\Sigma g^+)$ observed in the discharge products is formed by the "energy-pooling" process:

$$O_2(^1\Delta g) + O_2(^1\Delta g) \rightarrow O_2(^1\Sigma g^+) + O_2(^3\Sigma g^-) \qquad 4.1$$

Indeed, a steady state for $[O_2(^1\Sigma g^+)]$ may be set up if the rate of formation of $O_2(^1\Sigma g^+)$ is equal to the rate of the various loss processes, and it is probable that the early

observations that $O_2(^1\Sigma g^+)$ did not decay with time [42] can be explained on this basis. Arnold et al [97] have obtained rate constants for the quenching processes:

$$O_2(^1\Sigma g^+) + M \rightarrow O_2(^3\Sigma g^-) + M \qquad 4.2$$

by observing the effect on the steady state concentration of $O_2(^1\Sigma g^+)$ of added gas. The absolute rate constants depend on a value measured for the rate constant of reaction 4.1, but unfortunately there is an uncertainty of at least a factor of 20 in this rate constant [96,97] and thus in the rate constants for the quenching processes 4.2. A steady state for $[O_2(^1\Sigma g^+)]$ is not achieved if the loss process for $O_2(^1\Sigma g^+)$ is particularly efficient and, when ozone is added to the reaction system, $O_2(^1\Sigma g^+)$ decays as a result [95] by the reaction:

$$O_2(^1\Sigma g^+) + O_3 \rightarrow 2O_2 + O(^3P) \qquad 4.3$$

Nevertheless, the observed decay rates must be corrected for the formation of $O_2(^1\Sigma g^+)$ by the "energy-pooling" process. Thus, accurate measurement of the rate constants of the quenching processes represented by reaction 4.2 or the reaction 4.3 must be made in reaction systems where the ratio $[O_2(^1\Delta g)]/[O_2(^1\Sigma g^+)]$ is not so high that a significant contribution to $[O_2(^1\Sigma g^+)]$ is made by the "energy-pooling" process, 4.1.

Young and Black [37,38] have demonstrated that $O_2(^1\Sigma g^+)$ is produced by the ultra violet photolysis of oxygen as a

result of the sequence of reactions:

$$O_2 + h\nu \xrightarrow{\lambda=147nm} O(^1D) + O(^3P) \qquad 4.4$$

$$O(^1D) + O_2(^3\Sigma g^-) \rightarrow O_2(^1\Sigma g^+) + O(^3P) \qquad 4.5$$

It was considered worthwhile to investigate this system as a means of producing $O_2(^1\Sigma g^+)$ for kinetic studies.

4.3 Flow apparatus and materials.

The flow system is schematically shown in figure 40. An Edwards ES 250 vacuum pump maintained the flow. Jets J_1 and J_2 allowed for the introduction of gases into the flow line, before and after the irradiation area. Flow rates were measured by calibrated capillary flow meters. Linear flow velocities between 5.8 and 7.2 meters sec^{-1} were employed.

Ozone was prepared by a silent discharge through oxygen and was collected on silica gel at -80^oC as described in section 2.1a. Nitric oxide was prepared by the action of dilute sulphuric acid on sodium nitrite and distilled three times in vacuo (see section 2.1b). B.O.C. cylinder oxygen-free nitrogen and argon were dried by passing through P_2O_5 drying tubes and liquid nitrogen traps.

4.4 Optical components.

For photolysing the oxygen a xenon resonance lamp was constructed as described in section 2.4. This was found to give a fairly pure line at 147 nm, figure 11. The lamp discharge was excited by a "Microton 200" microwave supply.

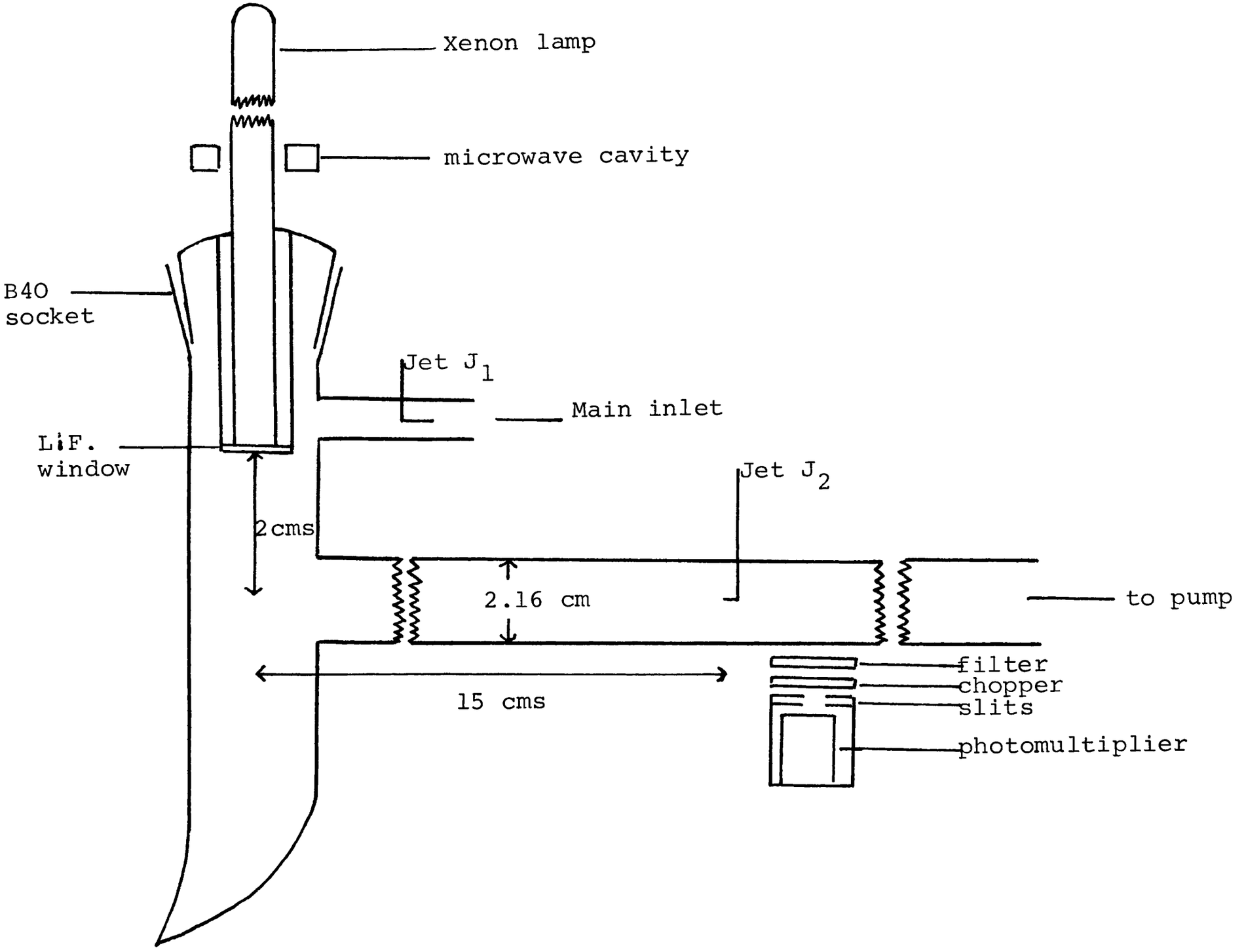


Figure 40. Schematic diagram of flow system

This could be varied in power and thus alter the lamp intensity.

An E.M.I. 9558A photomultiplier of the type described in section 2.6c was used to detect any emitted radiation from the photolysis products. The detector was used in conjunction with a mechanical chopper and phase sensitive detector as described in section 2.7. Narrow band interference filters were used to isolate particular spectral regions of interest.

4.5 Preliminary studies.

Preliminary experiments were carried out to establish if any emissions were produced on the irradiation of oxygen with λ = 147 nm. An emission was observed when viewed through the 762 nm narrow band interference filter. The fraction of emission intensity when no filter was present to that when the filter was in front of the detector was identical to the fractional transmission of the filter at λ = 762 nm, i.e. 45%. No radiation was detected at any other wavelength. The emission was therefore, almost entirely, that of the atmospheric band.

The variation of the O_2 ($^1\Sigma g^+$) band intensity with added oxygen was observed, the effect is shown in figure 41. In this run the lamp was 75 watts and the detector voltage 1200 volts. By adding a small amount of nitric oxide at J_2 a weak air afterglow was developed, by the reaction with the

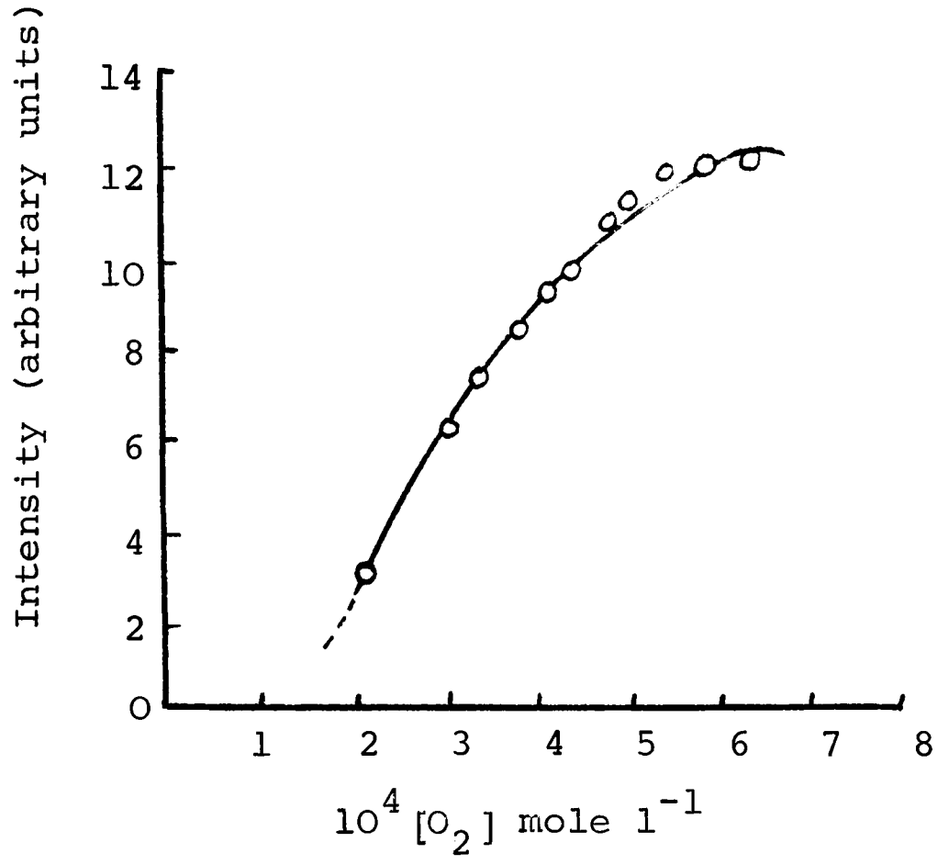


Figure 41. Variation of 762 nm intensity with [O_2]. Power 70 watts. E.H.T. 1100 volts.

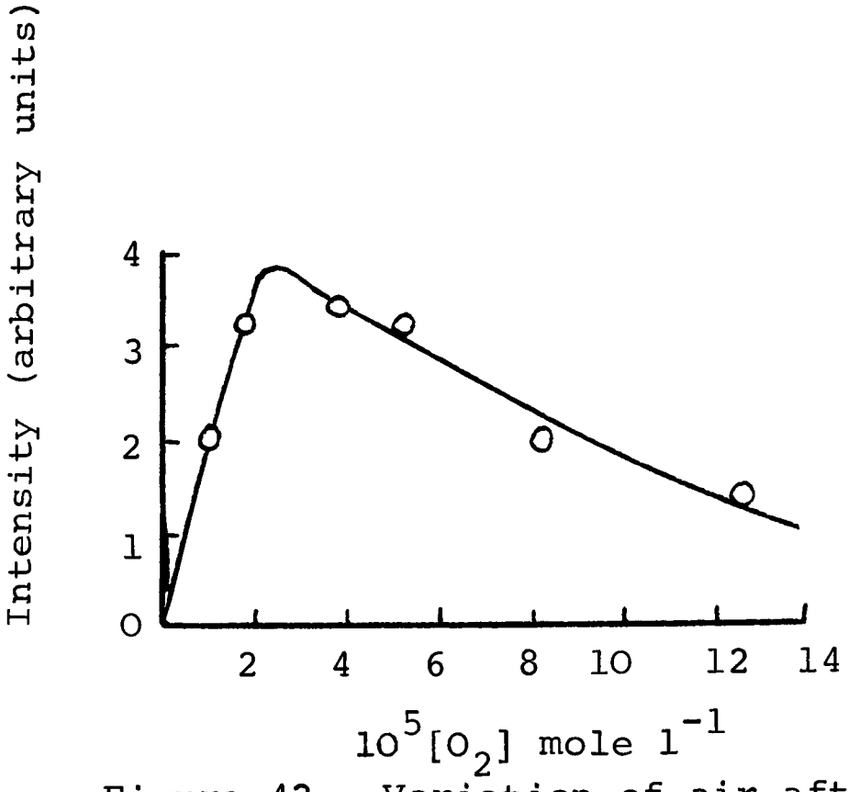


Figure 42. Variation of air afterglow intensity with [O_2] [NO] = 5 x 10^{-7} mole l^{-1}. Power 700 watts. E.H.T. 900 volts.

$O(^3P)$ atoms produced by the photolysis:

$$O(^3P) + NO \rightarrow NO_2 + h\nu \qquad 4.6$$

With a constant nitric oxide concentration (c.a. 7×10^{-7} mole l^{-1}), the variation in glow intensity with changing $[O_2]$ was observed. This is shown in figure 42. A OB2 glass with a Wratten 45 gelatine filter was used in front of the detector for the purpose, since it did not transmit the $O_2(^1\Sigma g^+)$ band. The lamp power was 75 watts and the detector voltage was 1000 volts.

The ability to observe $O_2(^1\Sigma g^+)$ readily using the photolytic system suggested that it was a good system for studying the reactions of $O_2(^1\Sigma g^+)$ kinetically.

4.6 Kinetic studies.

The apparatus adopted was identical to that shown in figure 40. An E.M.I. 9558A photomultiplier, operated at 1350 volts, equipped with two collimating slits could be moved along the observation length of the flow tube. The collimating slits allowed acceptance of radiation from a section of the flow tube about 0.6 cms long from the farthest point from the photomultiplier, which was equivalent in time to about 10^{-3} secs.

The concentration of $O_2(^1\Sigma g^+)$ at the observation point was determined from the absolute calibration of the detector against the air afterglow [78]. The procedure is described in detail in section 2.6a.

Atomic oxygen concentrations in the reaction system were determined from the intensity of the air afterglow, developed on the addition of a small concentration of nitric oxide (c.a. 10^{-7} mole l^{-1}). A Chance OB2 and Wratten type 45 filter was placed in front of the photomultiplier. The intensity (I_a) of the glow produced was compared with the intensity (I_b) of an after air glow produced by titrating nitrogen atoms. with nitric oxide, and then adding more nitric oxide:

$$N + NO \rightarrow N_2 + O(^3P) \qquad 4.13$$

$$NO + O(^3P) \rightarrow NO_2 + h\nu \qquad 4.6$$

The value of $I_b = k_6[NO]_b \ [O(^3P)]_b$ and I_a is given by

$$I_a = k_6[NO]_a[O(^3P)]_a$$

$$\text{hence} \quad [O(^3P)]_a = \frac{I_a[NO]_b[O(^3P)]_b}{I_b[NO]_a} \qquad 4.A$$

Both calibration and oxygen atom determination was carried out at the first observation position on the flow tube, i.e. near J_2, in order to minimize any error which could result from decay of the air afterglow or excited species.

The intensity of the atmospheric band was measured at 3 cm intervals down the observation section of the flow tube. Linear log (intensity) against time plots were used to determine an apparent first-order rate constant, α, for each experimental condition.

4.7 Effect of discharge power on α.

The effect of variation of discharge power on α at

three oxygen concentrations was studied and the results listed in Table 8.

Table 8. Effect of discharge power on α

$10^4[O_2]$ mole l^{-1}	lamp power W	α sec^{-1}	$10^{13}[O_2(^1\Sigma g^+)]_o$ mole l^{-1}	$10^{10}[O]_o$ mole l^{-1}	$\frac{10^{-2}[O]_o}{2[O_2(^1\Sigma g^+)]_o}$
1.67	100	134	1.48	1.71	5.8
	70	141	1.46	1.31	4.5
	45	143	1.12	0.97	4.3
2.36	100	106	1.38	1.65	6.0
	70	106	1.18	1.47	6.0
	45	108	0.84	0.99	5.9
3.62	100	90	1.47	1.42	4.8
	70	90	1.20	1.07	4.5
	45	90	0.82	0.72	4.4

The Table 8 also gives the absolute values of $[O_2(^1\Sigma g^+)]_o$ and $[O]_o$, the concentrations of $O_2(^1\Sigma g^+)$ and atomic oxygen leaving the irradiation zone. $[O_2(^1\Sigma g^+)]_o$ was calculated from $[O_2(^1\Sigma g^+)]$ at the first observation point and the measured value of α. Atomic oxygen was assumed to decay predominantly by the three body recombination reaction 4.7:

$$O + O_2 + M \rightarrow O_3 + M \qquad 4.7$$

Secondary reactions of atomic oxygen with ozone can be shown to be unimportant at the concentrations of ozone formed by equation 4.7. The rate constant for 4.7 is about 2×10^8

$mole^{-2}\ l^2\ sec^{-1}$ for M = O_2 [98], and the value was used to calculate $[O]_o$. The wall recombination rate constant is normally about 1 sec^{-1} [99] for a Pyrex reaction system of the dimension used. The wall effects were not, therefore, included in the calculation.

4.8 Reaction of $O_2(^1\Sigma g^+)$ with ozone.

Ozone was added at J_2, in concentration that would not affect the main flow conditions. The decay of the $O_2(^1\Sigma g^+)$ signal down the tube was observed. The α values for various ozone concentrations at two oxygen concentrations are listed in Table 9. Lamp power was 85 watts.

Table 9. Effect of α with added ozone.

$10^4[O_2]$ mole l^{-1}	$10^8[O_3]$ mole l^{-1}	α sec^{-1}
2.68	0	107
	1.26	157
	1.53	164
	2.07	189
	2.61	212
	3.15	240
3.67	0	112
	0.38	133
	1.12	180
	2.33	230
	3.18	252
	5.13	338

In the presence of ozone $O_2(^1\Sigma g^+)$ can take part

in the following reactions.

$$O_2(^1\Sigma g^+) + O_3 \rightarrow 2O_2 + O(^3P) \qquad 4.3$$

$$O_2(^1\Sigma g^+) + M \rightarrow O_2(^3\Sigma g^-) + M \qquad 4.2$$

$$O_2(^1\Sigma g^+) \xrightarrow{\text{wall}} O_2(^3\Sigma g^-) \qquad 4.8$$

From this the apparent first-order rate constant (α) is given by

$$\alpha = k_3[O_3] + k_2[M] + k_8 \qquad 4.B$$

The plots of α versus $[O_2]$ are shwon in figure 43. From the slope of the two "least squares" lines the values for k_3 obtained are (a) 4.34×10^9 mole^{-1} l sec^{-1} and (b) 4.18×10^9 mole^{-1} l sec^{-1} at 21°C. The possible cumulative error was about 10% in the measurement of time and ozone concentration. This yields the result for $k_3 = 4.26 \pm (.5) \times 10^9$ l m^{-1} s.$^{-1}$.

March et al [50] have made measurements of $[O_2(^1\Sigma g^+)]$ (optical emission at λ = 762 nm) and $[O_3]$ (multiple path absorption at λ = 253.7 nm) as a function of time in a system where ozone was added to discharged oxygen, from which atomic oxygen was removed by Hg O. They found that the $[O_2(^1\Sigma g^+)]$ decreased rapidly with time while the $[O_3]$ decreased long after $[O_2(^1\Sigma g^+)]$ had reached a very low value. These results indicated (a) that there was present a reactant species other than $O_2(^1\Sigma g^+)$ which consumed ozone, i.e. $O_2(^1\Delta g)$ and, (b) that $O_2(^1\Sigma g^+)$ was regenerated in the system. This latter observation is consistent with

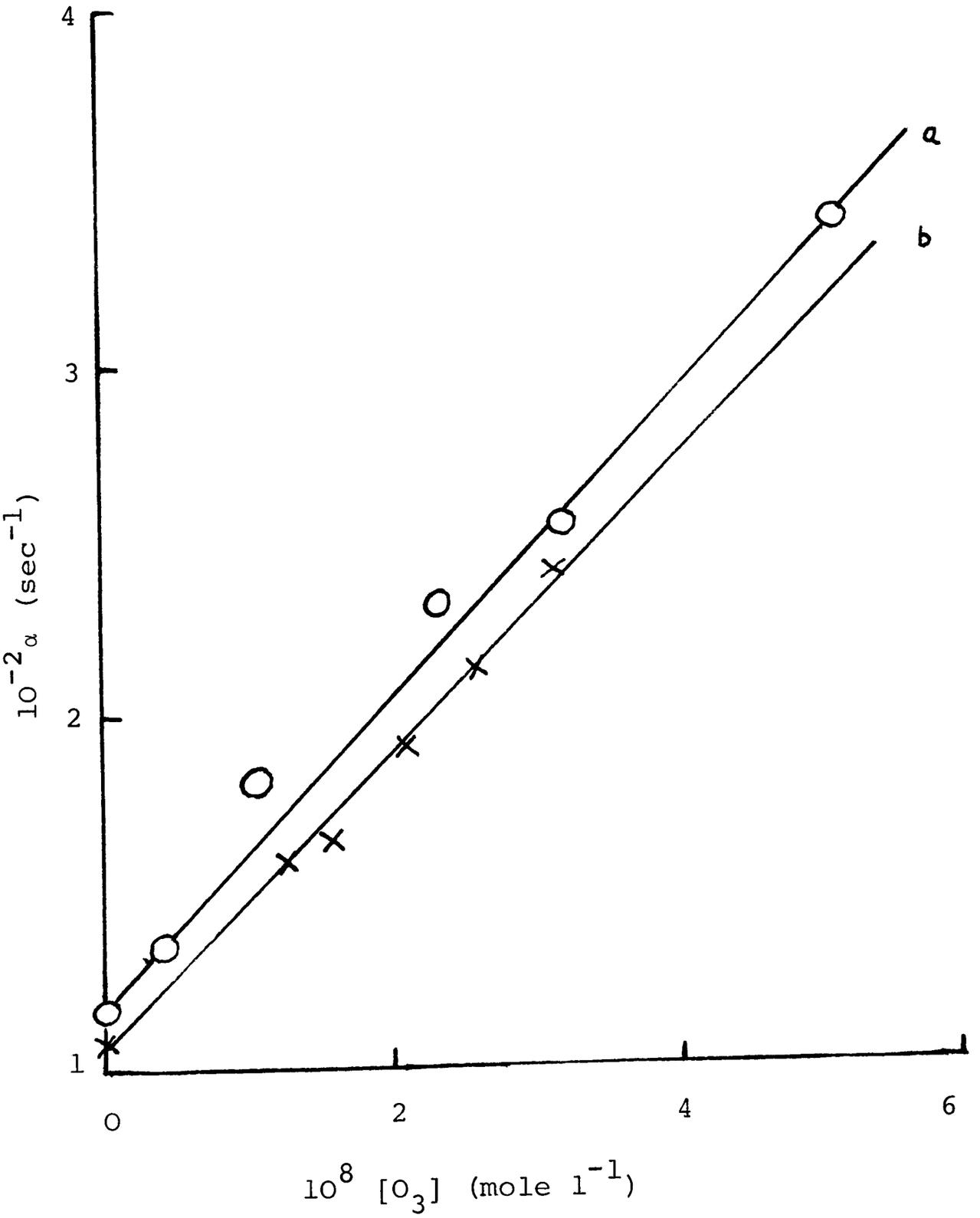


Figure 43. Variation of α with [O_3]

(a) O, [O_2] = 3.67 x 10^{-4} mole l^{-1}

(b) X, [O_2] = 2.68 x 10^{-4} mole l^{-1}

the production of the $O_2(^1\Sigma g^+)$ by the "energy-pooling process":

$$O_2(^1\Delta g) + O_2(^1\Delta g) \rightarrow O_2(^1\Sigma g^+) + O_2(^3\Sigma g^-) \qquad 4.1$$

Because of the participation of reaction 4.1, March et al found that the apparent value of k_3 decreased with reaction time and they made an assumed linear extrapolation of a log k_3-mean residence time plot to zero residence time, and obtained a value for $k_3 \sim 4 \times 10^8$ mole^{-1} l sec^{-1}. Accurate determination of k_3 in this system would require determination of $[O_2(^1\Delta g)]$ and a knowledge of k_1 to assess the correction $[O_2(^1\Sigma g^+)]$ needed at any reaction time. The value of k_3 obtained by March et al is ten times slower than that in this present work, but if a more realistic non-linear extrapolation of their results is considered then a much higher value of k_3 would be expected.

Recently, further evidence has been put forward by Noxon [39] for adopting the higher value of k_3. He has studied $O_2(^1\Sigma g^+)$ reactions in a static system involving the photolysis of oxygen with λ = 147 nm, and found that the $O_2(^1\Sigma g^+)$ signal decreased with time and attributed this to the reaction of $O_2(^1\Sigma g^+)$ with ozone, formed by the three body process:

$$O_2 + M \rightarrow O_3 + M \qquad 4.5$$

By considering the concentration of ozone produced in the system to give the required amount of $O_2(^1\Sigma g^+)$ decay Noxon

estimated $k_3 \sim 6 \times 10^9$ mole^{-1} l sec^{-1} which is in good agreement with the present work.

4.9 Quenching of $O_2(^1\Sigma g^+)$ by Argon and Nitrogen.

The decay of $O_2(^1\Sigma g^+)$ due to added argon and nitrogen was studied by adding these gases at J_1, before the irradiation unit. The reason for this being that the concentrations of added quencher were of the same order as the oxygen concentration and if added at J_2 would have disturbed the flow conditions. Table 10 lists the value of α, $[O_2(^1\Sigma g^+)]_o$, $[O]_o$ in the presence of nitrogen and argon. The discharge lamp power was 85 watts in these experiments and the photomultiplier operated at 1350 volts.

Figure 44 shows the variations of α with added nitrogen at two oxygen concentrations. In both cases $[N_2] << [O_2]$ and the effect on the total pressure is small. The average value for k_2 when $M = N_2$ obtained from figure 44 is 1.4×10^6 mole^{-1} l sec^{-1}. This value is in good agreement with that of Arnold et al [97] of $k_2 = 1.3 \times 10^6$ mole^{-1} l sec^{-1}. More recently Noxon [39], using a similar photolytic system as in the present experiments, has obtained a value for $k_2 = 9\ (\pm\ .3) \times 10^5$ mole^{-1} l sec^{-1}, and Stuhl et al [48] have obtained a value for $k_2 = 1.3 \times 10^6$ mole^{-1} l sec^{-1}.

The value of k_2 quoted by Arnold et al [97] was derived from a steady state value of $O_2(^1\Sigma g^+)$ set up by the "energy pooling" reaction 4.1, using a value for k_1 =

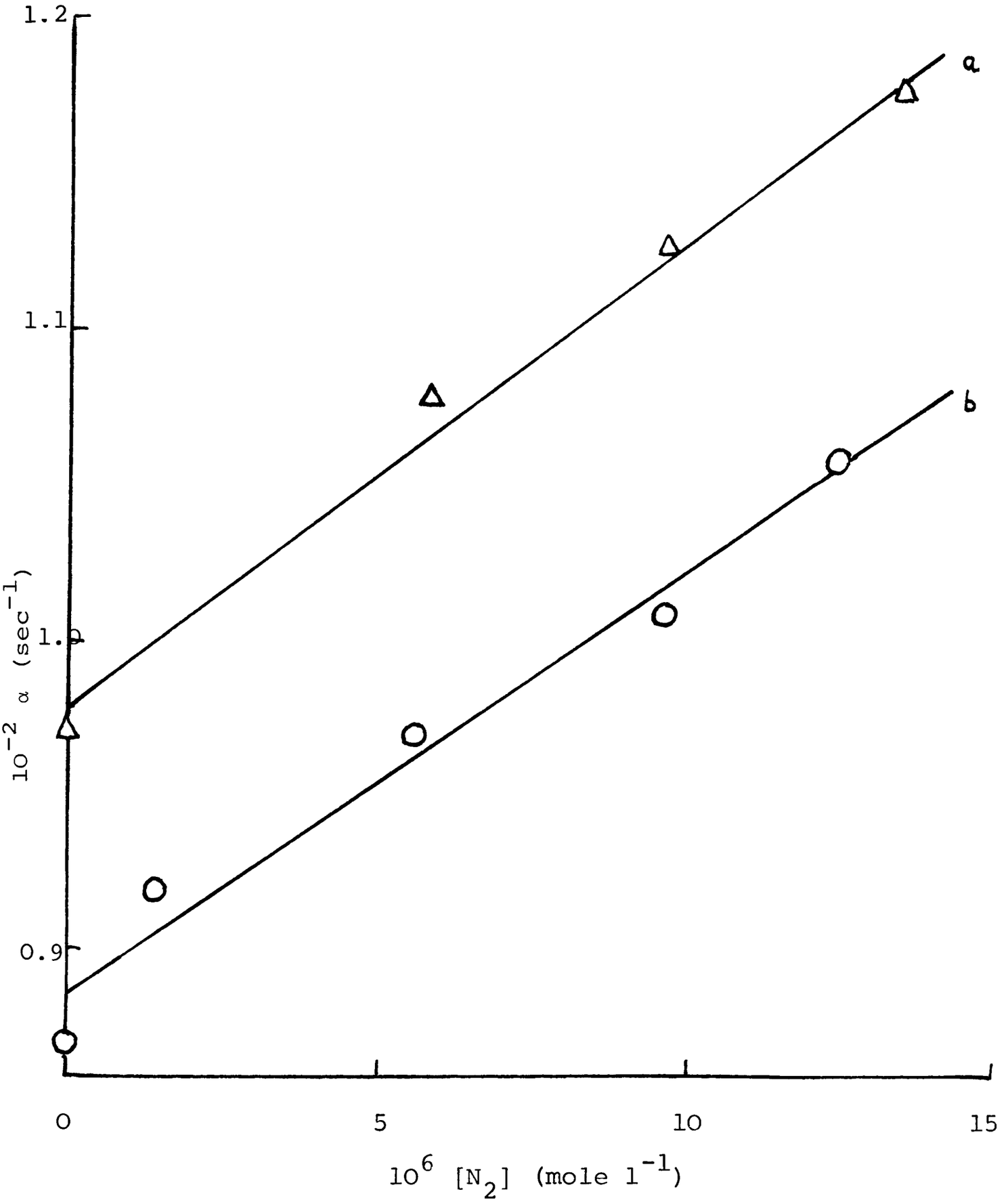


Figure 44. Variation of α with [N_2]. (a) Δ[O_2] = 4.00 x 10^{-4} m l^{-1}. (b) O, [O_2]= 3.28 x 10^{-4} mole l^{-1}.

Table 10. Dependence of α, $[O_2(^1\Sigma g^+)]_o$ and $[O]_o$ on [M].

$10^4[O_2]$ mole l^{-1}	$10^5[M]$ mole l^{-1}	nature of M	α (sec^{-1})	$10^{13}[O_2(^1\Sigma g^+)]_o$ mole l^{-1}	$10^{10}[O]_o$ mole l^{-1}	$\frac{10^2[O]_o}{2[O_2(^1\Sigma g^+)]_o}$
4.00	0	Nitrogen	37	1.27	1.1	4.33
	0.14		92	1.34		4.10
	0.56		97	1.27		4.33
	0.96		101	1.22		4.51
	1.25		106	1.20		4.58
3.28	0	Nitrogen	97	1.55	1.3	4.19
	0.58		108	1.44		4.51
	0.96		113	1.36		4.78
	1.33		118	1.37		4.74
3.67	0	Argon	99	1.27	1.2	4.72
	0.90		99	1.28		4.69
	2.34		97	1.25		4.80
	4.68		95	1.21		4.96
	7.55		90	1.18		5.08
2.88	0	Argon	110	1.46	1.4	4.79
	3.06		108	1.40		5.00
	6.30		103	1.35		5.19
	9.00		97	1.29		5.43

1.3×10^3 mole^{-1} l sec^{-1}. Adopting this approach and using the value of $k_2 = 1.4 \times 10^6$ mole^{-1} l sec^{-1}, the rate constant for reaction 4.1 is 1.4×10^3 mole^{-1} l sec^{-1}.

Argon is clearly an inefficient deactivator of $O_2(^1\Sigma g^+)$ and addition of argon to the gas stream inhibits diffusion to a greater extent than it quenches the excited species (Table 10). This result is in conflict with that of Arnold et al [97] who find nitrogen and argon to be of comparable efficiency in the deactivation reaction. The reason for this discrepancy is probably due to the different technique adopted.

4.10 Deactivation of $O_2(^1\Sigma g^+)$ by reaction with oxygen.

By increasing the total pressure of argon it was anticipated that α would increase with increasing [M]. However, it was found that α decreased with increasing $[O_2]$. The relatively high value of α obtained at low pressures suggest that surface deactivation on the walls of the flow tube, reaction 4.8, is efficient and it may be diffusion controlled. The condition for a reaction <u>not</u> to be diffusion controlled is that the time taken for the species to reach the surface should be short compared with the time taken for deactivation at the surface. An attempt to calculate exactly the effect of diffusion in order to obtain the value of k_8 seems unwise, since small relative errors in the diffusion term would

lead to larger errors in k_8. As an approximation the lifetime of $O_2(^1\Sigma g^+)$ can be regarded as the sum of the time taken for the species to diffuse to the wall and the time taken for it to be deactivated once it is there, and to omit any gas phase deactivator term. Thus for a cylindrical tube of radius r [100]:

$$k_8 = \left(\frac{r^2 M}{\phi D_o} + \frac{2r}{\bar{c}\gamma} \right)^{-1} \qquad 4.C$$

when D_o = pressure independent diffusion coefficient of O_2, (7.65×10^{-3} cm^2 mole l^{-1} sec^{-1})

$\bar{c}$ = mean thermal kinetic velocity of oxygen (about 4.3×10^4 cm^{-1})

γ = fraction of collisions of $O_2(^1\Sigma g^+)$ with the vessel walls that lead to deactivation.

and ϕ is a numerical constant whose value depends on the exact form of the solution of the diffusion equation, but is probably of the order of 10. Figure 45 shows α^{-1} as a function of $[O_2]$. A least squares analysis of the points, assuming a linear relationship, gives $\frac{\bar{c}\gamma}{2r} = 220$, so $\gamma \sim 10^{-2}$. The surface efficiency appears to vary slightly from one experimental run to another, especially if the reaction system has been open to the atmosphere between runs. For example, in figure 44, the higher $[O_2]$ line (a) lies <u>above</u> line (b), although the general trend in figure 45 makes it clear that increase in pressure reduces α. These considerations do not affect the

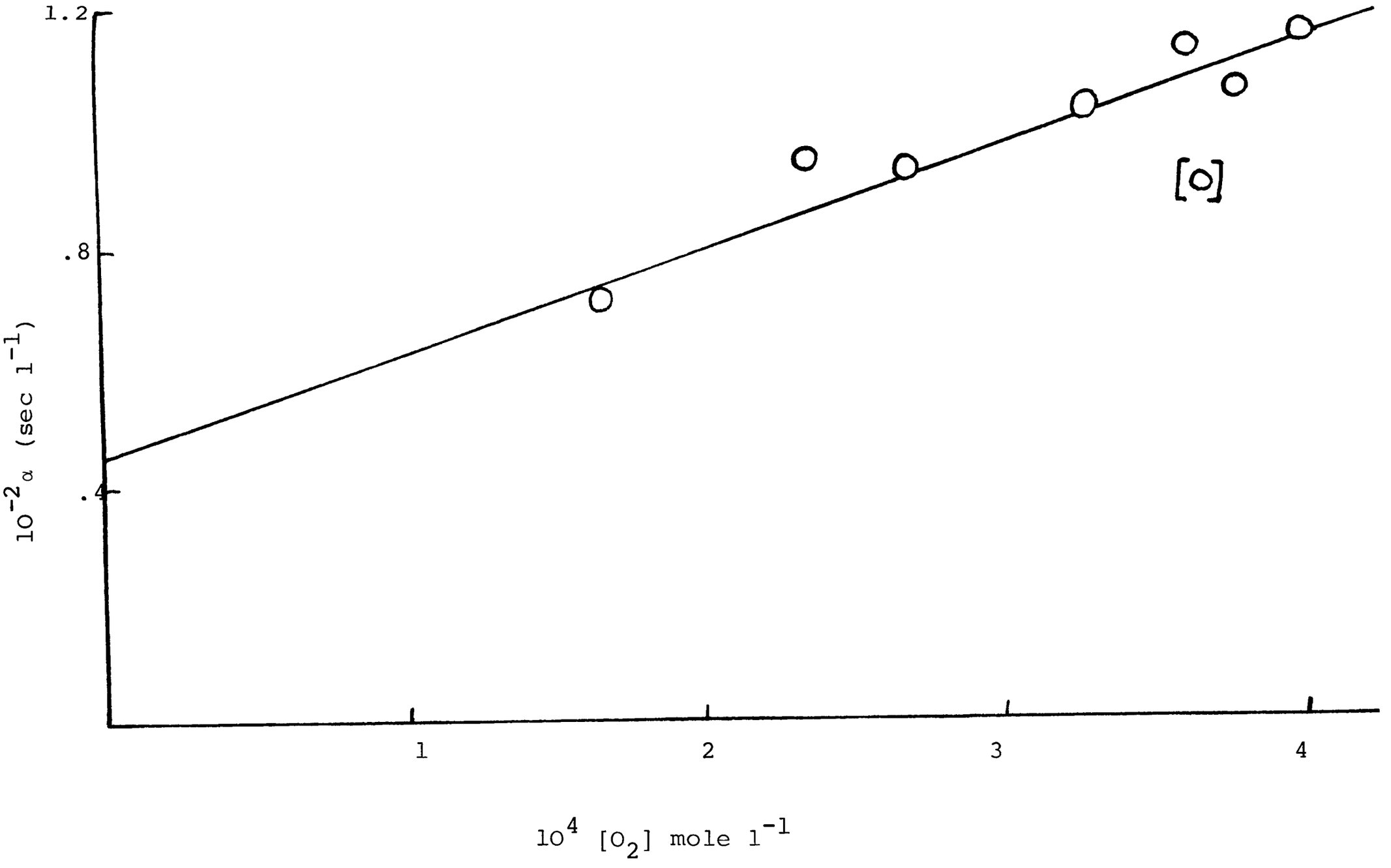


Figure 45. The function α^{-1} plotted against [O_2]

approximate value of α given above, since the variations are only of the order of 10%. However, this does stress the importance of obtaining in a single experimental run each set of points in investigations of α as a function of foreign gas pressure.

Arnold and Ogryzlo [96] found $\gamma = 2 \times 10^{-3}$, while Arnold et al [97] obtained $\gamma = 4 \times 10^{-2}$ for a Pyrex surface. In the earlier work there was no allowance for the diffusion term. Recently, Noxon [37] has estimated $\gamma = 10^{-2}$ which is in good agreement with the present result deduced from figure 45. The slope of the least squares line in figure 45 is 17.11 $mole^{-1}$ sec so that $\phi \sim 9$, which is consistent with expectation.

Oxygen is clearly a much less efficient deactivator of $O_2(^1\Sigma g^+)$ than is nitrogen. Some measure of an upper limit to k_2 can be obtained by assuming that the deviations from linearity in figure 45 all arise from participation of reaction 4.2 and not from experimental error. The largest deviation is for the point at $[O_2] = 2.36 \times 10^{-4}$ mole l^{-1}, where the predicted and observed values of α are 111 sec^{-1} and 106 sec^{-1}, which suggests that $k_2 \leq 6 \times 10^4$ $mole^{-1}$ l sec^{-1} for $M = O_2$. Recently Noxon [39] has obtained an exact value of $k_2 = 6 (\pm 3) \times 10^4$ $mole^{-1}$ l sec^{-1} and Stuhl and Welge [48] $k_2 = 6.3 \times 10^4$ $mole^{-1}$ l sec^{-1}. These results are in good agreement with the upper limit

set in the present work. It is difficult to account for the inefficiency of oxygen as a quencher of $O_2(^1\Sigma g^+)$. Arnold [46] has inferred that quenching efficiencies can be correlated to the magnitude of the intermolecular potential between $O_2(^1\Sigma g^+)$ and the quencher. Thus polar molecules might be expected to be better quenchers than non-polar molecules, which is in agreement with experimental data [46]. With the case in hand, however, it is possible that collisions between excited and ground state oxygen only results in a change of the molecule which carries the excitation.

A further deactivation reaction of $O_2(^1\Sigma g^+)$ has been proposed by Vallance Jones and Gattinger [35]:

$$O(^3P) + O_2(^1\Sigma g^+) \rightarrow O_2(^3\Sigma g^-) + O(^3P) \qquad 4.9$$

It could be argued that an increase of $[O_2]$, which has the effect of decreasing [O] in the observation region, would decrease the apparent value of α if reaction 4.9 was of importance. The concentration of O atoms is so small that it seems unlikely that the effect could be significant. However, to resolve this problem α was determined at different [O] under otherwise identical conditions by changing the incident light intensity. Table 8 shows that α is virtually unaffected by changes in $[O]_o$.

4.11 Reactions of $O(^1D)$ atoms.

The chemical properties and efficiencies of some of

the reactions of $O(^3P)$ and $O(^1D)$ atoms have been critically reviewed by Cvetanovic [101] and Zipf [52]. Their properties differ considerably, being due to the different electronic configuration which makes $O(^1D)$ a more electrophilic reagent than $O(^3P)$, and to differences in energy available. The excited $O(^1D)$ atom is 1.97 e.v. above the ground state $O(^3P)$ atom and has a life of 100 sec. The types of reactions expected of $O(^1D)$ atoms are as follows:

(1) Addition of $O(^1D)$ to stable molecules. This generally requires a third body. The order of the reaction, with respect to the third body, may be higher than one due to a stepwise vibrational deactivation of the excited association complex formed by the addition.

(2) Abstraction and fragmentation reactions. The $O(^1D)$ atom has the ability to add to simple molecules to form energy rich intermediates. These are stabilised by dissipation of their excess energy or are decomposed to give the final products which are themselves often energetically excited.

(3) Energy exchange reactions with oxygen containing molecules.

(4) Deactivation reactions.

The rate constants for the reactions of $O(^1D)$ atoms vary greatly from worker to worker. For example, the rate constant for the deactivation reaction 4.10:

$$O(^1D) + O_2 \rightarrow O(^3_{-1}P) + O_2 \qquad 4.10$$

is given as 2 x 10^6 mole 1 sec^{-1} by Warneck and Sullivan [102] and 3 x 10^{10} $mole^{-1}$ 1 sec^{-1} by Noxon [39]. Because of this inconsistency in laboratory determinations of $O(^1D)$ atom reactions it was considered worthwhile to make estimates of the efficiencies of some of the atom reactions occurring in our photolysis system.

Collisions which deactivate $O(^1D)$ may lead, apart from $O_2(^1\Sigma g^+)$, to either $O_2(^1\Delta g)$ on ground state oxygen and will be represented by equation 4.10:

$$O(^1D) + O_2 \rightarrow O(^3P) + O_2 \qquad 4.10$$

The other possible deactivation reactions in our system are surface deactivation and, in the presence of an added gas, quenching.

$$O(^1D) \xrightarrow{wall} O(^3P) \qquad 4.11$$

$$O(^1D) + M \rightarrow O(^3P) + M \qquad 4.12$$

The $O_2(^1\Sigma g^+)$ is produced by the energy transfer reaction 4.5:

$$O(^1D) + O_2(^3\Sigma g^-) \rightarrow O(^3P) + O_2(^1\Sigma g^+) \qquad 4.5$$

In a kinetic analysis the question arises of whether $[O(^1D)]$ can be treated as a stationary state within the irradiation zone. To solve the problem both stationary and non-stationary approaches were adopted and compared. Consider first a non-stationary state approach:

$$\frac{d[O(^1D)]}{dt} = I_o e^{-\varepsilon[O_2]_{ut}} \varepsilon[O_2] - (k_5+k_{10})[O_2][O(^1D)] - k_{11}[O(^1D)] - k_{12}[M][O(^1D)] \quad 4.D$$

where ε = decadic molar extinction coefficient of oxygen at λ = 147 nm (about 10^4 l mole^{-1} cm^{-1}).

I_o = intensity of radiation incident on the reaction gas.

u = flow velocity (cms sec^{-1}).

t = residence time in the irradiation unit.

$$[O(^1D)] = Ae^{-at} + \frac{I_o e^{-\varepsilon[O_2]_{ut}} \varepsilon[O_2]}{a - \varepsilon[O_2]_u} \quad 4.E$$

where $a = (k_5 + k_{10})[O_2] + k_{11} + k_{12}$

A = constant

when t = 0, $[O(^1D)] = 0$

$$\therefore [O(^1D)] = \frac{I_o \varepsilon[O_2]}{a - \varepsilon[O_2]_u} \left[e^{-\varepsilon[O_2]_{ut}} - e^{-at}\right] \quad 4.F$$

Now the rates of decay of $O_2(^1\Sigma g^+)$ and $O(^3P)$ in our system suggest that decay of these species can be neglected in the short (ca. 2 cm $\equiv$ 4 x 10^{-3} sec) irradiation zone. Thus $[O_2(^1\Sigma g^+)]$ can be treated as follows:

$$\frac{d[O_2(^1\Sigma g^+)]}{dt} = k_5[O_2][O(^1D)] \quad 4.G$$

Substituting F in equation G

$$\frac{d[O_2(^1\Sigma g^+)]}{dt} = \frac{k_5[O_2]^2 I_o}{a - \varepsilon[O_2]_u} \left[e^{-\varepsilon[O_2]_{ut}} - e^{-at}\right] \quad 4.H$$

$$[O_2(^1\Sigma g^+)] = \frac{k_5[O_2]^2 \varepsilon I_o}{a - \varepsilon[O_2]_u}\left[-\frac{e^{-\varepsilon[O_2]_{ut}}}{\varepsilon[O_2]_u} + \frac{e^{-at}}{a}\right] + \text{constant} \qquad 4.I$$

when $t = 0$, $O_2(^1\Sigma g^+) = 0$

$$\text{constant} = \frac{-k_5[O_2]^2 \varepsilon I_o}{a - \varepsilon[O_2]_u}\left[\frac{1}{a} - \frac{1}{\varepsilon[O_2]_u}\right] \qquad 4.J$$

$$\therefore [O_2(^1\Sigma g^+)]_t = \frac{k_5[O_2]^2 \varepsilon I_o}{a - \varepsilon[O_2]_u}\left[\frac{1}{\varepsilon[O_2]_u}(1-e^{-\varepsilon[O_2]ut}) - \frac{1}{a}(1-e^{-at})\right] \qquad 4.K$$

For the calculation of $[O(^3P)]$ it was assumed that 2 atoms are produced per quantum absorbed:

$$\frac{d[O(^3P)]}{dt} = 2I_o\, e^{-[O_2]_{ut}\varepsilon[O_2]} \qquad 4.L$$

$$= 2I_o \int_o^t [e^{-\varepsilon[O_2]_{ut}\varepsilon[O_2]dt}] + [\text{constant}] \qquad 4.M$$

$$\therefore [O(^3P)]_t = \frac{2I_o}{u}[1 - e^{-[O_2]_{ut}}] \qquad 4.N$$

Consider now a stationary approach for $[O(^1D)]$

$$\frac{d[O(^1D)]}{dt} = 0 = I_o\, e^{-\varepsilon[O_2]_{ut}\varepsilon[O_2]} - a[O(^1D)] \qquad 4.O$$

$$[O(^1D)] = \frac{I_o\, e^{-\varepsilon[O_2]_{ut}\varepsilon[O_2]}}{a} \qquad 4.P$$

Substituting P in G the equation for $O_2(^1\Sigma g^+)$ production is:

$$\frac{d[O_2(^1\Sigma g^+)]}{dt} = \frac{k_5 I_o\, \varepsilon[O_2]^2 e^{-\varepsilon[O_2]_{ut}}}{a} \qquad 4.Q$$

Integrating between $t = 0$ and $t = t$

$$[O_2(^1\Sigma g)]_t = \frac{k_5 I_o [O_2]}{au}[1 - e^{-\varepsilon[O_2]ut}] \qquad 4.R$$

If k_{11} and k_{12} are neglected then a will have its smallest value. In the above equations $[O_2]$ is typically 4×10^{-4} mole l^{-1}. The value of $k_5 + k_{10}$ is taken as about 2×10^{10} mole^{-1} l sec^{-1} [52]. This then gives a value of $a \approx 8 \times 10^6$ sec^{-1}. If the velocity $u \approx 5 \times 10^2$ cm sec^{-1} and $t \approx 4 \times 10^{-3}$ sec. then insertion of these values into the above equations gives an idea of the difference between the steady and non-steady state equation. It can be seen that there is very little difference between the two approaches and it is apparent that $[O_2(^1\Sigma g^+)]$ approaches closely the values predicted by a steady state treatment for $O(^1D)$. The approximate forms of $[O(^1D)]_o$ and $[O_2(^1\Sigma g^+)]_o$, i.e. the concentration of $O(^3P)$ and $O_2(^1\Sigma g^+)$ in the irradiation zone, may be used to obtain the relation:

$$\frac{[O]_o}{2[O_2(^1\Sigma g^+)]_o} = \frac{k_5 + k_{10}}{k_5} + \frac{k_{11}}{k_5[O_2]} + \frac{k_{12}[M]}{k_5[O_2]} \qquad 4.S$$

Table 8 shows the ratio $\frac{[O]_o}{2[O_2(^1\Sigma g^+)]_o}$ in the absence of any foreign gas. Clearly there is no systematic variation of the ratio with $[O_2]$, which suggests that the term $\frac{k_5+k_{10}}{k_5}$ is dominant. The magnitude of the ratio indicates that about one $O(^1D)$ is deactivated in reaction 4.5 for every 500 deactivated by reaction 4.10. If $k_5 + k_{10} = 2 \times 10^{10}$

$mole^{-1}$ 1 sec^{-1} [52] then $k_5 = 4 \times 10^7$ $mole^{-1}$ 1 sec^{-1}.

Figure 46 shows the effect of the addition of foreign gases to the reaction mixture. The values of $\frac{[O]_o}{2[O_2(^1\Sigma g^+)]_o}$ and [M] being obtained from Table 10. For M = N_2, the average value of k_{12} based on $k_5 = 4 \times 10^7$ $mole^{-1}$ 1 sec^{-1} is calculated as 7×10^{10} $mole^{-1}$ 1 sec^{-1}. For M = Ar, $k_{12} = 8 \times 10^9$ $mole^{-1}$ 1 sec^{-1}. Thus, these results indicate that nitrogen is about 3½ times more efficient than oxygen as a deactivator of $O(^1D)$.

The approximate expression derived for $[O]_o$ predicts that it should be a constant equal to $\frac{2I_o}{u}$. The results presented in Table 8 for $[O]_o$ are nearly constant at each value of the discharge power (i.e. I_o). The slight decrease observed with increasing $[O_2]$ is probably due to an underestimation of $O(^3P)$ in reaction 4.7 or at the walls. However, as this approach is only intended to give estimates of the efficiencies of the energy transfer and deactivation reactions, there seems little point in correcting the value of $[O]_o$ by adopting an accurately measured decay constant. At 100 watts power fed to the photolytic lamp, $[O]_o$ is about 2×10^{-10} mole l^{-1} so that I_o is about 5×10^{-11} einstein cm^{-2} sec^{-1} ≡ 3×10^{13} quanta cm^{-2} sec^{-1}, which is consistent with published data for the type of lamp employed. Noxon [103] has suggested that

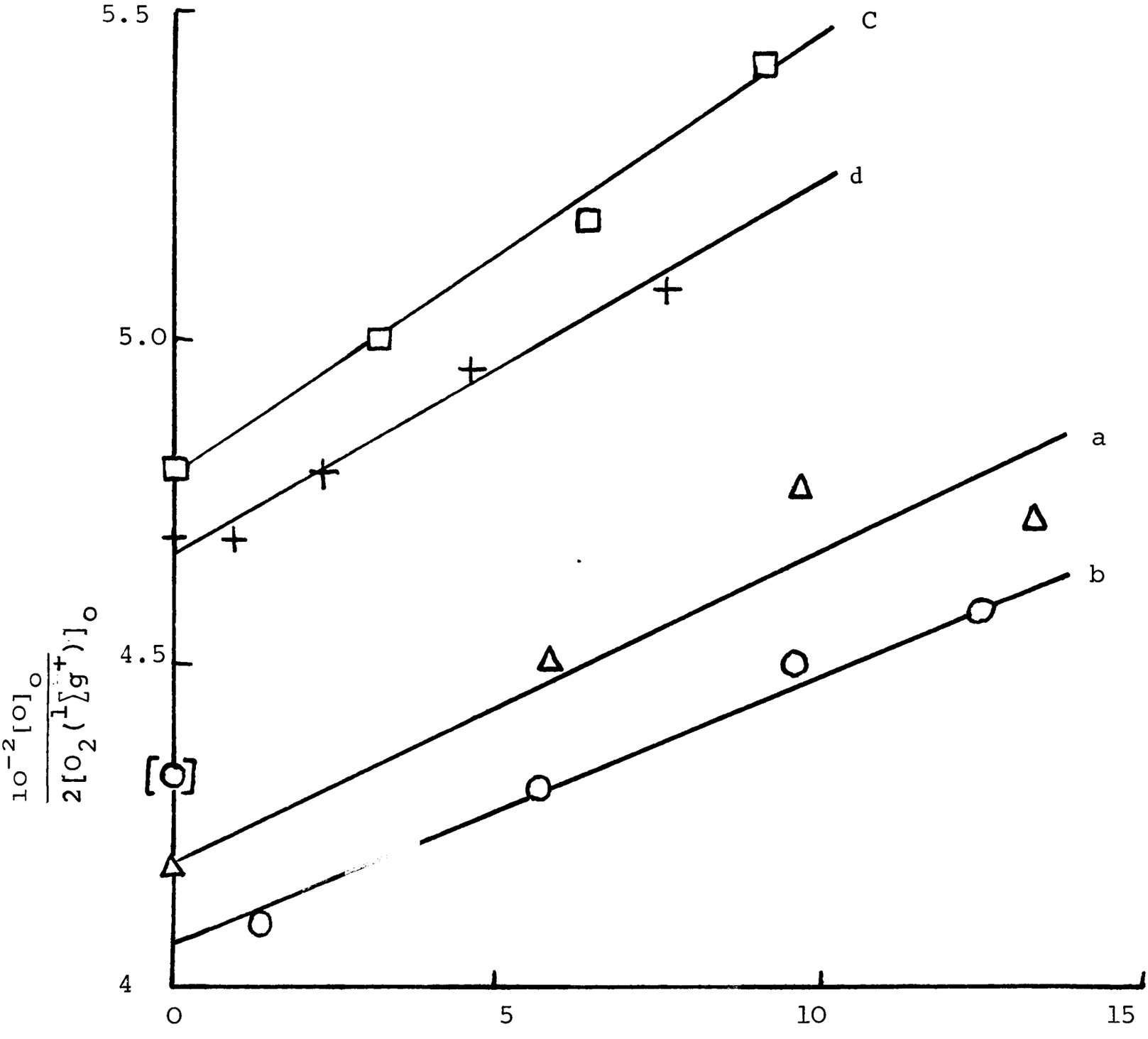


Figure 46. Dependence of function $\frac{[O]_o}{2[O_2(^1\Sigma g^+)]_o}$ on M. (a) Δ, M = N_2; $[O_2]$ = 3.28 x 10^{-4} mole l^{-1}, (b) O, M = N_2;$[O_2]$= 4.00 x 10^{-4} mole l^{-1}, (c) ¤, M = Ar; $[O_2]$= 2.88= 10^{-4} mole l^{-1}, (d)+M = Ar; $[O_2]$ = 3.67 x 10^{-4} mole l^{-1}.

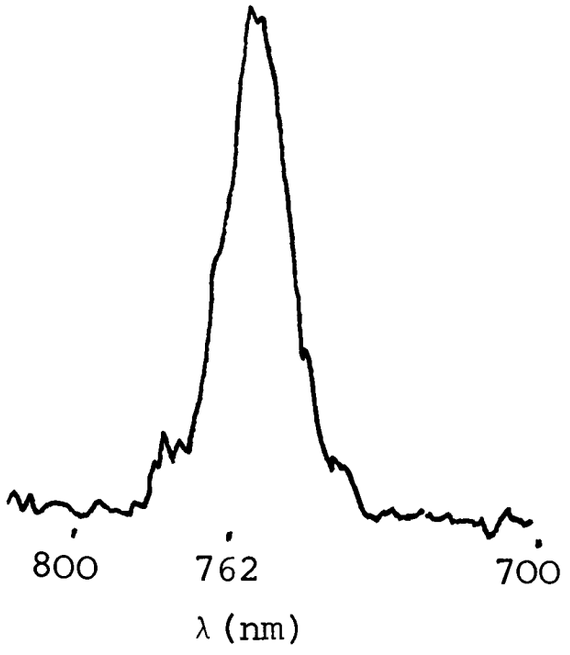


Figure 47. Scan of oxygen photolysed at λ = 147 nm using 9558A detector. Lamp power 150 watts. E.H.T. 1350 volts.

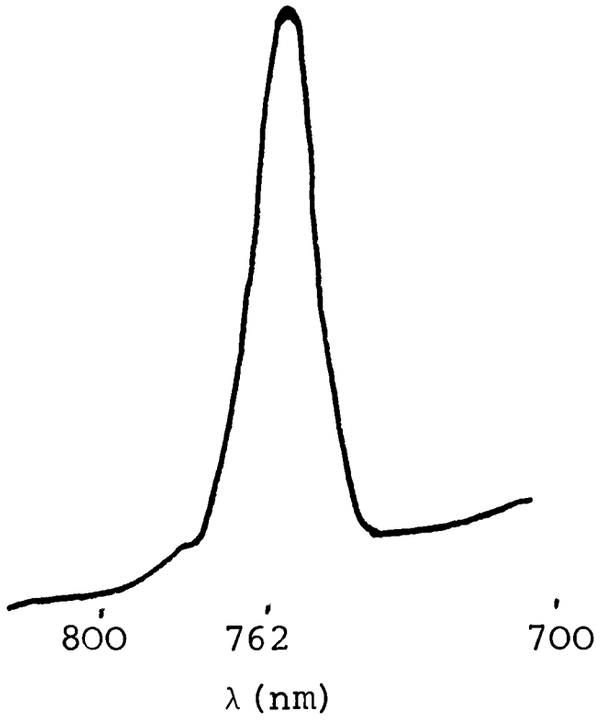


Figure 47(a). Scan of discharge products of oxygen using 9558A detector. E.H.T. 1100 volts. Microwave power 150 watts.

using an interference filter, which has not been sufficiently well collimated, when calibrating a detector against the air afterglow could lead to errors due to the shift of the band pass to shorter wavelengths. In addition, the calibration for determining $[O_2(^1\Sigma g^+)]$ required that the EHT supplied to the photomultiplier was less for observing the air afterglow than for the atmospheric band. A sensitivity scaling factor obtained from figure 21 was applied in the calculation, but this approach could be open to error and it was thought desirable to carry out all observations at the same applied voltage.

The calibration experiments carried out in section 4.6 were repeated using a Bausch and Lomb monochromator instead of an interference filter. An identical flow system to that used before (figure 40) was adopted. The detector (E.M.I. 9558A) and monochromator were not moved. The lamp power was set at 150 watts and the applied voltage at 1310 volts. A scan of the products of irradiated oxygen at λ = 147 nm is shown in figure 47a and if compared to a scan of the products of a discharge through oxygen (figure 47b) then it is clear that $O_2(^1\Sigma g^+)$ is present in figure 47. The background signal in figure 47b is due to a residual air afterglow produced by nitrogeneous impurities in the discharge. Calibrations were carried out as described in section 2.6c, the applied voltage being kept

constant throughout all experiments. The $O_2(^1\Sigma g^+)$ signal at the observation point was recorded and the [O] atom concentration was measured by adding a known amount of nitric oxide to the flow. The $[O_2(^1\Sigma g^+)]_o$ and $[O]_o$ values were calculated as described in section 4.6 using α values from these earlier results, and are listed in Table 11.

It is apparent that the ratio $\frac{[O]_o}{2[O_2(^1\Sigma g^+)]_o} \times 10^{-2}$ is about 2 which is not far removed from the value of 5 obtained in earlier experiments. If k_{10} for $M = O_2$ is taken as 2×10^{10} mole^{-1} l sec^{-1} then k_5 is given as 1×10^8 mole^{-1} l sec^{-1}. These calibrations indicate that the errors incurred by using a filter system and variable applied voltage to the detector are in fact not very large.

The results of other workers for reactions of $O(^1D)$ atoms vary considerably. However, recently Zipf [52] has reported a number of rate constants which clearly suggest that nitrogen is a more efficient deactivator of $O(^1D)$ atoms than oxygen, with a rate constant for k_{12} with $M = N_2$, of $3 - 6 \times 10^{10}$ mole^{-1} l sec^{-1}. This is in good agreement with the present result. Since the present results were estimated using an assumed value of k_{10} ($M = O_2$) it is probably more meaningful to discuss them in relative terms with other workers. The ratio $\frac{k_{10}}{k_{12}} = 0.3$ which is in good agreement with the value quoted by Le Blanc

Table 11.

$10^4[O_2]$ mole l^{-1}	$10^{13}[O_2(^1\Sigma g^+)]_t$ mole l^{-1}	α sec^{-1}	$e^{-\alpha t}$	$10^{12}[O_3(^1\Sigma g^+)]_o$ mole l^{-1}	$10^{10}[O]_t$ mole l^{-1}	$e^{-\alpha' t}$	$10^{10}[O]_o$ mole l^{-1}	$\frac{10^{-2}[O]_o}{2[O_2(^1\Sigma g^+)]_o}$
1.60	1.47	140	.07	2.10	5.0	0.90	5.55	1.3
2.20	2.20	109	.14	1.60	3.82	0.84	4.55	1.4
2.62	2.40	100	.19	1.25	3.16	0.79	4.00	1.6
2.94	2.16	96	.23	0.94	3.04	0.76	4.00	2.1
3.20	2.00	93	.24	0.83	2.34	0.73	3.20	1.9
2.04	2.20	118	.12	1.85	4.1	0.86	4.80	1.2

et al [115] of 0.25 and Young and Black [37] of 0.6. The ratio of $\frac{k_{12(M=Ar)}}{k_{12(M=N_2)}} \sim 10^{-1}$ for the present set of experiments, which is higher than the value of Preston et al [116] of 4×10^{-2} and Young and Black [37] of 3.6×10^{-2}. The present results suggest that in the energy transfer process 4.5 one molecule of $O_2(^1\Sigma g^+)$ is formed for about 200 $O(^1D)$ atoms quenched, which is in conflict with Noxon [39] who quotes a value of 1 in 5.

4.12 Attempts to detect $O_2(^1\Delta g)$.

The energy transfer process reaction:

$$O(^1D) + O_2 \rightarrow O_2(^1\Delta g) + O^3P \qquad 4.14$$

has been observed in the photolysis of ozone-oxygen mixtures with $\lambda = 253.7$ nm (see Chapter 3, [32]). Attempts were made to detect radiation at 1270 nm from $O_2(^1\Delta g)$ in the photolysis products of oxygen using the same flow system shown in figure 40. The detector employed was the R.C.A. 7102 photomultiplier. The minimum detectable concentration of $O_2(^1\Delta g)$ was about 3×10^{-13} mole l^{-1} in the apparatus, while the maximum $[O_2(^1\Sigma g^+)]$ at the observation point; 2×10^{-14} mole l^{-1} in the experiments described in section 4.6. Thus if $O_2(^1\Delta g)$ decays at a similar decay rate to that of $O_2(^1\Sigma g^+)$ then reaction 4.14 would have to proceed at 15 times faster than k_5 for $O_2(^1\Delta g)$ to be observable, i.e. $k_{14} < 6 \times 10^8$ mole^{-1} l sec^{-1}. A fuller discussion of $O_2(^1\Sigma g^+)$ and

Table 12.

Reaction	Rate constant $l\ mole^{-1} sec^{-1}$	Remarks
$O_2(^1\Sigma g^+)+O_3 \rightarrow 2O_2+O$	4.3×10^9	direct assessment.
$O_2(^1\Sigma g^+)+N_2 \rightarrow O_2+N_2$	1.4×10^6	direct assessment.
$O_2(^1\Sigma g^+)+O_2 \rightarrow O_2+O_2$	$\leq 6 \times 10^4$	upper limit from figure 45
$O_2(^1\Sigma g^+) \xrightarrow{wall} O_2$	($\gamma \sim 10^{-2}$)	extrapolation to $[O_2] = 0$ in figure 45
$O_2(^1\Delta g)+O_2(^1\Delta g) \rightarrow O_2(^1\Sigma g^+)+O_2$	1.4×10^3	based on comparison of quenching results for $M=N_2$ with data of Arnold et al (1968)[97]
$O(^1D)+O_2 \rightarrow O_2(^1\Sigma g^+)+O^3P$	4×10^7 } 1×10^8 }	estimates based on k_5+k_{10} = $2 \times 10^{10} mole^{-1}$ l sec^{-1} [52]
$O(^1D)+O_2 \rightarrow O_2(^1\Delta g)+O$	$\leq 6 \times 10^8$	
$O(^1D)+N_2 \rightarrow O+N_2$	7×10^{10}	
$O(^1D)+Ar \rightarrow O+Ar$	8×10^9	

$O_2(^1\Delta g)$ production in ozone photolysis is presented in Chapter 3.

All the results measured or estimated in this chapter are brought together in Table 12, mentioning the assumptions made in deriving the constants.

4.13 Further work on oxygen photolysis.

The temperature dependence of reaction 4.3:

$$O_3 + O_2(^1\Sigma g^+) \rightarrow 2O_2 + O(^3P) \qquad 4.3$$

should be examined in order to obtain the activation energy. The low temperature values of k_3 would be exceedingly useful in atmospheric calculations. The photolysis system should be improved to obtain an accurate measurement of the quenching rates for $O_2(^1\Sigma g^+)$ with oxygen and argon, and to show , as has been suggested, whether $O_2(^1\Delta g)$ is the quenching product of reaction 4.2:

$$O_2 + O_2(^1\Sigma g^+) \rightarrow O_2(^1\Delta g) + O_2 \qquad 4.2$$

Further attempts, using a more refined optical apparatus, should be made to observe $O_2(^1\Delta g)$ as a product of the photolysis of oxygen with $\lambda = 147$ nm.

The system is clearly a useful source of $O(^1D)$ atoms. Attempts should be made to observe the $O(^1D) \leftrightarrow O(^3P)$ transition at 634 nm, so that more direct measurements of $O(^1D)$ atom reactions can be made. In particular, the reactions of $O(^1D)$ with CO_2, CO and H_2O should be studied as their rate constants have not been well established.

CHAPTER 5

MISCELLANEOUS REACTIONS

Chapter 5 considers other possible reactions which might lead to excited singlet oxygen. These include atom recombination reactions, the nitric oxide-ozone reaction and some preliminary studies of photosensitization reactions with organic gases.

5.1 Atom recombination.

The reaction between two ground state oxygen atoms with a third body was suggested as a means of producing excited singlet molecular oxygen in the atmosphere [13]. Indeed Young and Sharpless [41,100] have observed $O_2(^1\Sigma g^+)$ and $O_2(^3\Sigma_u^+)$ as products of the reaction

$$O(^3P) + O(^3P) + M \rightarrow O_2(^1\Sigma g^+) + M \qquad 5.1$$

The rate constant for this reaction for $O_2(^1\Sigma g^+)$ production was given as $k_1 = 5 \times 10^4$ mole^{-2} l^2 sec^{-2} for M = nitrogen, although there was some inconsistency in their experimental results.

An analogous reaction for $O_2(^1\Delta g)$ production would be

$$O(^3P) + O(^3P) + M \rightarrow O_2(^1\Delta g) + M \qquad 5.2$$

No experimental evidence for such a reaction has yet been presented.

Experiments were thus carried out in an attempt to detect $O_2(^1\Delta g)$ by reaction 5.2. The source of $O(^3P)$ atoms was

obtained by titration of nitrogen atoms, produced by a microwave discharge through molecular nitrogen, with nitric oxide:

$$N + NO \rightarrow N_2 + O(^3P) \qquad 5.3$$

Addition of too much nitric oxide resulted in the appearance of the air afterglow.

The flow system is shown in figure 48 and the monochromator with germanium detector was employed to observe $O_2(^1\Delta g)$. In an experiment various nitrogen atom concentrations were titrated with nitric oxide and any signal at 1270 nm was recorded. In addition, the region between 1100 nm and 1400 nm was scanned with the monochromator. The apparatus was calibrated with the air afterglow, as described in section 2.6c, in order to obtain a value for the minimum detectable signal at 1270 nm. The minimum measurable signal on the pen recorder was taken as one centimeter and this corresponded to the emission from an $O_2(^1\Delta g)$ concentration of 3×10^{-10} moles l^{-1}. Table 13 lists the results and experimental conditions for a number of runs. In all experiments, no $O_2(^1\Delta g)$ was observed

Although no $O_2(^1\Delta g)$ was observed some limiting estimate of the rate constant of reaction 5.3 was made. A simplified reaction scheme for the reactions of $O(^3P)$ atoms was adopted.

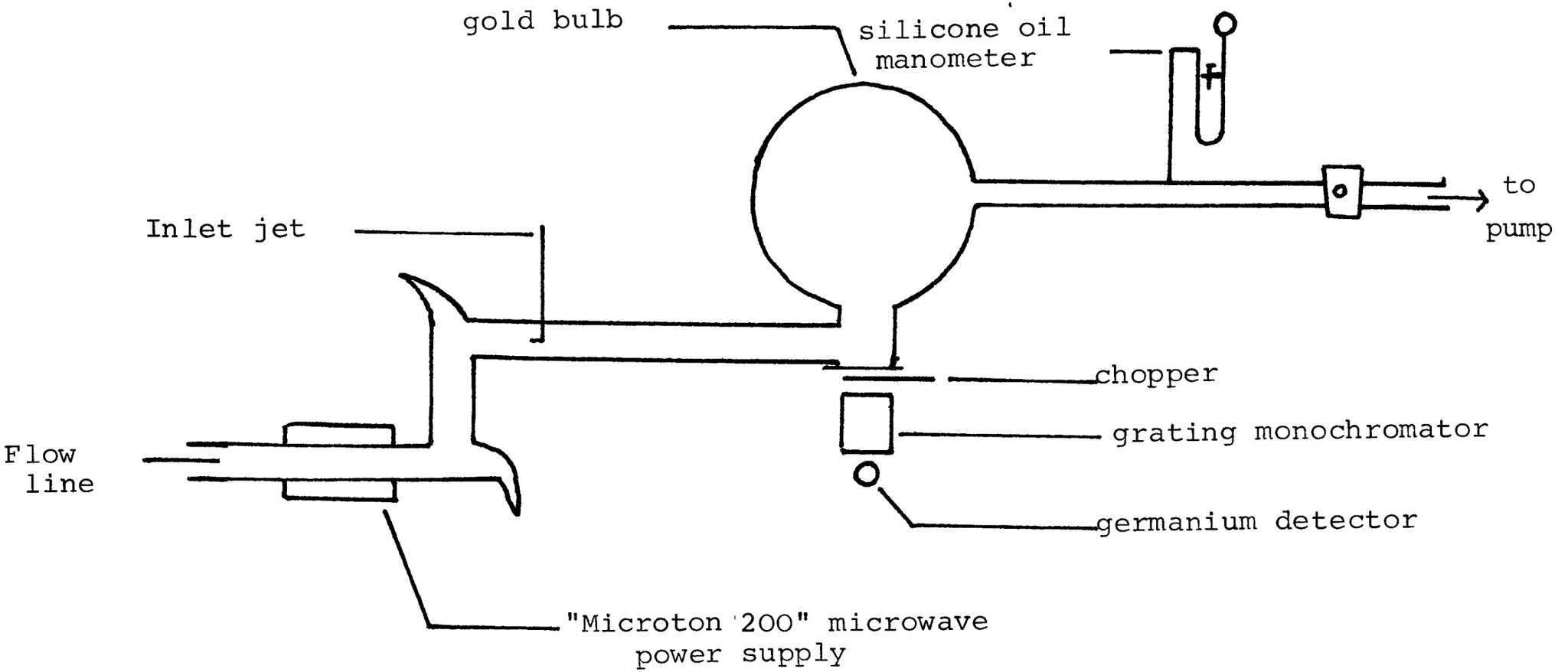


Figure 48. Flow system for studying atom recombination reactions

Table 13.

$10^5[N_2]$ mole l^{-1}	Power watts	$10^7[NO]$ mole l^{-1}	Nature of M	Detector	Volts	$O_2(^1\Delta g)$ emission	Min. detect. $O_2(^1\Delta g)$ mole l^{-1}
1.2	40	4.0	Nitrogen	Germanium	6	None	3×10^{-10}
1.7	40	6.65	Nitrogen	"	"	"	"
2.8	40	10.7	Nitrogen	"	"	"	"
3.0	80	14.0	Nitrogen	"	"	"	"

$$O(^3P) + O(^3P) + M \rightarrow O_2(^1\Delta g) + M \qquad 5.2$$

$$O_2(^1\Delta g) \xrightarrow{\text{wall}} O_2 \qquad 5.4$$

$$O_2(^1\Delta g) \rightarrow O_2 + h\nu \qquad 5.5$$

Oxygen was not used as the third body in any of the experiments, and ozone formation via reaction 5.6:

$$O(^3P) + O_2 + M \rightarrow O_3 + M \qquad 5.6$$

was thus not important in our system.

A steady state approximation was adopted

$$\frac{d[O_2(^1\Delta g)]}{dt} = k_2[O(^3P)]^2[M] - k_4[O_2(^1\Delta g)]$$

$$k_2 = \frac{k_4[O_2(^1\Delta g)]}{[O(^3P)]^2[M]}$$

Deactivation of $O_2(^1\Delta g)$ by nitrogen was not considered since the rate constant for this quenching reaction was evaluated by Clark and Wayne as 2.4×10^2 mole^{-1} l sec^{-1} and is clearly very slow. The value of wall deactivation was taken as .2 sec^{-1} which, according to Clark and Wayne, is a reasonable value for a pyrex surface. Using the results in Table 13, the upper limit for the rate constant at reaction 5.2 was $k_2 \leq 10^6$ moles^{-2} l^2 sec^{-2}.

The magnitude of this rate constant is discussed in Chapter 6 with respect to its importance in producing significant amounts of singlet excited molecular oxygen in the atmosphere.

5.2 Nitric oxide-Ozone reaction.

The chemiluminescent reaction between nitric oxide

and ozone was suggested as a source of $O_2(^1\Delta g)$ in polluted atmospheres [105]. Clough and Thrush [44] have made an extensive study of the kinetics of this highly exothermic reaction and found that chemiluminescence was produced. The maximum intensity for the NO + O_3 glow occurs at an energy of 23 K.cals $mole^{-1}$ which is ℘ w for an electronic transition. The reaction scheme proposed was as follows:

$$NO + O_3 \rightarrow NO_2^* \text{ (excited state)} + O_2 \qquad 5.7$$

$$NO + O_3 \rightarrow NO_2 \text{ (ground state)} + O_2 \qquad 5.8$$

$$NO_2^* \rightarrow NO_2 + h\nu \qquad 5.9$$

$$M + NO_2^* \rightarrow NO_2 + M \qquad 5.10$$

Clyne, Thrush and Wayne [43] found that the pre-exponential factors for the reactions yielding ground state and electronically excited NO_2 were virtually the same. Thus it was argued that $O_2(^1\Delta g)$ and $O_2(^1\Sigma g^+)$, with electronic excitation energies of 22 and 37 K.cals $mole^{-1}$ respectively could be formed in the reaction. Attempts were made by Clough and Thrush to observe $O_2(^1\Delta g)$ and $O_2(^1\Sigma g^+)$ but proved negative and it was suggested that the excitation of NO_2 in preference to O_2 was associated with the fact that it contains the newly formed bond, whereas the O-O linkage takes no active part in the reaction.

Experiments were carried out to confirm this result, using different detectors to those of Clough and Thrush.

The observations fall into two categories (a) using the photomultiplier and various interference filters and (b) the monochromator and germanium detector. The flow system was the same as described in 5.1 (figure 48). Ozone and nitric oxide were prepared as described in section 2.1.

When using the photomultiplier-filter system the intensities through the 643 nm, 701 nm, 762 nm, 801 nm, 807 nm and 1270 nm filters were recorded. The percentage relative intensities (relative to the 801 nm filter for the 7102 and the 762 nm filter for the 9558A photomultiplier) are listed in Table 14. Carrier gases when used were either oxygen or nitrogen at concentrations of 4×10^{-5} moles l^{-1}.

It is clear from Table 14 that, within the experimental error of about 3 - 5% in the relative intensities, there is no significant deviation at 762 nm or 1270 nm over the experimental conditions employed and so $O_2(^1\Delta g)$ or $O_2(^1\Sigma g^+)$ was not produced by this chemiluminescent reaction.

An attempt was made using the germanium detector and monochromator to scan the NO + O_3 glow to see if there was any deviation at 1270 nm. A typical run is shown in figure 49 indicating the recorded intensity change with increasing wavelength. Over the experimental runs no

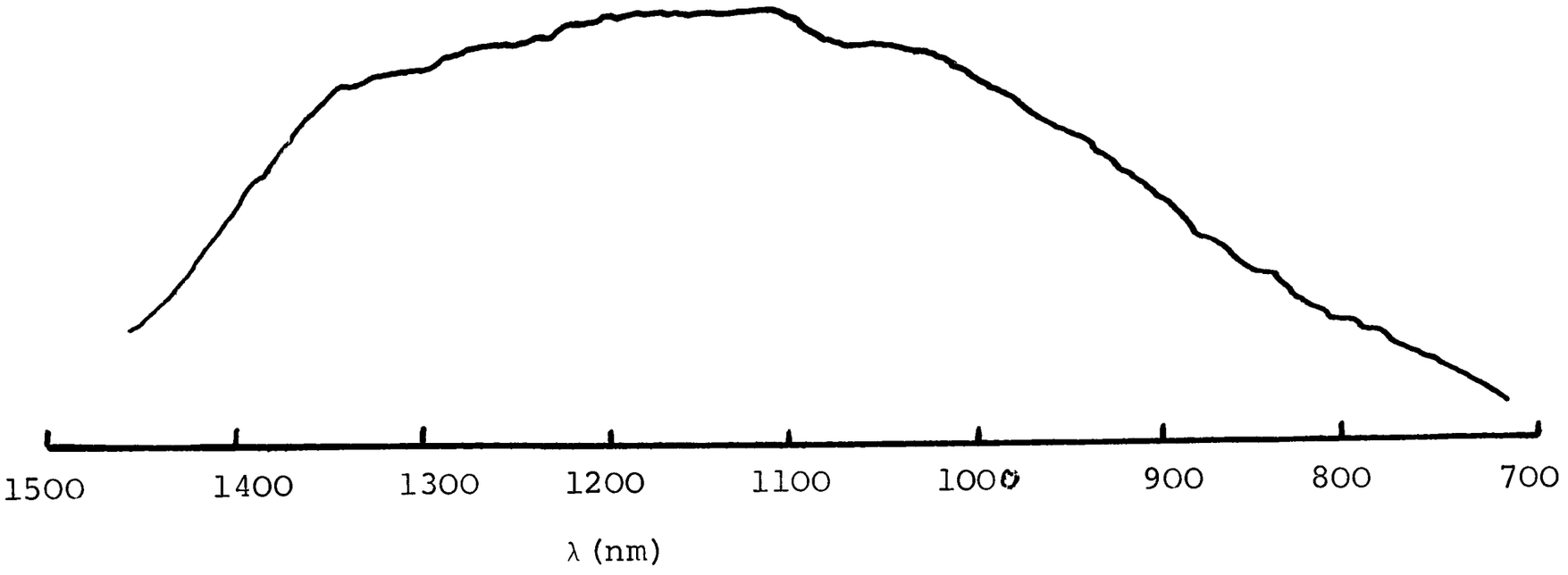


Figure 49. Scan of NO + O_3 glow using monochromator and germanium detector. [NO] $\approx 10^{-6}$ mole l^{-1}, [O_3] $\approx 10^{-6}$ mole l^{-1}

Table 14. Relative filter intensities of the NO + O_3 glow

$[O_3]$ mole l^{-1}	[NO] 10^7 mole l^{-1}	643 nm	701 nm	762 nm	801 nm	870 nm	1270 nm	E.H.T. volts	Nature of M 10^5 mole l^{-1}	Detector
		← relative filter intensities →								
1.9	1.30	28.8	46.0	49.5	100		6.8	1200	None	R.C.A.
1.2	1.30	28.0	45.0	48.0	100		7.0	1100	"	7102
0.8	1.30	29.0	47.0	49.5	100		7.15	1100	"	"
3.6	1.30	-	47.5	50.0	100		6.4	1100	"	"
0.84	0.68	29.0	45.0	50.0	100		7.25	1100	"	"
1.2	0.68	-	46.0	50.0	100		7.2	1100	"	"
3.6	4.65	-	49.0	51.5	100		6.8	1100	"	"
0.65	7.74	29.0	46.0	49.5	100		7.3	820	"	"
1.1	5.00	-	45.5	49.5	100		7.4	820	"	"
1.5	5.5				100		7.4	1400	O_2	7102
3.5	5.5				100		7.0	1000	N_2	"
3.5	5.5				100		6.8	1160	O_2	"
1.0	3.2			100.	38.0	11.0	11.0	1080	O_2	9558A
2.1	3.2			100.	38.0	11.5		1080	O_2	"
2.6	3.2			100.	37.5	12.5		1080	O_2	"
1.7	5.3			100.	39.0	11.0		800	O_2	"
1.7	5.3			100.	39.0	11.0		800	N_2	"
1.7	5.3			100.	36.0	11.0		1100	N_2	"

significant deviation at 1270 nm was observed. Wayne [106] has also attempted to detect $O_2(^1\Delta g)$ using essentially the same system but with greater resolution, and finds noevidence for $O_2(^1\Delta g)$. For this set of experiments it was concluded that the nitric oxide-ozone reaction does not produce detectable quantities of $O_2(^1\Sigma g^+)$ or $O_2(^1\Delta g)$.

5.3 Photosensitisation reactions.

Khan et al [105] have suggested that any one of a variety of organic compounds that absorb radiation at wavelengths greater than the atmospheric cut off at about 300 nm could act as donors (D) in an energy transfer mechanism.

$$D(S_o) + h\nu \longrightarrow D^*(S_1) \qquad 5.12$$

$$D^*(S_1) \xrightarrow[\text{crossing}]{\text{intersystem}} D^{**}(T_1) \qquad 5.13$$

$$D^{**}(T_1) + O_2(^3\Sigma g^-) \longrightarrow D(S_o) + O_2(^1\Delta g \text{ or } \Sigma g^+) \qquad 5.14$$

(S) and (T) refer to singlet and triplet states. It was suggested [107] that simple organic compounds prevalent in polluted atmospheres might yield excited singlet oxygen molecules.

Experiments were carried out in an attempt to detect $O_2(^1\Delta g)$ or $O_2(^1\Sigma g^+)$ by the above mechanism in irradiated mixtures of methane, ethane and ethylene (all supplied by Matheson Gas Co.) with oxygen. The absorption curves for methane, ethane and ethylene are shown in figure 50. From

these curves it is clear that radiation < 180 nm was required and a low pressure hydrogen lamp was employed. This had identical design and mode of preparation to those described in section 2.4. This type of lamp, if not getterised, was found to give a rather impure spectrum from the lithium fluoride cutoff at 104 nm upwards. However, in these experiments the quantity of ultra violet radiation rather than the purity of radiation was of importance. The flow system employed was as in figure 48, and photomultiplier-interference filters were used to observe any $O_2(^1\Delta g)$ or $O_2(^1\Sigma g^+)$.

No emission was observed with methane-oxygen, ethane-oxygen, ethylene-oxygen, mixtures.

The same procedure was adopted using benzene-oxygen mixtures. The benzene was degassed under vacuum. The irradiation source employed was a low pressure mercury resonance lamp, yielding λ = 253.7 nm. Consideration of the absorption curve for benzene, figure 51, shows that benzene has a maximum absorption near 253.7 nm. Some evidence for the presence of $O_2(^1\Delta g)$ was observed using the 7102 photomultiplier and 1270 nm interference filter. No $O_2(^1\Sigma g^+)$ was observed in this system when using the 9558 photomultiplier and 762.0 nm interference filter. However, Snelling [108] has obtained emission at 1270 nm from a similar system and has carried out a detailed kinetic study. He found that the production of $O_2(^1\Delta g)$

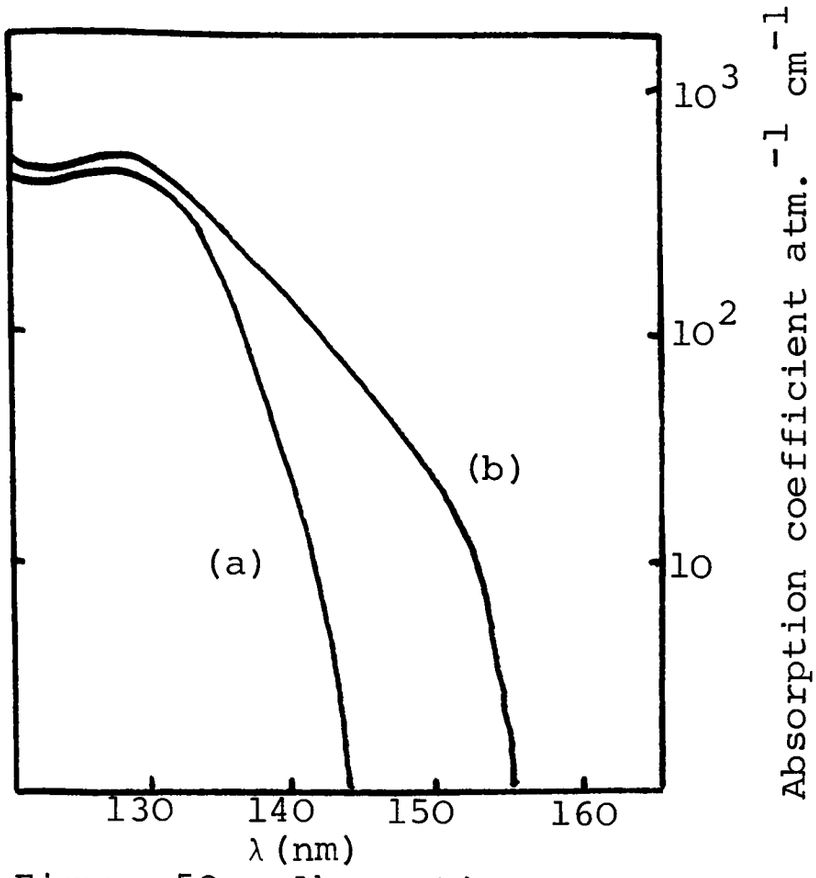


Figure 50a. Absorption spectrum of (a) methane and (b) ethane [88]

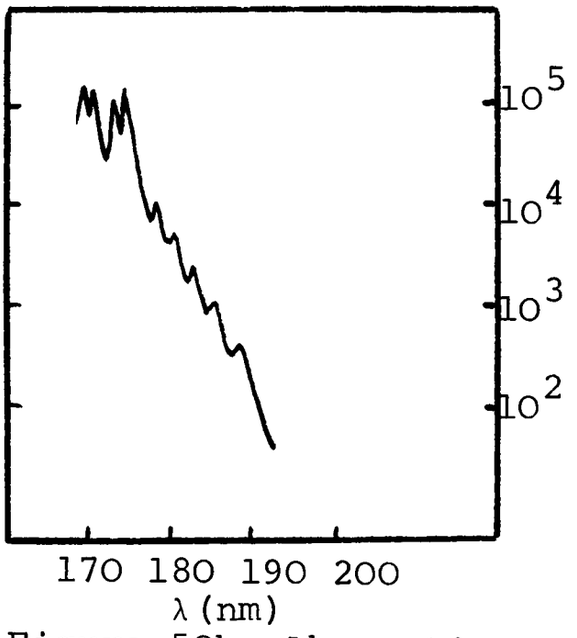


Figure 50b. Absorption spectrum of ethylene [88]

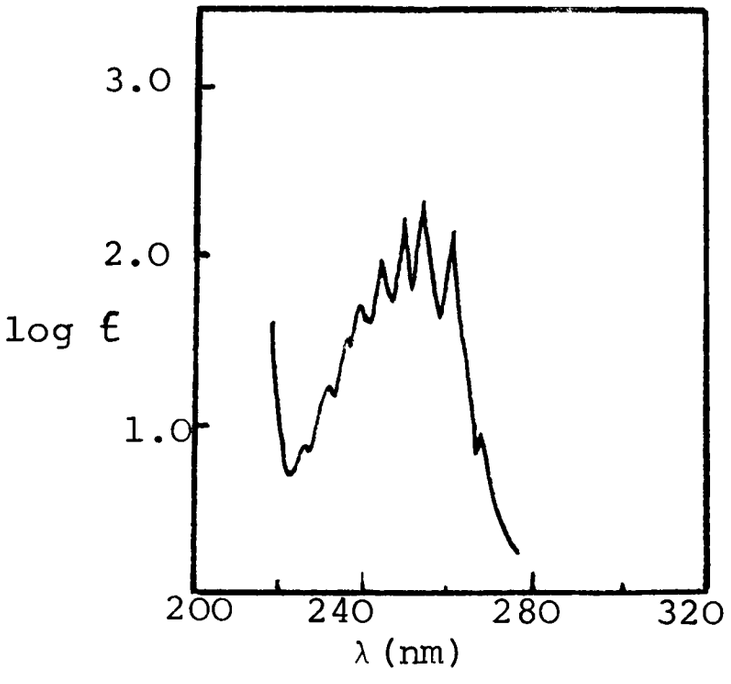


Figure 51. Absorption spectra of benzene, cyclohexane [88] being the solvent.

can be attributed to the quenching of triplet benzene by oxygen, and has suggested a rate of 3×10^{10} l mole^{-1} sec^{-1} for this process.

Numerous workers [109] have subsequently detected $O_2(^1\Delta g)$ by means of the transfer of energy from the triplet states of a selection of organic molecules to ground state oxygen.

CHAPTER 6

ATMOSPHERIC DISCUSSION

One of the aims of this thesis was to try and elucidate some of the likely mechanisms that could produce singlet excited oxygen molecules in the atmosphere. The results of observations described in this thesis suggest:-

a) Photolysis of pure ozone at λ = 253.7 nm does not produce $O_2(^1\Delta g)$ in significant quantities in the primary photolytic step.

b) Photolysis of pure ozone at λ = 253.7 nm may produce $O_2(^1\Sigma g^+)$ but observation made difficult by the rapid deactivation of the species by ozone.

c) Photolysis of ozone-oxygen mixtures at λ = 253.7 nm produces $O_2(^1\Delta g)$ by an energy transfer process.

d) Photolysis of pure ozone at λ > 266 nm does not produce any excited species, though the lack of observation could be due to experimental limitations.

e) Photolysis of oxygen at λ = 147 nm produces $O_2(^1\Sigma g^+)$ by the energy transfer reaction.

f) The atom recombination of ground state oxygen atoms with a third body does not produce significant concentrations of $O_2(^1\Delta g)$.

Comparison of the day and night time intensities of the atmospheric and infra-red atmospheric band [15]

suggests that the ultimate source of excitation of singlet oxygen is photochemical, below altitudes of 100 KM. Houghton [21] has pointed out that direct absorption of solar radiation by molecular oxygen is not likely to be the main source of singlet oxygen since, in order to produce the observed emission intensities, 50% of the energy absorbed at all wavelengths would have to be re-radiated in the two atmospheric bands. Ozone would be a more probable source of the energy, since the excitation and emission from singlet oxygen would only have to be .3% efficient.

No radiation from $O_2(^1\Sigma g^+)$ was observed in the photolysis of pure ozone at λ = 253.7 nm, but as deactivation reactions play a major role in the laboratory system, it is not clear whether or not $O_2(^1\Sigma g^+)$ is produced. Wallace and Hunter [13] have shown that such a production mechanism would fit their observed intensity-altitude data for the atmospheric band in the day-glow.

In the case of $O_2(^1\Delta g)$ no emission was observed from photolytic studies of pure ozone. This suggests that some other mechanism may be producing $O_2(^1\Delta g)$ in the atmosphere. The energy transfer process does produce $O_2(^1\Delta g)$, and a rate constant for the reaction was evaluated. Calculations were carried out to determine (1) whether the energy transfer could yield sufficient $O_2(^1\Delta g)$, (2) how important

was the role of any $O_2(^1\Delta g)$ production in the primary step and (3) the main quenching mechanisms in the atmosphere.

The following reaction scheme was proposed.

$$O_2 + h\nu \xrightarrow{J[O_3]} \begin{cases} \xrightarrow{\alpha} O_2 + O(^1D) & 6.1a \\ \xrightarrow{\beta} O_2(^1\Delta g) + O(^1D) & 6.1b \end{cases}$$

$$O(^1D) + O_2 \longrightarrow O(^3P) + O_2 \qquad 6.2$$

$$O(^1D) + N_2 \longrightarrow O(^3P) + N_2 \qquad 6.3$$

$$O(^1D) + O_2 \longrightarrow O_2(^1\Delta g) + O(^3P) \qquad 6.4$$

$$O(^1D) + O_3 \longrightarrow 2O_2 \qquad 6.5$$

$$O_2(^1\Delta g) + O_2 \longrightarrow 2O_2 \qquad 6.6$$

$$O_2(^1\Delta g) + O_3 \longrightarrow 2O_2 + O \qquad 6.7$$

$$O_2(^1\Delta g) \longrightarrow O_2 + h\nu \qquad 6.8$$

A stationary state is assumed to be set up, i.e. $\frac{d[O(^1D)]}{dt} = \frac{d[O_2(^1\Delta g)]}{dt} = 0$. This gives

$$[O(^1D)] = \frac{J[O_3]\ (\alpha + \beta)}{(k_2+k_4)[O_2]+k_3[N_2]+k_5[O_3]} \qquad 6.A$$

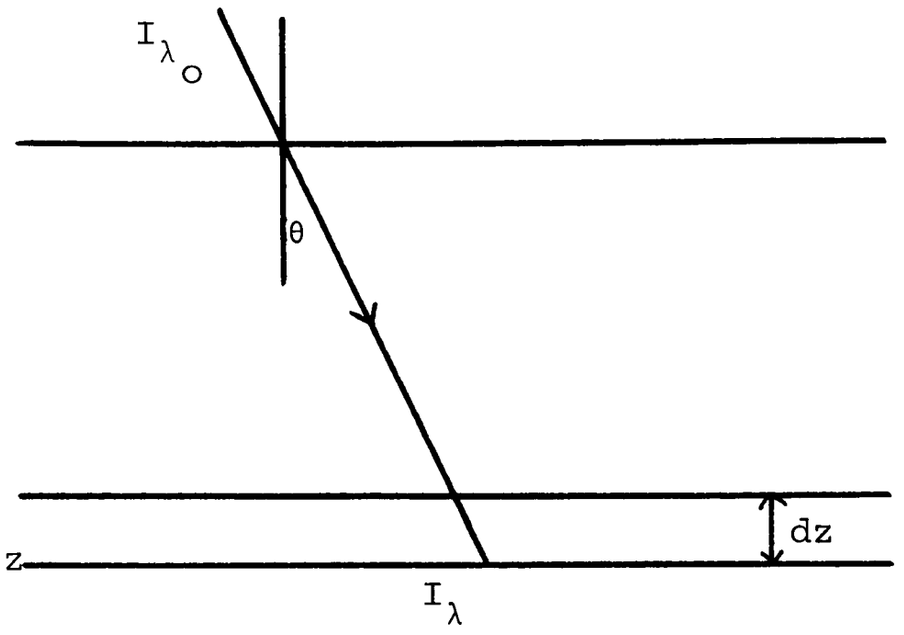
$$[O_2(^1\Delta g)] = \frac{J[O_3](1-\alpha)+k_4[O_2][O(^1D)]}{k_6[O_2] + k_7[O_3] + k_8} \qquad 6.B$$

The intensity of the "infra-red atmospheric" band I for an atmospheric layer of thickness d cms is given by

$$I = k_8[O_2(^1\Delta g)]d. \qquad 6.C$$

The J values were computed by Dr. D.P. Edwards [110] and their significance can be understood by consideration

of the following figure:



The solar intensity I_λ at a height z is related to the ozone concentration $[O_3]$ and the ozone absorption cross section α_λ by

$$I_\lambda = I_{\lambda_o} e^{-\sec\theta \int_z^\infty \alpha_\lambda [O_3] dz} \qquad 6.D$$

where θ is the solar zenith angle.

The decomposition of ozone is given by

$$\frac{-d[O_3]}{dt} = I_\lambda \alpha_\lambda [O_3] = J_\lambda [O_3] \qquad 6.E$$

Integration of this over the wavelength considered gives

$$\int \frac{-d[O_3]}{dt} . d\lambda = \int J_\lambda [O_3] d\lambda \qquad 6.F$$

$$= J[O_3] \qquad 6.G$$

The values of I_{λ_o} between 200 nm and 350 nm were taken

from Allen [89]. The ozone distribution was taken from two sources, Hering's observations at the Canal Zone [19] and values presented at the U.G.G.I. Symposium at Lucerne. These values were recently confirmed by unpublished results from the Meteorological Office [111]. The J values were computed for $\lambda \leq 310$ nm for a solar zenith angle of 60^{o}.

Rate constants in this chapter are expressed in cm^3 molecules sec^{-1} units, since virtually all atmospheric data employs these units. Intensity units are given in Rayleighs. This unit is generally used by atmospheric physicists in airglow measurements and corresponds to an apparent emission rate of 10^6 photons sec^{-1} in a column of area 1 cm^2.

A number of computations, using an ALGOL programme, were carried out firstly using rate constants derived from this work and secondly, using other values to test which mechanisms are important in either production or removal of $O_2(^1\Delta g)$. Table 15 lists a series of runs stating the value and reference of the rate constants used. All values are taken at room temperature. The value of $\log_{10}I$ is given where I is the total emission from a column above 27 K.m in Rayleighs. $O(^1D)$ atoms and $O_2(^1\Delta g)$ concentrations are also listed in logs. These are taken at a spot height of 49.6 Km. In each run concentration and intensity values were computed between 27 and 80 Km. and

selecting a spot height of 49.6 Km for each run was done for convenience of tabulation in order to indicate the important processes more easily. A complete run is discussed later. Table 15 also lists the number of reactions per sec per cm^3, in logs, at 49.6 Km for each reaction over a selected number of runs.

Before being able to consider the computed results it is necessary to know the magnitude of the various parameters observed in the atmosphere. Atmospheric observation requires a total intensity I of 3×10^7 Rayleighs, i.e. $\log_{10} I = 7.5$.

Using this value it is possible to assess the results of Table 15. The conclusions drawn are listed as follows:

(1) In run B only the energy transfer process for producing $O_2(^1\Delta g)$ and the radiation process 6.8 occur which was to see what was the maximum possible intensity that could be attributed to the energy transfer process. The calculated value of I was $\log_{10} I = 9.1$ and so there is plenty of energy available to give the required intensity. However, this value is obtained without considering all the deactivation mechanisms. The effect of these are considered below.

(2) In run C the rate constants for each reaction were included in the computation and the resulting intensity is $\log_{10} I = 3.8$. This value is very much smaller than the

Table 15.

Run	α	β	k_2	k_3	k_4	k_5	k_6	k_7	k_8	$\log_{10}\frac{I}{F}$	$\log_{10}(O^1D)$	$\log_{10}(^1\Delta g)$	references of k values
B	1	0	0	0	3×10^{-13}	0	0	0	2.6×10^{-4}	9.1	5.3	12.0	k_4: this work k_8: [14]
C	1	0	3.4×10^{-10}	1.3×10^{-10}	3×10^{-13}	4×10^{-10}	2.2×10^{-18}	2×10^{-15}	2.6×10^{-4}	3.8	1.9	7.1	k_2: [52] k_5: this work k_3: this work k_6, k_7: [44]
D	1	0	"	"	"	1×10^{-13}	"	"	"	3.8	1.9	7.1	k_3: varied
G	1	0	4×10^{-15}	2×10^{-14}	"	"	"	"	"	7.0	5.1	10.3	k_2, k_3 : [102]
H	1	0	"	8×10^{-14}	"	"	"	"	"	6.8	4.9	10.0	k_3: varied
I	0	1	3.4×10^{-11}	1.3×10^{-10}	"	"	"	"	"	7.2	1.9	10.4	$\beta = 1$
J	0.7	0.3	"	"	1×10^{-12}	4×10^{-10}	"	"	"	6.6	1.9	9.9	k_4: [33]
L	1	0	"	"	3.4×10^{-11}	"	"	"	"	5.9	1.9	9.1	$k_2 = k_4$: [52]
M	0	1	"	"	"	"	"	2×10^{-15}	"	7.2	1.9	10.4	
N	0	1	"	"	"	"	"	6×10^{-15}	"	7.2	1.9	10.4	k_7: varied
P	0	1	"	"	"	"	"	2×10^{-15}	7.8×10^{-4}	7.6	1.9	10.4	k_8: varied

M	8.4	7.1	8.4	7.1	3.1	8.4	6.3	6.8
N	"	"	"	"	"	"	0.8	"
L	"	"	"	"	"	7.1	5.0	5.3
P	"	"	"	"	"	8.4	6.3	7.3
J	"	7.2	"	5.0	3.2	7.9	5.8	6.8

$\log_{10}$ of numbers of reactions sec^{-1} cm^{-3} at 49.6 KM.

required $\log_{10}I = 7.5$, and shows how important the deactivation reactions are. In addition it is apparent that the reaction 6.4 with the rate constant of 3×10^{-13} cm^3 molecules sec^{-1} does not produce sufficient $O_2(^1\Delta g)$. Indeed in run L where the value of k_4 has been increased to that of k_2, i.e. an $O_2(^1\Delta g)$ molecule produced for every collision of $O(^1D)$ atom with oxygen, the intensity is $\log_{10}I = 5.9$. This is still a factor of fifty too small.

It is clear that the deactivation reactions play an important role in $O_2(^1\Delta g)$ production scheme. It is necessary to consider each reaction in turn to evaluate which are the most important quenchers of the excited species $O_2(^1\Delta g)$ and $O(^1D)$.

(3) Comparison of runs C and D in which k_5 was varied indicate that there is no significant change in the final calculated intensity. $O(^1D) + O_3 \rightarrow O_3$. Thus although k_5 has a very high rate constant it is not that important as a quencher in the atmosphere.

(4) Comparison of runs C, G and H indicate that changes in the rate constant of reaction 6.3:

$$N_2 + O(^1D) \rightarrow N_2 + O(^3P) \qquad 6.3$$

cause large changes in the final intensity value. Indeed in G where k_3 is given the low value evaluated by Warneck and Sullivan [102], $\log_{10}I = 7.0$ which is close to the observed value. However, the higher values of k_3 are now

generally regarded as correct. These runs show how important reaction 6.3 is in removing $O(^1D)$.

(5) In run L, β is put at 1. Thus all oxygen molecules formed in the primary process are $O_2(^1\Delta g)$. This gives an intensity of $\log_{10}I = 7.2$, which is very close to the observed value. Clearly, the production of $O_2(^1\Delta g)$ in the primary step seems an essential requirement to give sufficient intensity values.

(6) In runs M and N the rate constant of reaction 6.7:

$$O_3 + O_2(^1\Delta g) \rightarrow 2O_2 + O(^3P) \qquad 6.7$$

is varied. This results in no change in the intensity value and it is concluded that the loss of $O_2(^1\Delta g)$ by reaction of ozone is not a very important loss process in the atmosphere.

(7) In run P the transition probability is varied and increasing it by a factor of three to $k_8 = 7.8 \times 10^{-4}$ sec^{-1} results in an intensity of $\log_{10}I = 7.6$ which is greater than that required by observation. However, at the present time there is no reason to doubt the accepted value of $k_8 = 2.6 \times 10^{-4}$ sec^{-1} [14].

(8) The lower section of Table 15 presents the reactions cm^{-3} sec^{-1} in logs for each reaction of runs M to I. This shows that reaction 6.3 is very important as mentioned above. In addition, it shows that reaction 6.6:

$$O_2 + O_2(^1\Delta g) \rightarrow O_2 + O_2 \qquad 6.6$$

is quite significant in controlling the $O_2(^1\Delta g)$ concentration despite its low rate constant [44]. The lesser roles of the other reactions can also be seen from these runs.

Before discussing these conclusions further, the importance of the atom recombination reaction must be assessed:

$$O(^3P) + O(^3P) + M \rightarrow O_2(^1\Delta g) + M \qquad 6.9$$

An upper limit was put on $k_9 \leq 10^6$ moles^{-2} l^2 sec^{-2} for $M = N_2$ (i.e. 3.0×10^{-35} molecules^{-2} cm^6 sec^{-2}) as a result of experiments described in Chapter 5. Using this value an estimation of the intensity of the "infra-red atmospheric" band could be evaluated. The radiation I, from a layer of thickness d cms, due to reaction 6.9 is given by:

$$I = 10^{-6}\, k_8 k_9 [O(^3P)]^2 [N_2] d \quad \text{rayleighs} \qquad 6.H$$

At about 50 Km, $[O(^3P)] \approx 10^{11}$ particles cm^3 [112] and $[N_2] \approx 5 \times 10^{14}$ molecules cm^3 [112]. Thus for an emitting layer of thickness 10 Km,

$$I \approx 1.3 \times 10^{-1} \quad \text{Rayleighs}$$

This is a negligible amount and if reaction 6.9 were to be important then k_9 would have to be a factor of 10^8 faster than estimated in section 5.1.

From all these calculations described it is clear that the production of $O_2(^1\Delta g)$ in the primary step is

Table 16. ⟵ (Reaction cm^{-3} sec^{-1} log_{10}) ⟶

-log P	KM	$[O_3]$	J	1	2	3	4	5	6	7	8	$[O^1D]$	$[O_2{}^1\Delta_g]$	R/KM	R above
11·0	77·3	8·1	-2·1	6·0	4·7	5·4	4·7	-0·3	5·7	2·6	5·7	1·0	9·2	-99·9	-99·9
10·8	74·6	8·2	-2·1	6·1	4·8	6·0	4·8	-0·1	5·8	2·8	5·8	1·3	9·4	4·7	5·2
10·0	71·6	8·3	-2·1	6·2	4·9	6·2	4·9	-0·1	6·1	2·9	5·7	0·9	9·2	4·7	5·5
9·5	68·5	8·6	-2·1	6·5	5·2	6·5	5·2	0·3	6·5	3·4	5·9	1·1	9·5	4·8	5·7
9·0	68·2	9·0	-2·1	7·0	5·9	6·9	5·7	0·9	6·9	4·1	6·1	1·3	9·7	5·0	5·9
8·5	61·6	9·5	-2·1	7·4	6·1	7·4	6·1	1·7	7·4	4·8	6·4	1·6	10·0	5·3	6·2
8·0	57·8	9·9	-2·1	7·8	6·5	7·8	6·5	2·3	7·8	5·5	6·7	1·8	10·2	5·6	6·5
7·5	53·8	10·3	-2·1	8·2	6·9	8·1	6·9	2·8	8·2	6·0	6·8	1·9	10·4	5·7	6·7
7·0	49·6	10·6	-2·2	8·4	7·1	8·4	7·1	3·1	8·4	6·5	6·8	1·9	10·4	5·8	6·9
6·5	45·4	10·9	-2·3	8·6	7·3	8·5	7·3	3·2	8·6	6·5	6·7	1·8	10·3	5·8	7·0
6·0	41·4	11·2	-2·5	8·7	7·4	8·6	7·4	3·5	8·7	6·7	6·6	1·7	10·2	5·7	7·1
5·5	37·5	11·6	-2·8	8·7	7·4	8·7	7·6	3·7	8·7	6·9	6·4	1·5	10·0	5·8	7·1
5·0	33·9	12·0	-3·2	8·9	7·6	8·8	7·6	4·1	8·9	7·3	6·3	1·4	9·9	5·4	7·2
4·5	30·4	12·5	-3·6	8·9	7·6	8·9	7·6	4·3	8·9	7·5	6·1	1·2	9·7	5·2	7·2
4·0	27·0	12·7	-4·0	8·7	7·4	8·7	7·4	4·1	8·7	7·3	5·7	0·8	9·3	4·9	7·2

1 $\alpha = 0$
$p = 1$

2 = $3·4 \times 10^{-11}$ cm^3 m^{-1} s^{-1}

3 = $1·2 \times 10^{-10}$ .. ..

4 = $3·4 \times 10^{-11}$ .. ..

5 = $4·0 \times 10^{-10}$ .. ..

6 = $2·0 \times 10^{-18}$ .. ..

7 = $2·0 \times 10^{-15}$ .. ..

8 = $2·6 \times 10^{-4}$ sec^{-1}

necessary to explain the observed atmospheric intensities. This infers that the results of Jones and Wayne [29] are correct. However, the laboratory experiments described in Chapter 3 show that $O_2(^1\Delta g)$ is not produced in detectable quantities in the primary step of ozone photolysis at λ = 253.7 nm. It is difficult to reconcile these two observations. Perhaps, as Evans [34] has suggested, $O_2(^1\Delta g)$ is formed mainly at wavelengths greater than 266 nm, where most of the atmospheric absorption by ozone occurs.

The distribution of the calculated intensities of the "infra-red atmospheric" band can be seen from consideration of Table 16. This shows a complete analysis of run M. Figure 52 shows the intensity and concentration profile of $O_2(^1\Delta g)$, which indicates a maximum at about 50 Km and another small peak at about 75 Km. This is also compared with some rocket observations of Evans [34]. The observed results show a similar distribution to the calculated results, although there is some discrepancy in the height of the small secondary peak. It should be pointed out that in calculations on the $O_2(^1\Delta g)$ distribution carried out by Evans [113], no secondary peak at high altitudes was calculated. A closer examination of run M indicates that the peak at about 75 Km cannot be attributed to variations in the ozone profile. However, further calculations are necessary to decide the importance and nature of this small

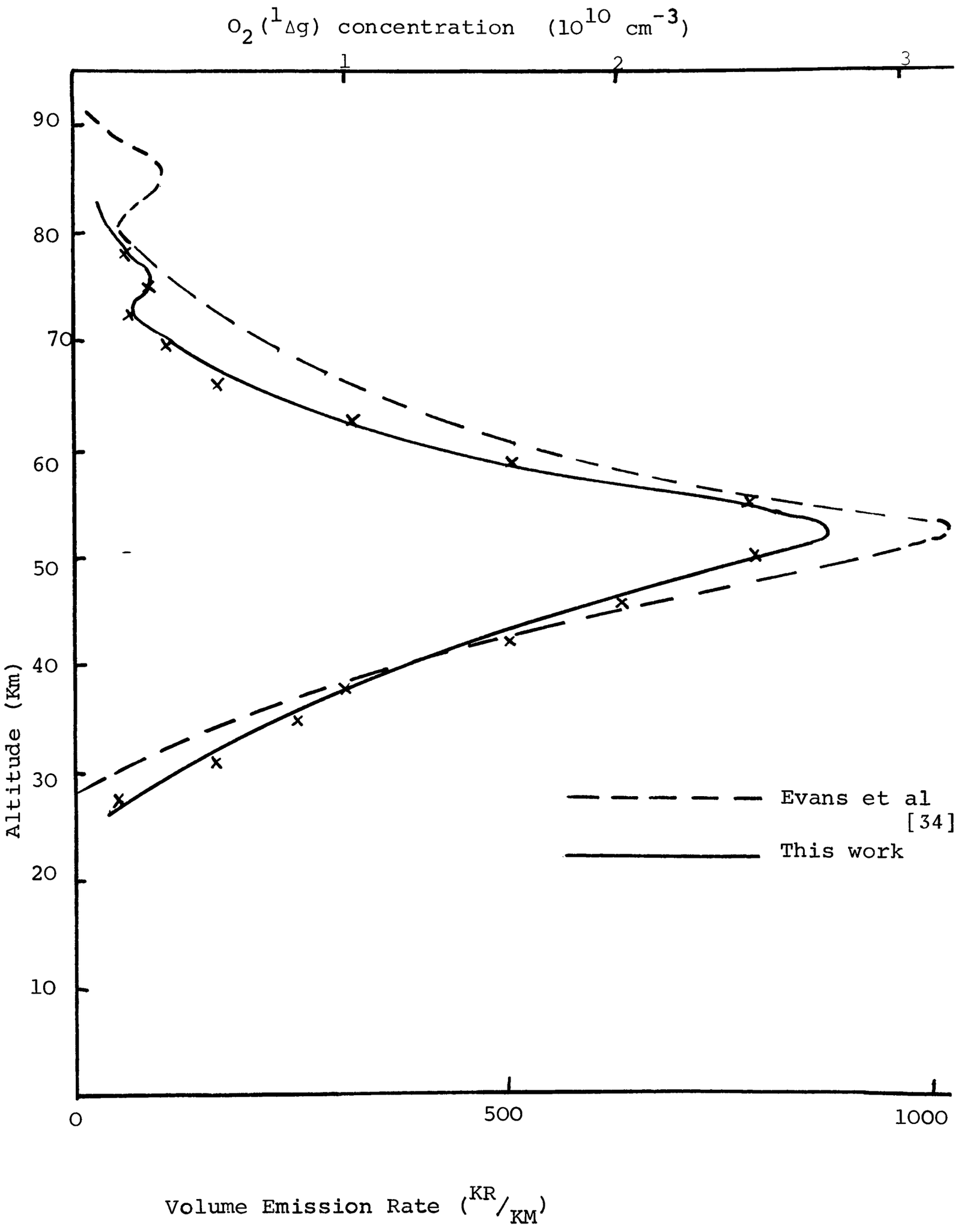


Figure 52. Concentration-intensity profile of the infra-red atmospheric band.

peak. There is also an increase in the $[O(^1D)]$ at the higher altitudes but these values cannot be compared with other workers since no reliable observations of $[O(^1D)]$ at these heights are available.

This initial calculation scheme in its present form does differentiate between the importance of mechanisms that yield $O_2(^1\Delta g)$ and also indicate the major reactions removing the excited species. The scheme, however, requires refinements. The J values should be extended to $\lambda \leq 350$ nm and all values computed to several places of decimals. In addition, the scheme should be extended to altitudes below 27 Km and a temperature correction for the rate constants introduced into the calculation. Further, various ozone profiles should be used since the ozone profiles used in the calculations are sometimes different, for geographical and atmospheric reasons, to those where rocket observations of the "infra-red atmospheric" bands are carried out.

REFERENCES

1. Goody, R.M., Atmospheric Radiation I, Oxford University Press (1964).

2. Ratcliffe, J.A., Physics of the Upper Atmosphere, Academic Press (19610).

3. Farkas, A. and Melville, H.W., Experimental Methods in the Gas Phase, Macmillan & Co. (1939).

4. Watanabe, K., Zelikoff, M. and Lin, C.Y., AFCRC Technical Report No. 52-53, Geophysical Research Paper No. 21 (1953).

5. Meinel, A.B., Astrophys. J. 112 464 (1950).

6. Gush, H.P. and Buijs, H.L., Canad. J. Phys. 42, 1037 (1964).

7. Gilmore, F.R., J. Quant. Spec. Radiative Trans. 5, 369 (1965).

8. Herzberg, G. and Herzberg, G., Astrophys. J. 105, 353 (1948).

9. Vallance Jones, A. and Harrison, A.W., J. Atmos. Terr. Phys. 13, 45 (1958).

10. Alberti, F., Ashby, R.A. and Douglas, A.E. Can. J. Phys. 46, 337 (1968).

11. Childs, W.H.J. and Mecke, R., Z. Physik. 68, 344 (1931).

12. Wark, D.Q. and Mercer, D.M., Applied Optics, 4, 839 (1968).

13. Wallace, L. and Hunten, D.M., J. Geophys. Res. 73, 4813 (1968).

14. Badger, R.M., Wright, A.C. and Whitlock, R.F., J. Chem. Phys. 43, 4345 (1965).

15. Wayne, R.P., Advance in Photochemistry, in press.

16. Bates, D., Physics of the Upper Atmosphere, Academic Press, p.219-267 (1960).

17. Wayne, R.P., Quat. J. Met. Soc. 93, 69 (1967).

18. Noxon, J.F., Space Sci. Revs. 8, 1 (1968).

19. Herring, W.S., A.F.C.R.C. 64-30-1 (1963).

20. Dütsch, E. and Grindberg, W., Pure and Appl. Geophys. 72, 204 (1969).

21. Houghton, J., Proc. Roy. Soc. A288, 545 (1965).

22. Norrish, R.G.W. and Wayne, R.P., Proc. Roy. Soc., A288, 200, 361 (1965).

23. De More, W.B. and Raper, O.F., J. Chem. Phys. 37, 2048 (1962).

24. McGrath, W.D. and Norrish, R.G.W., Proc. Roy. Soc., A242, 265 (1957).

25. McGrath, W.D. and Norrish, R.G.W., Proc. Roy. Soc., A242, 317 (1960).

26. De More, W.B. and Raper, O.F., J. Chem. Phys. 40, 1053 (1964).

27. De More, W.B. and Raper, O.F., J. Chem. Phys. 44, 1780 (1966).

28. Huffman, R.E., Larrabee, J.S. and Tanaka, Y., J. Chem. Phys. 47, 4462 (1967).

29. Jones, I.T.N. and Wayne, R.P., J. Chem. Phys., to be published(1969).

30. Castellano, E. and Schumacher, H.J., J. Chem. Phys. 36, 2238 (1962).

31. Castellano, E. and Schumacher, H.J., Z. Physik Chem. 34, 198 (1962).

32. Izod, T.P.J. and Wayne, R.P., Nature 217, 947 (1968).

33. Izod, T.P.J. and Wayne, R.P., Proc. Roy. Soc. A308, 81 (1968).

34. Evans, W.F.J., Hunter, D.M., Llewellyn, E.J. and Vallance Jones, A., J. Geophys. Res. 73, 2885 (1968).

35. Vallance Jones, A. and Gattinger, R.L., Plan. Space Sci., 11, 961 (1963).

36. De More, W.B. and Raper, O.F., Astrophys. J. 139, 1381 (1964).

37. Young, R.A. and Black, G., J. Chem. Phys. 47, 2311 (1967).

38. Young, R.A. and Black, G., J. Chem. Phys. 48, 2067 (1968).

39. Noxon, J. - to be published.

40. Young, R.A. and Black, G. and Slanger, T.G., J. Chem. Phys. 49, 4758 (1968).

41. Young, R.A. and Sharpless, R.L., J. Geophys. Res. 67, 3871 (1962).

42. Clyne, M.A.A., Thrush, B.A. and Wayne, R.P., Photochem. & Photobiol. 4, 957 (1965).

43. Clyne, M.A.A., Thrush, B.A. and Wayne, R.P., Trans. Farad. Soc. 60, 359 (1964).

44. Clough, P. and Thrush, B.A., Trans. Farad. Soc. 918 (1967).

45. Wayne, R.P., Photochem. & Photobiol. 5, 693 (1966).

46. Arnold, S.J., Ph. D. Thesis, U.B.C. (1966).

47. Brown, R.L., J. Phys. Chem. 71, 2492 (1967).

48. Stuhl, F. and Welge, K., Canad. J. Chem. 47, 1870 (1969).

49. Young, R.A. and Black, G., Symposium on Chemiluminescence; Symposium Reprints 1, (1965).

50. March, R.E., Furnival, S.G. and Schiff, H.I., Photochem. & Photobiol. 4, 971 (1965).

51. McGrath, W.D. and McGarvey, J.J., Planet Space. Si. 15 427 (1967).

52. Zipf, E.C., Symposium on Laboratory Measurements of Aeronomic Interest, York University, Toronto (1968).

53. Packer, D., An.. Geophys. 17, 67 (1961).

54. Schofield, K., Plan. Space Sci. 15, 643 (1967).

55. Briner, E., Ozone Chemistry and Technology. Advances in Chemistry Series 21, 1 (1954).

56. Sear, J. and Sutherland, H., J. Phys. Chem. 72, 117 (1968).

57. Griggs, M. and Kaye, S., Rev. Sci. Inst. 39, 1685 (1968).

58. Jenkins, A.C., Ozone Chemistry and Technology. Advances in Chemistry Series 21, 13 (1954).

59. Clough, P. and Thrush, B.A., Chem. and Ind. 33, 1971 (1966).

60. White, I.F., Part II Thesis, Oxford (1967).

61. Vigraux, E., Annls. Phys. 8, 709 (1953).

62. Inn, Y. and Tanaka, C., J. Opt. Soc. Am. 43, 870 (1953).

63. Griggs, M., J. Chem. Phys. 49, 857 (1968).

64. Hearn, A., Ph. D. Thesis, Cambridge (1959).

65. Caldwell, W.C., J. Applied Physics 12, 779 (1941).

66. Wayne, R.P., Luminescence in Chemistry, Edt. E.J. Bowen, p.42-47 (Van Nostrand 1968).

67. McNesby, J.R. and Okabe, H., Adv. in Photochem. Edt. Noyes, W.A., p.157 (Wiley & Sons 1964).

68. Okabe, H., J. Opt. Soc. Am. 54, 478 (1964).

69. Clark, I.D., private communication.

70. Wayne, R.P., Ph. D. Thesis, Cambridge (1963).

71. Gowenlock, G.R. and Melville, H.W., Experimental Methods in the Gas Phase. Figure 2.82b, p.110 (Macmillan & Co. 1964).

72. Clyne, M.A.A., Ph. D. Thesis, Cambridge (1962).

73. Gunter, R., Jenning, A. and Grant, H., J. App. Opt. 7, 2143 (1968).

74. Moss, T.S., Rep. Prog. Phys. 28, 15 (1965).

75. Zwerdling, S. and Lux, B., Phys. Rev. 106, 51 (1957).

76. Kaufman, F., Proc. Roy. Soc. A247, 123 (1958).

77. Clyne, M.A.A. and Thrush, B.A., Trans. Farad. Soc. 58, 511 (1962).

78. Fontijn, A., Meyer, C.B. and Schiff, H.I., J.Chem. Phys. 40, 64 (1964).

79. Fontijn, A. and Ellison, R., J. Phys. Chem. 72, 3701 (1968).

80. Jonathan, N. and Petty, R., Trans. Farad. Soc. 64, 1240 (1968).

81. Bausch and Lomb manufacturers' manual.

82. Lucy, J.G., Electronic Eng. 39, 148 (1967).

83. Wayne, R.P., Photochem. & Photobiol. 5, 889 (1966).

84. White, I.F. and Wayne, R.P., Berichte 72, 131 (1968).

85. Bowen, E.J., J. Chem. Soc. 76, (1935).

86. Jones, I.T.N., private communication.

87. Benson, S. and Axworthy, W., J. Chem. Phys. 42, 2614 (1965).

88. Calvert, J. and Pitts, J.N., Photochemistry, p.493, 494, and 499 (Wiley & Sons Inc. 1967).

89. Allen, C.W., Astrophysical Quantities, p.172 (Athlone Press 1962).

90. Snelling, D.R. and Bair, E.J., J. Chem. Phys. 48, 5737 (1968).

91. Katakis, D., J. Chem. Phys. 47, 3319 (1967).

92. McNeal, R.J. and Cook, G.R., J. Chem. Phys. 47, 5385 (1967).

93. Wayne, R.P. and Pitts, J.N., J. Chem. Phys. 50, 3644 (1969).

94. Clark, I.D. and Wayne, R.P., Proc. Roy. Soc. in press (1969).

95. Clyne, M.A.A., Thrush, B.A. and Wayne, R.P., Nature 199, 1057 (1963).

96. Arnold, S.J. and Ogryzlo, E.A., Canad. J. Phys. 45, 2053 (1967).

97. Arnold, S.J., Kubo, M. and Ogryzlo, E.A., Adv. in Chem. 78, (1968).

98. Kaufman, F. and Kelso, J.R., J. Chem. Phys. 46, 541 (1967).

99. Kaufman, F., Progress in Reaction Kinetics 1, Chapter 1 (Pergamon Press).

100. Carslaw, H.S. and Jaeger, J.C., Conduction of Heat in Solids (Clarendon Press, Oxford, 1959).

101. Cvetanovic, R.J., Adv. in Photochem. 1, 115 (1964).

102. Warneck, P. and Snelling, O.J., J. Chem. Phys. 46, 953 (1967).

103. Noxon, J., private communication.

104. Young, R.A. and Sharpless, R.L., J. Chem. Phys. 39, 107 (1965).

105. Pitts, J.N., Khan, A., Wayne, R.P. and Smith, E.B., Envir. Sci. Tech. 3, 241 (1968).

106. Wayne, R.P., unpublished results.

107. Pitts, J.N., private communication.

108. Snelling, D.R., Chem. Phys. Letters 2, 346 (1968).

109. Wilson, T., J. Am. Chem. Soc. 91, 2387 (1969).

110. Edwards, D.P. unpublished results.

111. Walshaw, C.D., private communication.

112. Hunt, B.G., J. Atmos. Sci. 23, 88 (1966).

113. Evans, W., Ph. D. Thesis, Univ. Saskatchewan (1966).

114. Dixon Lewis, G., Wilson, W.E. and Westenberg, A.A., J. Chem. Phys. 44, 2877 (1967).

115. Carleton, N.P., Le Blanc, F.J. and Oldenberg, O., Bull. Am. Phys. Soc. 11, 503 (1966).

116. Preston, K.F. and Cvetanovic, R.J., J. Chem. Phys. 45, 2888 (1966).